EXPERIMENTAL AND PREDICTED PERFORMANCE FOR THE COMBUSTION OF A LOW HEATING VALUE GAS IN A SWIRL BURNER

by

James G. Rice

Dissertation submitted to the Graduate Faculty of the
Virginia Polytechnic Institute and State University
in partial fulfillment of the requirements for the degree of
DOCTOR OF PHILOSOPHY
in
Mechanical Engineering

APPROVED:

W. C. Thomas, Chairman

F. J. Pierce

C. H. Long

H. L. Moses

L. L. Grigsby

February, 1979

Blacksburg, Virginia

ACKNOWLEDGMENTS

First of all, I would like to thank my wife and my two children, for their patience and understanding during all my years of schooling. I would also like to thank them for the many sacrifices that they have made in my behalf during these years. I hope I can repay them.

I would like to express my appreciation to the members of my advisory committee: Professors W. C. Thomas, F. J. Pierce, H. L. Moses, C. H. Long and L. L. Grigsby. In particular, I would like to thank Professor Thomas for his advice and assistance. During the past few years his help has been valuable, not only in the areas concerned with this dissertation, but also in his influence on my professional development in general.

Finally, I would like to thank the other graduate students with whom I have worked on this project. did an excellent job on the design, construction, and experimentation during the first phases of this work. His work provided me with a firm basis to proceed on. I would also like to thank for the long hours of work that he put in during the data collection and data reduction.

TABLE OF CONTENTS

TABLE OF CONTENTS, Cont.

LIST OF FIGURES

LIST OF FIGURES, cont.

LIST OF TABLES

NOMENCLATURE

a - finite difference coefficient

C - convection transport term defined by equation (2.25)

C_1 - empirical constant

C_2 - empirical constant

C_μ - empirical constant in equation (2.14)

D - diffusion transport tern defined by equation (2.11)

f - mixture fraction

f_{st} - stoichiometric mixture fraction

G_x - axial flux of axial momentum

G_ϕ - axial flux of tangential momentum

G_k - production rate for turbulence energy

k - turbulence kinetic energy

ℓ - mixing length

n - number of moles

n_o - number of moles of oxidant

n_F - number of moles of fuel

n_P - number of moles of combustion products

P - static pressure

Pe - Peclet Number

R_o - characteristic dimension

r - radial coordinate

S - swirl number

S_ϕ - source of ϕ per unit volume

T - temperature

T_{ref} - reference temperature

U_o - average inlet axial velocity

u - axial velocity

v - radial velocity

W_o - average inlet tangential velocity

w - tangential velocity

x - axial coordinate

ε - dissipation rate for turbulence kinetic energy

ρ - density

θ - tangential coordinate

ϕ - general dependent variable

τ - shear stress

σ - turbulent Prandtl number

μ - laminar viscosity

μ_t - eddy or effective viscosity

SUBSCRIPTS

E - value at the "east" node

e - value at the "east" face of the control volume

N - value at the "north" node

n - value at the "north" face of the control volume

P - value at the current node, P

S - value at the "south" node

s - value at the "south" face of the control volume

W - value at the "west" node

w - value at the "west" face of the control volume

SUPERSCRIPTS

* - trial value

' - correction to a trial value

1.0 INTRODUCTION

1.1 Background

The study of the combustion process in stationary combustion systems, such as those in gas turbines or power plants, has received considerable attention in the literature in the recent past. The combined effects of the energy shortage and pollution control efforts have created the demand for careful analyses of such systems. The study and analysis of the combustion in such systems involves the interactive application of fluid mechanics, heat transfer, and thermodynamic analyses to realistically model the physical process. The current availability of high-speed digital computers and recent advances in analytical techniques has made the numerical modeling of such a process a realistic goal. The object of the current investigation was to formulate a mathematical model that accurately represents the physical situation and to develop the methodology for a solution technique, consistent with the current state-of-the-art, to solve for the velocity and temperature fields associated with the combustion system. The theoretical analysis was also to be verified with a simultaneous experimental program. The system chosen for this program was chosen such that the combustion system itself would provide some new and valuable information. For these reasons, the fuel chosen was a low heating value (low HV) gas which can be produced at a relatively low cost from coal and, consequently, is a fuel of future importance. A swirl burner was used in the investigation for reasons which will be discussed.

The main emphasis of the investigation was on the development

of the analytical technique. Prior to discussing the analysis, however, the basic geometry and the combustion system will be described to give physical insight into the methodology of the analysis development. Since the current investigation includes an experimental verification of the analysis to be developed, a review of the previous experimental work in this area is included in this first chapter. The actual development of the analytical method will be covered in Chapter Two. Chapter Three will provide a brief description of the experimental apparatus and procedures used to obtain the supporting data. The predicted and measured results will be presented in Chapter Four and the conclusions reached for the overall investigation will be given in Chapter Five.

The analysis that will be presented here is an outgrowth of the author's earlier experience with numerical analyses utilizing the stream function and vorticity formulation approach [1]. Due to the fact that the author had previously developed a code based around this type of formulation, an approach to a primitive variables (velocity and pressure) formulation for the flow field was taken that is different from those most often encountered in the literature. This approach will be explained in more detail, but the essential difference is that a "non-staggered" grid system was utilized in the current analysis as opposed to a "staggered" grid system used in many other such analyses appearing in the literature. These terms will be explained in more detail in the following discussions. In retrospect, the present method has turned out to be a fortunate choice since the resulting solution algorithm is considerably simpler to incorporate into a computer code and is much simpler to apply. The resulting solution requires

roughly one-third of the computations required in a staggered grid system for a two-dimensional problem and one-fourth of those required for a three-dimensional problem. The solution algorithm is given the acronym, CENCIS (CENtered Cell, Implicitly Staggered). The computer code is called PRIMCO (PRIMitive variables COmbustion).

1.2 Combustion System

1.2.1 Low Heating Value Fuel

The composition of the low HV gas used in this investigation is shown in Table I with the properties of propane shown for comparison. As shown, the low HV gas has a heating value of only 4.77 MJ/scm compared to a heating value of 91.2 MJ/scm for the propane. Because of this low heating value, the burner required for the combustion process and the actual combustion process is considerably different from that of the more conventional fuels with higher heating values. As shown in Table I, the air-fuel ratio required for the low HV gas is approximately one whereas the air-fuel ratio for the more conventional fuels is in the range of 15-20.

Low HV gas is an attractive fuel for several reasons. First, it is relatively inexpensive to produce from coal. In fact, the gas used in this study is representative of an "in-situ" coal gas, i.e., the coal gas is produced in place (underground). An additional benefit of the low HV gas is that the flame temperatures produced are relatively low and NO_x pollution levels should be minimal. The combustion of low HV gas, however, presents many new and challenging problems for the burner designer. The low HV gas is difficult to burn in a stable combustion

Table I Volumetric Analysis and Properties of Burner Fuels*

Constituent	Propane	Low-HV Gas
N_2	---	49
H_2	---	18
CH_4	---	5
C_3H_8	100	--
CO	---	7
CO_2	---	21
Higher Heating Value		
MJ/scm (B/scf)	91.2 (2448)	4.77 (128)
MJ/kg (B/lbm)	50.4 (21649)	4.44 (1909)
Stoichiometric Air/Fuel Ratio		
By Mass, σ_m	15.6	1.18
By Volume	23.9	1.07
Specific Gravity, SG_f**	1.53	0.904
Molecular Weight	44.1	26.1
Adiabatic Flame Temperature, K (F)***	2267 (3621)	1723 (2641)

*When necessary, properties were calculated from gas composition using Reference 2.

**Air standard.

***Reactants were assumed to be at 298 K (77 F) and atmospheric pressure.

process, particularly at low excess air levels because of the lower heating value. A comprehensive and accurate analysis of the swirl burner combustion system is expected to be extremely useful to the burner designer.

1.2.2 Swirl Burner

The swirl burner was chosen as a means of providing stable combustion with low HV gas. The swirl burner is characterized by an intensive mixing process and thus should provide for a stable combustion process even with the low heating value fuel. The swirl burner used consists of two concentric annular flow passages as illustrated in Fig. 1.1. The fuel enters the combustion chamber through the center passage and the combustion air enters through the surrounding annulus. The air has axial and tangential, or swirl, velocity components. The fuel normally has only an axial component of velocity. The secondary swirl velocity and the resulting radial pressure gradient may result in the deceleration of the flow in the central region of the flow. At high degrees of swirl, a recirculation region is formed in the center of the flow field, as illustrated in Fig. 1.2. This recirculation zone is similar to the flow pattern produced by a bluff body flame holder and promotes stable combustion. As a result of the recirculating flow, a complete form of the Navier-Stokes equations must be used to model the flow field. The governing equations are elliptic in nature. Solution techniques developed for boundary layer type flows, where the simplified governing equations are parabolic in nature, are not directly applicable. The consequences of the elliptic governing equations will

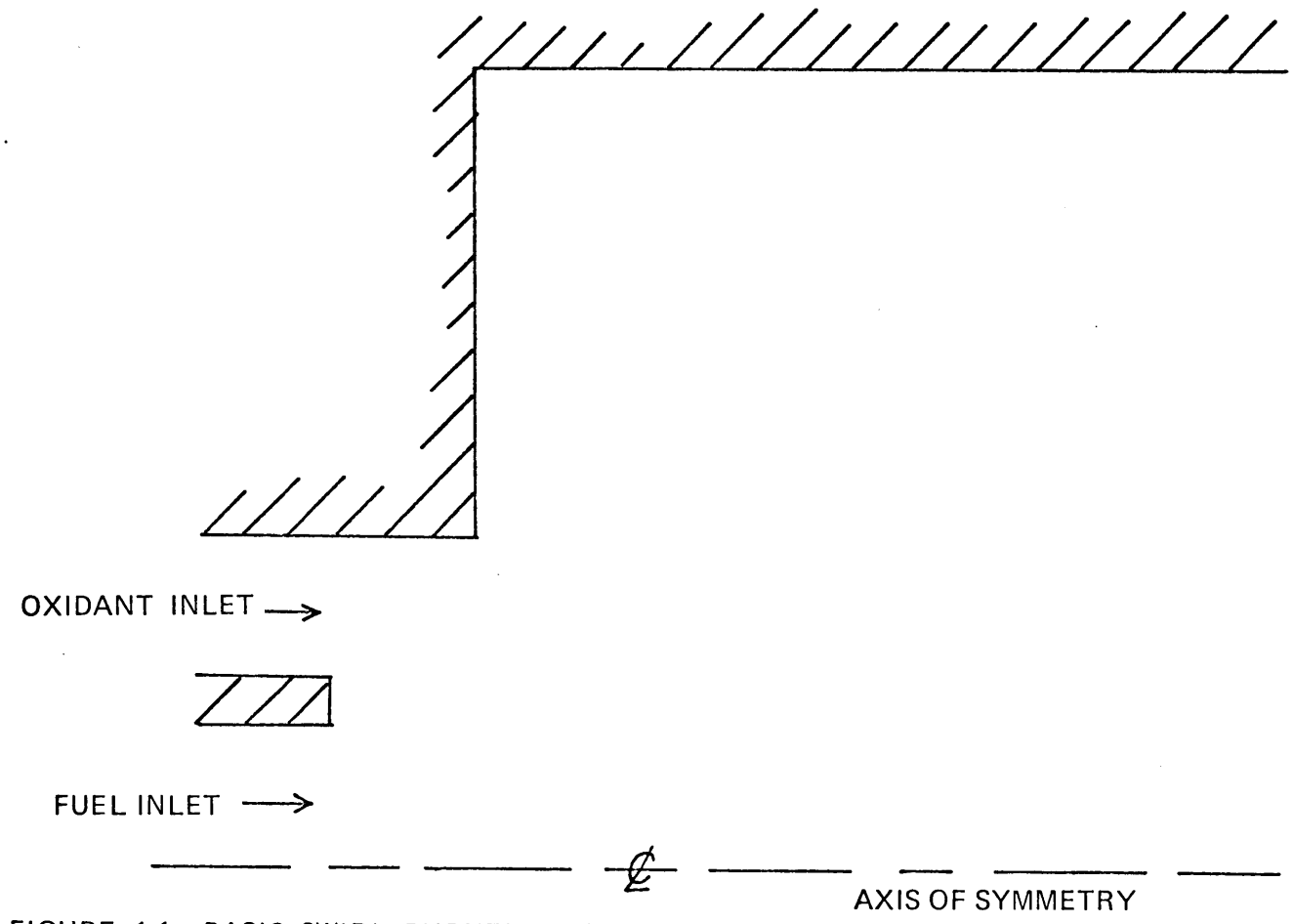

FIGURE 1.1 BASIC SWIRL BURNER GEOMETRY

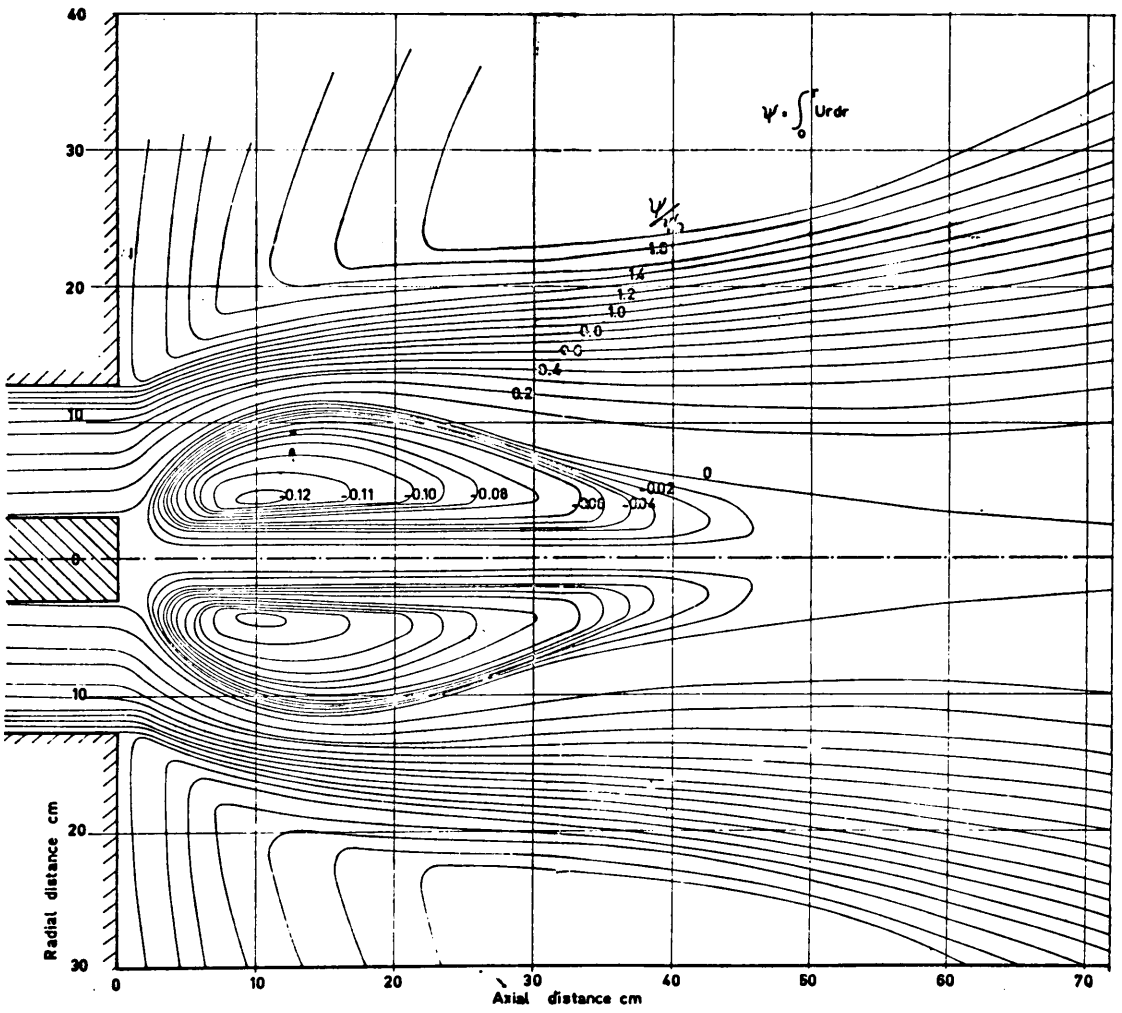

(reference 3)

FIGURE 1.2 TYPICAL SWIRLING FLOW PATTERN

be discussed further in Chapter Two.

A means of characterizing the degree of swirl is required to discuss the swirl burner. The dimensionless parameter used most frequently in the literature is the swirl number. The swirl number is defined as

$$S = \frac{G_\phi}{RG_x} \tag{1.1}$$

where G_ϕ is the axial flux of tangential momentum, G_x is the axial flux of axial momentum, and R is a characteristic burner dimension. Thus, for a flow with no tangential velocity component, the swirl number is zero. If the flow was completely tangential (no axial velocity), the swirl number would be infinite. A maximum practical value for the swirl number is approximately 3.

1.3 Analytical Background

The discussion of the analytical background in the following section will center on the analysis of the flow field since this is the most complex part of the solution. The solution of the governing equations for the combustion processes is coupled to the flow field solution, but the coupling is relatively weak. The analysis of the heat transfer and combustion processes is an important part of the overall solution. However, the emphasis in the present investigation is on the solution of the flow field. The combustion models that are employed will be discussed in Chapter Two.

Two basic approaches have been used in attempting a solution of the elliptic equations governing the flow field. In one approach, the

governing equations are formulated in terms of the stream function and vorticity. In the second approach, the "primitive variables" of velocity and pressure are used. Since there are inherent advantages and disadvantages to both approaches, the relative merits of each of the two techniques will be noted. In the following discussion, the governing equations for modeling a steady-state, two-dimensional flow in cartesian coordinates are considered. The flow variables are the two velocity components, u and v, and the static pressure, P. The governing conservation equations are the two momentum equations and the continuity equation.

1.3.1 Stream Function - Vorticity Formulation

In the stream function-vorticity approach, the two momentum equations are cross-differentiated and manipulated algebraically to derive the vorticity transport equation [4,5]. The pressure is eliminated from the resulting equation. The continuity equation is formulated in terms of the stream function. The governing equations are thereby reduced to two equations with two unknowns--the stream function and the vorticity. The number of equations and the number of unknowns has thus been reduced by one with the pressure eliminated, but the partial differential equation for the vorticity transport is of one order higher than the two momentum equations it replaces. The more troublesome aspects of solving the stream function-vorticity system involve the specification of the vorticity at the boundaries. In addition, convergence problems are often encountered in solving the vorticity equation.

1.3.2 Primitive Variables (PV) vs Stream Function Vorticity (SFV)

Based on the available literature up through approximately 1972, it had not been apparent as to whether a PV or SFV formulation offered a significant advantage for different classes of flow problems. In fact, Roache [4] states that "there is no clear advantage". The situation has changed since then principally as a result of improved pressure solution techniques. Earlier PV formulations employed a Poisson-type equation for the pressure distribution which indirectly included information from the continuity equation. The resulting equation for pressure was as troublesome as the vorticity transport equation in an SFV formulation. More recent PV formulations do not use this approach. With these problems eliminated in the more recent techniques, there are several advantages to a PV formulation, although the pressure is still the most sensitive variable. The major advantages are:

- More stable and rapid convergence
- More physically meaningful variables to work with
- Much easier boundary conditions to formulate
- Much simpler formulation.

1.3.3 Primitive Variables

In the primitive variables formulation, the flow variables are the velocity components and the static pressure. For the two-dimensional example being considered, the governing equations consist of the two momentum equations and the continuity equation. The first difficulty encountered in the solution of this set of equations is simultaneously solving the set of three equations for these three unknowns. For exam-

ple, a finite-difference equation can be derived for each of the velocity components from each of the momentum equations, but there is no obvious finite difference equation that principally governs the pressure distribution. Two basic approaches are found in the literature to solve the problem. The first technique involves deriving a "Poisson" type equation for pressure [4]. This equation is obtained by differentiating each of the momentum equations and adding them to obtain the desired equation for the pressure. The governing equation for the pressure is then [4]

$$\frac{\partial^2 P}{\partial x^2} + \frac{\partial^2 P}{\partial y^2} = - \frac{\partial^2 (u^2)}{\partial x^2} - 2 \frac{\partial^2 (uv)}{\partial x \partial y} - \frac{\partial^2 (v^2)}{\partial y^2} \qquad (1.2)$$

Information from the continuity equation is included by substituting the following relation directly into equation (1.2):

$$\frac{\partial u}{\partial x} = - \frac{\partial v}{\partial y} \qquad (1.3)$$

This technique thus supplies an explicit differential equation for the pressure distribution. This approach was used in the first of the primitive variables formulations, but the technique does not attack the problem of satisfying the continuity equation directly. The pressure solution in this technique may be as troublesome as the vorticity equation in the stream function vorticity formulation.

The second method [5,6] is an implicit technique which involves solving for a pressure correction term to simultaneously satisfy continuity along with the momentum equations. Most of the current algorithms found in the literature are based on this approach. The following section will illustrate the process. In this approach, the two momentum

equations are solved for the trial velocities u*, v*, based on an assumed initial pressure distribution. It should be noted that these velocities do not necessarily satisfy the continuity equation. Thus if these velocities are substituted into the continuity equation, the result is a nonzero residual, i.e.,

$$\frac{\partial u^*}{\partial x} + \frac{\partial v^*}{\partial y} = R \tag{1.4}$$

The basic solution procedure involves varying the pressure such that the continuity equation residual is reduced to zero. The residual is a function of the velocities which in turn are implicit functions of pressure. Therefore,

$$\frac{\partial R}{\partial P} = \frac{\partial R}{\partial u}\frac{\partial u}{\partial P} + \frac{\partial R}{\partial v}\frac{\partial v}{\partial P} \tag{1.5}$$

where the pressure-velocity relations in the above equation are deduced from the two momentum equations. Thus, the pressure variation required to reduce the continuity equation residual to zero may be found from

$$\Delta P = R/[\partial R/\partial P] \tag{1.6}$$

This general approach is used in the dominant solution techniques appearing in the literature. There are several algorithms based on this approach. The most convenient and efficient appears to be the SIMPLE algorithm of Patankar and Spalding [8]. In the SIMPLE algorithm, it is assumed that the trial velocities are related to the true velocities (u,v) by a velocity correction, i.e.,

$$u = u^* + u' \tag{1.7}$$

$$v = v^* + v' \tag{1.8}$$

It is assumed that these velocity corrections are proportional to a pressure correction P', i.e.

$$u' = D_u \frac{\partial P'}{\partial x} \tag{1.9}$$

$$v' = D_v \frac{\partial P'}{\partial y} \tag{1.10}$$

The D_u and D_v values are derived from the x and y direction momentum equations, respectively. While this assumption is only approximate as the solution converges to the true velocity field, both the pressure and velocity corrections diminish to zero. The true or corrected velocities are given by

$$u = u^* + D_u \frac{\partial P'}{\partial x} \tag{1.11}$$

$$v = v^* + D_v \frac{\partial P'}{\partial y} \tag{1.12}$$

These relations are substituted into the continuity equation to obtain a finite difference equation for the pressure corrections. The equation for the pressure correction is solved and the velocity field is corrected to satisfy continuity and momentum. The general solution procedure is outlined in Fig. 1.3.

An additional feature of solutions using the primitive variables is the use of a staggered grid system [6,7,8,9]. Although there has not been much explanation published in the finite-difference literature on the reasons for using a staggered grid system, articles have been published [10] in finite-element literature on mixed interpolation schemes

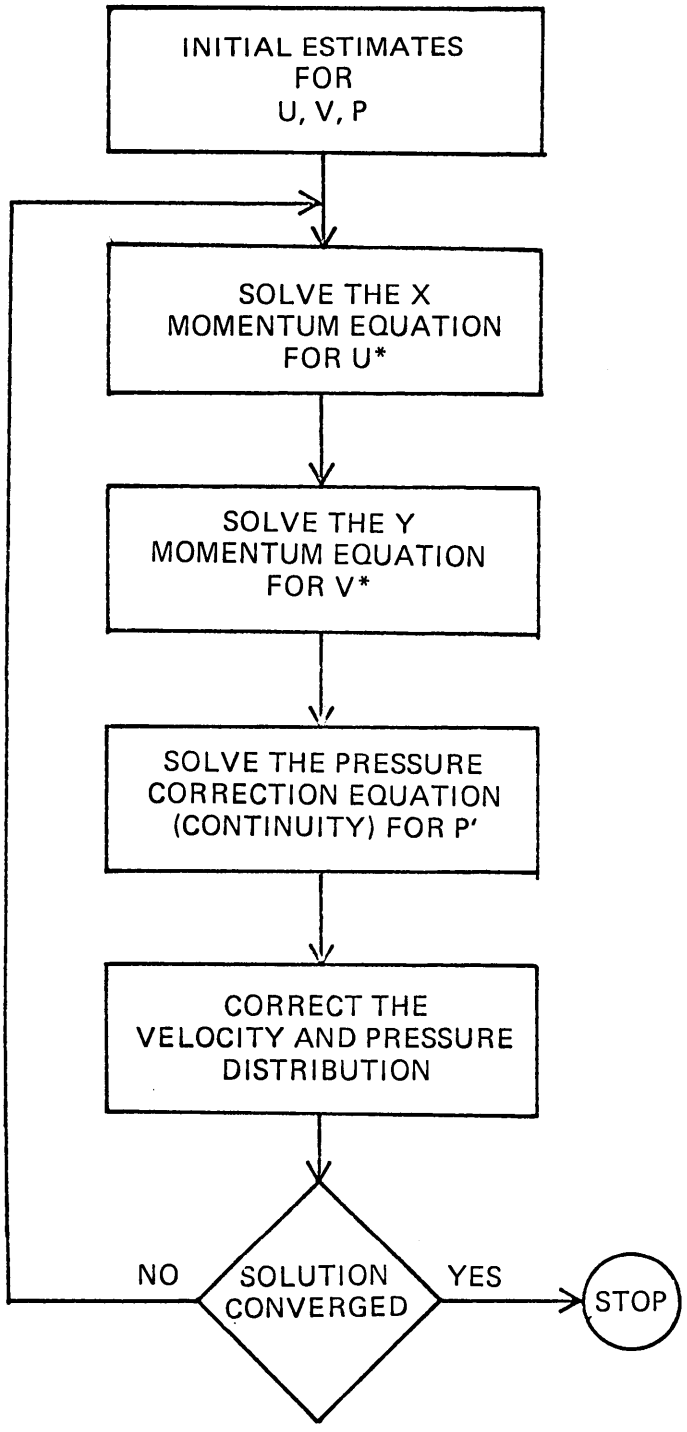

FIGURE 1.3 PRIMITIVE VARIABLES SOLUTION PROCEDURE

which achieve the same effect as a staggered grid system. A staggered grid system is illustrated in Fig. 1.4. Dependent variables other than the velocities are assigned values at the central node points of the control volume and the velocities are located on the faces of the control volume. From the control volume shown for the axial momentum equation, it can be seen that the second derivatives for velocity in the axial momentum equation are approximated by three points and the first-order pressure derivative is approximated with two points. Studies have shown [11] that a more accurate and stable solution results from such mixed approximations since the order of accuracy is equal for all terms. The staggered grid system is, however, somewhat cumbersome to apply. The following section will illustrate the basic physical reason for using a staggered grid system.

Staggered Grid Systems

As explained in the preceding section, many of the dominant solution procedures in the recent literature employ a staggered grid system. This section will illustrate the reasons for using such a grid system and introduce the scheme by which the current approach eliminates this requirement. The following discussion is based on the SIMPLE algorithm [8]. Recall that the basic approach involves finding a pressure correction, P', such that the continuity equation is satisfied. In addition, it is assumed that the pressure correction is related to the velocity correction at each node by

$$u' = D_u \frac{\partial P'}{\partial x} \tag{1.13}$$

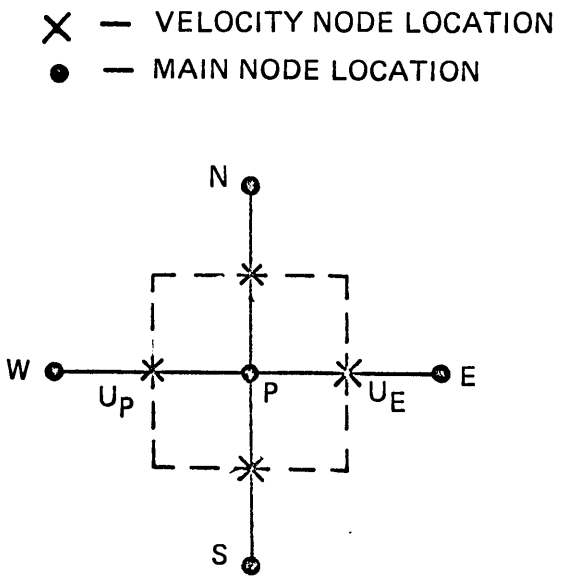

a) MAIN CONTROL VOLUME

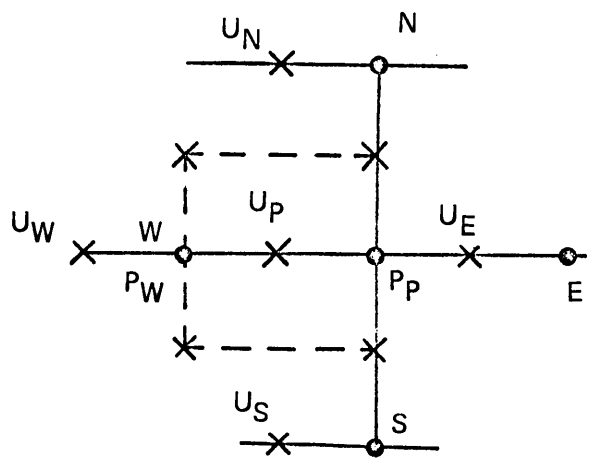

b) AXIAL MOMENTUM CONTROL VOLUME

FIGURE 1.4 STAGGERED GRID SYSTEM

$$v' = D_v \frac{\Delta P'}{\Delta y} \tag{1.14}$$

These relationships are then used similarly for the surrounding nodes to derive finite difference equations for the pressure corrections in the form

$$C_p P'_p = C_E P'_p + C_W P'_W + C_N P'_N + C_S P'_S \tag{1.15}$$

In order that a finite-difference equation for the pressure correction, such as equation (1.15), may be derived, it is essential that the velocity correction at node P be expressed as a function of the pressure correction at node P, or

$$u'_p = f(P'_p) \tag{1.16}$$

In more basic terms, referring to equation (1.11), it is required that at the node P,

$$\left.\frac{\partial u}{\partial P}\right|_p = f(P_p) \tag{1.17}$$

Referring to equation (1.13), it is essential that the finite-difference expression used to represent this relation includes P'_p. Consider the control volume illustrated in Fig. 1.5. The control volume is represented by a non-staggered grid system with velocity and pressure values located at the same node points. For convenience, let the grid system be uniformly spaced with equal increments in both directions. A central difference approximation to the first derivative for the pressure yields

$$\left.\frac{\partial P'}{\partial x}\right|_p = \frac{P'_E - P'_W}{2\Delta x} \tag{1.18}$$

NON-STAGGERED AXIAL MOMENTUM
CONTROL VOLUME

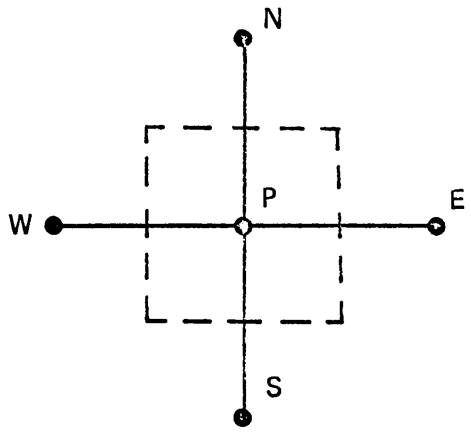

FIGURE 1.5 PRESSURE GRADIENT CALCULATION

Substitution of this relation into equation (1.13) yields

$$u'_p = D_u \frac{P'_E - P'_W}{2\Delta x} \tag{1.19}$$

The influence of the pressure at the node point, P, is completely omitted. This result is always true if the velocity and the pressure are at the same spacial location. The uniform grid example illustrates clearly the problem. Using a three-point finite-difference to approximate a first derivative may be viewed as using a quadratic polynomial to approximate the function. The polynomial is then differentiated to obtain an estimate of the derivative. The slope of the polynomial is a linear function and is thus specified by the two end points. The influence of the middle point on the slope is minimal. In the equal interval example shown here, the influence of the middle point is zero.

The use of a staggered grid system circumvents this problem. Referring to the grid system shown in Fig. 1.4, the velocity corrections are on the faces of the control volume. For the axial momentum control volume, the resulting relationships are of the form

$$\frac{\partial P}{\partial x} = \frac{P_p - P_w}{\Delta x} \tag{1.20}$$

or

$$u'_p = D_u \frac{\Delta P'}{\Delta x} \tag{1.21}$$

where

$$\Delta P' = P'_p - P'_W \tag{1.22}$$

The value of the pressure at the node appears explicitly. This

approach enables the straightforward derivation of a finite difference equation for the pressure.

The approach that is used in the current work also allows the derivation of such a finite-difference equation but without the added complexity of a staggered grid system. The current approach will be called an "implicitly staggered" solution procedure since the grid system is not actually staggered, but the same effect is obtained by the manner in which the finite difference pressure corrections are derived. As with the staggered grid system, the velocities to be corrected and the pressure corrections are at different spacial locations. The method will be described in detail in Chapter Two.

1.3.4 Turbulence Closure Schemes

An essential requirement in solving turbulent transport processes in any of the previously mentioned approaches is the closure of the problem. It is necessary to relate turbulent exchange coefficients, such as an eddy viscosity, to the local flow properties. Because of the fact that turbulence and the resulting turbulent transport is a flow property rather than a fluid property, general schemes for calculating turbulent transport properties that are universal have eluded formulation. In the problem at hand, there is a turbulent transport mechanism for mass, momentum and energy. The basic approach used in the current analysis is to model all of the turbulent transport processes by using an analogy with the turbulent transport of momentum. The turbulent transport of momentum is modeled using the effective viscosity concept. The turbulent exchange coefficients for mass and energy are then related to

the effective viscosity. For example, the turbulent exchange coefficient for energy, the eddy or effective diffusivity, would be related to the eddy viscosity through the use of a turbulent Prandtl number. In the following discussion, various models for eddy viscosity are discussed.

1.3.5 Mixing Length Models

The starting point for the discussion of turbulence models is Prandtl's mixing length model which has formed the basis for a majority of earlier eddy viscosity models. Prandtl's hypothesis was that the eddy viscosity, in flows where one velocity is dominant, such as boundary layer flows, could be calculated from

$$\mu_t = \rho \ell^2 \left| \frac{\partial u}{\partial y} \right| \tag{1.23}$$

where ℓ is the mixing length. The mixing length concept can be extended to multi-dimensional flows as [7]

$$\mu_t = \rho \ell^2 \left\{ \frac{u_i}{x_j} + \frac{u_j}{x_i} \right\} \frac{u_i}{x_j} \tag{1.24}$$

where standard index notation is used. In Prandtl's hypothesis, the mixing length represents the length scale over which turbulent eddys interact. Thus, in relatively simple boundary layer flows, for example, the length scale is of the same order as the distance from the wall and is easily calculated. In more complex flows where the mixing length model is used to calculate an eddy viscosity algebraic models may be used to specify the mixing length as a function of the flow geometry [12,13]. Specifying the required mixing length in complex multi-dimensional prob-

lems is virtually impossible, and other techniques must be used. An additional problem with the mixing length model is the dependence on the velocity gradient. Thus in regions of complex flows where the velocity gradients are small, the mixing length model predicts eddy viscosities that are too low.

1.3.6 Two-Equation Turbulence Models

Two-equation turbulence models differ from mixing length models essentially in that the two-equation models provide a means of calculating the mixing length. The major drawback of the mixing length models is eliminated. Two-equation models use the turbulence kinetic energy, k, rather than the velocity gradient to correlate the eddy viscosity. The eddy viscosity is related to the kinetic energy by

$$\mu_t = \rho k^{\frac{1}{2}} \ell \tag{1.25}$$

It should be noted, however, that this model is not essentially different from Prandtl's hypothesis and, in fact, under boundary-layer type flow conditions where the mixing length is known, the two-equation model yields the same results as the mixing length model.

The basic premise in such models is that the turbulence energy production is related to the mean strain rate tensor for the flow field. The rate of generation of the turbulence energy is given by [12]

$$G_K = \mu_t \left\{ \frac{\partial u_i}{\partial x_j} + \frac{\partial u_j}{\partial x_i} \right\} \frac{\partial u_i}{\partial x_j} \tag{1.26}$$

With the turbulence energy thus related to mean flow properties, a partial differential equation is derived which accounts for the convection, diffusion, dissipation and formation of this quantity throughout the flow field. This equation can then be solved simultaneously with the other conservation equations for the flow field [11].

In all two-equation turbulence models found in the literature, the first dependent variable is the kinetic energy of turbulence. However, there are a variety of models used, where each is distinguished by the choice of the second variable. In all models, the second variable forms the means by which the mixing length is specified. Table II shows some of the two-equation models used currently. From reviewing the literature [14,15], one concludes that there is little significant difference between the models other than some advantages of convenience for some of the models. The most frequently used second variable now appears to be the dissipation rate for turbulence energy. The dissipation rate is related to the turbulence energy by

$$\varepsilon = C_\mu k^{3/2}/\ell \tag{1.27}$$

The dissipation rate is the second variable employed in the current analysis. The governing equations used for the turbulence kinetic energy and the dissipation rate along with the boundary conditions and the solution procedure for these equations will be presented in the analysis chapter.

This discussion concludes the analytical background. The analysis to be developed in Chapter Two is based on the background work that has been described. The analysis will use the primitive variables of velocity

Table II Two-Equation Turbulence Models

Reference	2nd Variable	Symbol
16	$k^{1/2}/\ell$	f
17	$k^{3/2}/\ell$	ε
18	ℓ	ℓ
19	$k\ell$	$k\ell$

and pressure. A pressure solution algorithm will be outlined which follows the same basic approach as the Patankar-Spalding SIMPLE algorithm. The current algorithm will not be based on a staggered grid system, however. The analysis will also include provisions for variable density, combustion, and a two-equation turbulence model.

1.4 Experimental Background

There have been a number of papers dealing with experimental studies of combustion processes in swirl burners. For the most part, however, these studies have dealt with the more conventional fuels with heating values considerably higher than those under consideration here. Grant [20] has presented a comprehensive review of the literature up to 1974. A summary of the literature referenced by Grant is listed in Table III. As noted by Grant, several of the workers have compared analytical calculations with experimental measurements but a limited number have used the two-equation turbulence model that will be employed with present work. In addition, none of these workers has considered a low-HV fuel. The low-HV fuel introduces a considerably different flow situation. A detailed review of the current literature in this area is given by Lilley [21] and Syred and Beer [31]. As pointed out by Lilley, there is a considerable need for the further development and verification of these analytical techniques, particularly in flows with recirculation. In particular, he notes that the calculation of pollutant formation requires an accurate analysis.

Although there have been no papers in the literature that deal explicitly with the combustion of a low HV gas in a swirl burner, there are

Table III Experimental Investigations of Swirling Flow and Combustion

Authors	Year	Ref. No.	Type of Flow		Flow Measurements				Maximum Swirl
			Iso.	Comb.*	Temp.	Vel.	Turb.	Press.	
Chigier and Beér	1964	3	X	--	-	X	-	X	1.43
Chigier and Chervinsky	1967	22	X	--	-	X	-	X	0.64
Mather and Maccallum	1967	23	X	--	-	X	-	X	2.7
Leukel, et al.	1970	24	X	N.G.	X	X	-	X	1.4
Bafuwa and Maccallum	1970	25	X	T.G.	X	X	-	X	1.25
Syred, et al.	1972	26	X	T.G.	X	X	X	-	2.2
Beltagui and Maccallum	1973	27	-	T.C.	X	X	-	X	***
Manheimer - Timnat, et al.	1973	28	-	N.G.	X	X	-	-	0.5
Baker, et al.	1974	29	X	N.G.	-	X	X	-	0.52
Chigier and Dvorak	1974	30	X	N.G.	X	X	X	-	0.3

*N.G. is natural gas; T.G. is town gas.

**Values of swirl number are not given in paper.

papers dealing with similar areas, such as, for example, the combustion of low HV gases in gas turbines and intermediate heating value gas combustion. In the case of the gas turbine combustion processes, studies have indicated [32,33] that, as stated earlier, the low HV gas combustion produces low NO_x formation. These studies also indicate, however, that hydrocarbon emissions may be a problem. These results point out again the need for an accurate analysis of such combustion processes.

1.5 Objectives

The current dissertation represents one facet of a larger overall project in swirling flow combustion research. The overall goals of the total project are:

(1) To design and construct a variable-swirl burner capable of stable combustion with a wide variety of fuels.

(2) To provide an instrumentation system for detailed measurements of the distributions of velocity, pressure, and temperature in the combustion system.

(3) To develop a computer-aided analysis to predict the performance of the swirl burner.

(4) To compare the predicted and measured performance of the swirl burner and to verify the analysis technique.

The emphasis of this investigation will be on the development of the analysis technique and the demonstration of the validity of the technique by comparisons of predicted and measured results. This investigation will address essentially the third and fourth goals listed above. For more information on the overall project and, in particular, the

details on the other phases of the projects, the reader is referred to references 20 and 34.

2.0 ANALYSIS

This chapter discusses the development of the analytical method. The first sections of the chapter will introduce the basic geometry and assumptions in the analysis. The governing conservation equations for the system will then be discussed. The finite difference analysis that is applied to the conservation equations is presented next. With the general form of the finite difference equations as a reference, the development of the pressure solution algorithm follows. The last portion of the chapter is devoted to the description of a sample program to illustrate the basic solution algorithm. The sample program is included in the appendix.

2.1 Geometry

The basic geometry under consideration for the purpose of analysis is illustrated in Fig. 2.1. The solution domain is shown enclosed by the dashed line. The problem is described using a cylindrical coordinate system with the origin as shown in the figure. The flow pattern in the swirl burner is assumed to be axisymmetric and can be described using two spatial coordinates. The centerline is an axis of symmetry, and the solution considers one-half of the flow field. It should be noted that the third velocity component, in the tangential direction, is non-zero. All quantities have zero gradients in the tangential direction, however. The fuel enters through the center tube and the combustion air enters through the annular passage surrounding the fuel passage. The incoming air has both an axial and tangential, or swirl, velocity component. In

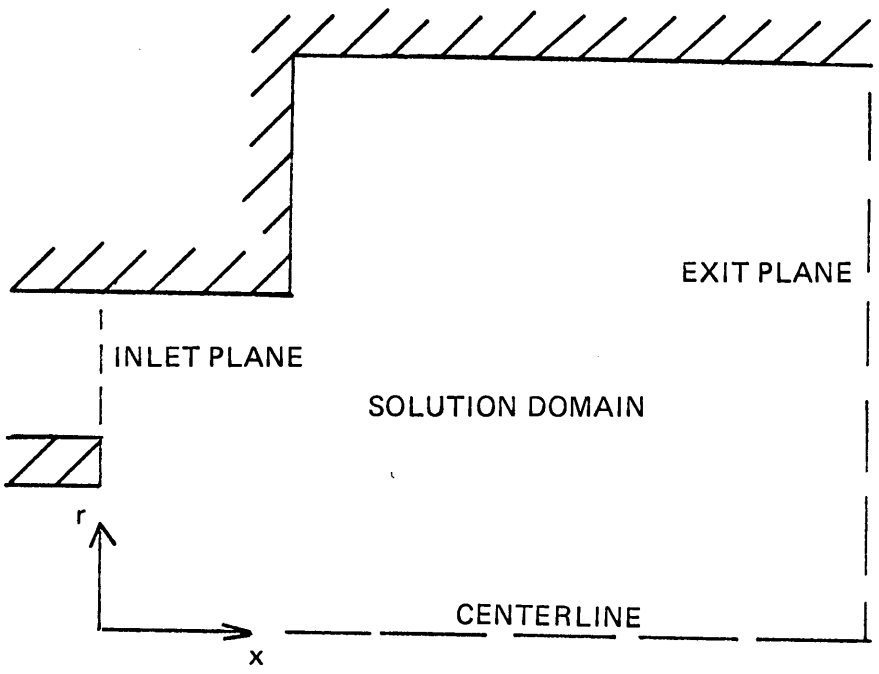

FIGURE 2.1 FLOW GEOMETRY

general, the inlet fuel does not have a swirl velocity.

2.2 Basic Assumptions

Relatively few assumptions are made in simplifying the governing equations for the current analysis. The first assumption is that the flow is steady. The flow is turbulent and all quantities appearing in the equations are time averaged. The most essential assumption in the analysis is the handling of the turbulent transport terms in the governing equations. The basic approach is that it is assumed that the turbulent transport terms, i.e., the Reynolds stress terms, can be represented by the product of an eddy viscosity and a velocity gradient in the same form as a laminar diffusion term. The combustion reactions are assumed to be physically-controlled rather than rate-controlled and equilibrium conditions are assumed. The full form of the governing conservation equations for momentum, i.e., the Navier Stokes equations, are employed. No diffusion terms are neglected and the governing equations are elliptic.

2.3 Governing Equations

As mentioned earlier, the primitive variables of pressure and velocity are employed for the representation of the flow field. These variables, together with the other variables shown in Table IV completes the description of the flow and combustion processes. The discussion of the governing equations will be in four separate sections consisting of the flow field conservation equations, the turbulence model, the combustion process model and, finally, a description of the generalized form for all of the conservation equations. This generalized conservation

Table IV Dependent Variables

Variable	Conservation Equation
u - Axial Velocity	Axial Momentum
v - Radial Velocity	Radial Momentum
w - Tangential Velocity	Tangential Momentum
P - Pressure	Continuity Equation
f - Mixture Fraction	Conservation of Mass Species
k - Turbulent Kinetic Energy	Turbulence Energy Transport
ε - Dissipation Rate for Turbulence	Decay of Turbulence

equation is used as the basis for the derivation of the finite-difference relations that are used for all of the governing equations.

2.3.1 Flow Field Conservation Equations

The conservation equations for the flow field are the three momentum equations for the axial, radial and tangential directions, and the continuity equation. The governing momentum equations are [35]:

Axial Momentum

$$u\frac{\partial}{\partial x}\{\rho u\} + v\frac{\partial}{\partial r}\{\rho u\} = -\frac{\partial P}{\partial x} + \frac{1}{r}\frac{\partial}{\partial r}\left\{r\mu_t\left[\frac{\partial u}{\partial r} + \frac{\partial v}{\partial x}\right]\right\} + \frac{\partial}{\partial x}\left\{2\mu_t\frac{\partial u}{\partial x}\right\} \qquad (2.1)$$

Radial Momentum

$$u\frac{\partial}{\partial x}\{\rho v\} + v\frac{\partial}{\partial r}\{\rho v\} - \frac{w^2}{r} = -\frac{\partial P}{\partial r} + \frac{1}{r}\frac{\partial}{\partial r}(2r\mu_t\frac{\partial v}{\partial r}) - 2\mu_t\frac{v}{r^2} + \frac{\partial}{\partial x}\left\{\mu_t(\frac{\partial u}{\partial r} + \frac{\partial v}{\partial x})\right\} \qquad (2.2)$$

Tangential Momentum

$$u\frac{\partial}{\partial x}\{\rho w\} + v\frac{\partial}{\partial r}\{\rho w\} + \rho\frac{vw}{r} = \frac{1}{r}\frac{\partial}{\partial r}\left\{r\mu_t(\frac{\partial w}{\partial r})\right\} - \frac{\mu_t w}{r^2} - \frac{w}{r}\frac{\partial \mu_t}{\partial r} \qquad (2.3)$$

The assumptions associated with this set of equations are as follows. The Reynolds Stress terms are being modeled using an effective or eddy viscosity in the form

$$\rho\,\overline{u'u'} = \mu_t\frac{\partial u}{\partial x} \qquad (2.4)$$

$$\rho\,\overline{u'v'} = \mu_t\frac{\partial u}{\partial r} \qquad (2.5)$$

This Reynolds Stress model and the fact that a single direction independent, or isotropic, eddy viscosity is employed in the momentum equations

is perhaps the most important assumption in the complete analysis. This model implies that the turbulence in the flow field is isotropic. In addition, the assumptions for the turbulence model employed in the momentum equations have important implications for the other conservation equations, i.e., the combustion model for example. This importance is not only because of the dependence of the other conservation equations on the flow field solution, but the turbulence model employed in the other conservation equations is based on Reynolds' analogy and is linearly related to the effective viscosity.

The governing momentum equations include variable property effects which account for density and viscosity variation.

Continuity Equation

The continuity equation completes the set of governing equations for the flow field. The steady state form of the continuity equation for the cylindrical coordinate system is

$$\frac{\partial}{\partial x}\{\rho u\} + \frac{1}{r}\frac{\partial}{\partial r}\{r\rho v\} = 0 \qquad (2.6)$$

The continuity equation together with the three momentum equations constitutes a set of four equations for the four unknown flow variables, i.e., the three velocity components (u,v,w) and the static pressure, P.

2.3.2 Turbulence Model

As stated earlier, an essential feature of the solution procedure is the turbulence model that is employed. The turbulent transport of momentum will be considered first. Recall that the turbulence transport is expressed in terms of the Reynolds Stresses, or

$$\tau_{ij} = \rho\overline{u_i' u_j'} \tag{2.7}$$

which is, for example, in cylindrical coordinates

$$\tau_{xr} = \rho\overline{u'v'} \tag{2.8}$$

The basic assumption in the momentum equations is that these terms can be expressed in the same form as the laminar viscous stresses, i.e.,

$$\tau_{ij} = \mu_t\left[\frac{\partial u_i}{\partial x_j} + \frac{\partial u_j}{\partial x_i}\right] \tag{2.9}$$

which becomes in cylindrical coordinates

$$\tau_{xr} = \tau_{rx} = \mu_t\left\{\frac{\partial v}{\partial x} + \frac{\partial u}{\partial r}\right\} \tag{2.10}$$

The fluid viscosity in the above equations has been replaced by an effective or eddy viscosity.

For all of the governing equations to be considered, the turbulent diffusion terms are expressed as

$$D_\phi = \frac{\partial}{\partial x_i}\{\Gamma_\phi \frac{\partial \phi}{\partial x_i}\} \tag{2.11}$$

where the turbulent exchange coefficient, Γ_ϕ, is given in each case in terms of the eddy viscosity. The key element in accurately closing the problem thus lies in an accurate model of the eddy viscosity. As pointed out earlier, the major deficiency in utilizing a mixing length model is the inability to specify the mixing length in complex flow geometries. The two-equation turbulence model provides a solution to this problem.

The basic model that is employed was proposed by various authors as

early as 1942. The high speed digital computer made the use of such models a reality only in the late 1960s [11].

The two variables that are used in the model are the turbulence kinetic energy, k, and the dissipation rate for turbulence energy, which are defined respectively as

$$k \equiv \tfrac{1}{2} \overline{u_i' u_i'} \tag{2.12}$$

and

$$\varepsilon \equiv \mu \frac{\partial u_i}{\partial x_j} \frac{\partial u_i}{\partial x_j} \tag{2.13}$$

The dissipation rate provides a means of calculating the required mixing length. The local mixing length is related to the local values of k and ε by

$$\ell = C_\mu k^{3/2}/\varepsilon \tag{2.14}$$

The turbulent viscosity is then calculated from the local values of k and ε by

$$\mu_t = \rho C_\mu k^2/\varepsilon \tag{2.15}$$

An extensive discussion of the differential equations for all of the principle turbulence models found in the literature may be found in references 12 and 36. The essential features of the model employed in the current investigation will be described here. The governing partial differential equation for the turbulence kinetic energy is not a conservation equation since turbulence kinetic energy is not a conserved quantity. The governing equation is thus called the turbulence kinetic energy transport equation. The equation considers the convection,

diffusion, production and dissipation of the turbulence kinetic energy. The governing equation, in cylindrical coordinates, is [35]

$$\rho\left[u\frac{\partial k}{\partial x} + v\frac{\partial k}{\partial r}\right] = \frac{1}{r}\frac{\partial}{\partial r}\frac{r\mu_t}{\sigma_k}\frac{\partial k}{\partial r} + \frac{\partial}{\partial x}\frac{\mu_t}{\sigma_k}\frac{\partial k}{\partial x} + G_k - \rho\varepsilon \qquad (2.16)$$

The terms on the left-hand side of the governing equation are the convection terms. The first two terms on the right-hand side represent the diffusion of k. The next term on the right-hand side represents the production of the turbulence kinetic energy and the last term represents the dissipation of turbulence energy. The generation rate of k is given by

$$G_k = \mu_t\left[2\{(\frac{\partial u}{\partial x})^2 + (\frac{\partial v}{\partial r})^2 + (\frac{v}{r})^2\} + (\frac{\partial u}{\partial r} + \frac{\partial v}{\partial x})^2 + (\frac{\partial w}{\partial x})^2 + (\frac{\partial w}{\partial r} - \frac{w}{r})^2\right] \qquad (2.17)$$

In addition to the transport equation for the turbulence kinetic energy, a similar equation is employed for the dissipation rate. The governing equation for the transport of the dissipation rate, ε, is

$$\rho\{u\frac{\partial \varepsilon}{\partial x} + v\frac{\partial \varepsilon}{\partial r}\} = \frac{1}{r}\frac{\partial}{\partial r}\frac{r\mu_t}{\sigma_\varepsilon}\frac{\partial \varepsilon}{\partial r} + \frac{\partial}{\partial x}\frac{\mu_t}{\sigma_\varepsilon}\frac{\partial \varepsilon}{\partial x} + c_1 G_k \varepsilon/k - \frac{c_2\rho\varepsilon^2}{k} \qquad (2.18)$$

Notice that this equation is quite similar to the transport equation for the turbulence kinetic energy. As in the previous case, the terms on the left represents the convective transport terms, and the first two terms on the right represent diffusion transport. The next term on the right-hand side represents a source term for the dissipation rate and the last term represents a loss.

The transport equations for the two variables, i.e., the dissipation rate and the turbulence kinetic energy will be solved simultaneously

with the other conservation equations. With these two variables specified, the effective viscosity may be calculated. The problem is strongly nonlinear and requires an iterative solution technique.

2.3.3 Combustion Process

The combustion process is modeled using a simplified approach in the current analysis. It should be pointed out, however, that this simplified approach is not a limitation on the current analysis. A more complex combustion model can readily be incorporated into the current analysis. The current effort, however, is centered on the development of the more basic features of the analysis. The basic approach taken is that the combustion process is physically-controlled rather than rate-controlled. Alternately, this model may be viewed as assuming that all reaction rates are infinite. The combustion process is completely controlled by the mixing of the fuel and oxidant. At each point within the flow field, the fuel and oxidant are assumed to react instantaneously to attain an equilibrium composition.

The mixing of the fuel and oxidant is described by a single conservation equation expressed in terms of the mixture fraction, f. The mixture fraction is the local mass fraction of fuel initially present prior to combustion. The combustion gases are assumed to be a two-component mixture of ideal gases which react to produce a third mixture of ideal gases. The two components are the fuel and the oxidant. For the present analysis these are the low HV gas and air, respectively. The governing conservation equation for the mixture fraction is then the continuity equation for the particular species. The conserved quantity is

thus the mass of the fuel and the mass of the air. The governing equation is then

$$\rho\left\{u\frac{\partial f}{\partial x} + v\frac{\partial f}{\partial r}\right\} = \frac{1}{r}\frac{\partial}{\partial r}\frac{r\mu_t}{\sigma_f}\frac{\partial f}{\partial r} + \frac{\partial}{\partial x}\frac{\mu_t}{\sigma_f}\frac{\partial f}{\partial x} \tag{2.19}$$

Notice that the governing equation accounts for the convection and diffusion of the conserved quantity. As will be shown in a later section, the finite difference solution of this equation will readily fit into the solution algorithm for the other dependent variables in the flow field.

Once the mixture fraction distribution has been determined, the thermodynamic properties of the mixture are calculated. The properties required are the density and temperature. Recall that the mixture is assumed to be at an equilibrium state. If the mixture fraction is greater than the stoichiometric value, the resulting equilibrium mixture contains combustion products and excess oxidant. If the mixture fraction is less than the stoichiometric value, the equilibrium mixture consists of the excess fuel and the products of combustion. Because the variation in static pressure is quite small for the current problem, the pressure is assumed to be atmospheric for the purpose of calculating the mixture density and temperature. The mixture density may be expressed in terms of the local mixture fraction as [7]

$$f \leq f_{st}: \quad \rho = \frac{Pf_{st}}{[T_o(f_{st}-f) + T_{st}\, f]R} \tag{2.20}$$

$$f > f_{st}: \quad \rho = \frac{P(1-f_{st})}{[T_F(f-f_{st}) + T_{st}(1-f)]R} \tag{2.21}$$

The mixture density is calculated from the ideal gas equation of state at the local mixture temperature. Because the mixture is assumed

to be in equilibrium and conduction and radiation heat transfer effects have been neglected, the mixture temperature is a function only of the mixture fraction and the pressure. Since the pressure is assumed constant for the calculation of thermodynamic properties, the mixture temperature is simply a function of the local mixture fraction. The present analysis utilizes a separate computer code to generate the mixture temperatures as a function of the local mixture fraction [2]. A typical plot of this function is shown in Fig. 2.2. A straightforward interpolation scheme is utilized to calculate the mixture temperature from the given value of the mixture fraction.

As stated earlier, the current analysis is a very simplified approach. The basic approach may be viewed as a three-component mixture of ideal gases, the three components being the fuel, oxidant and products of combustion. A more complex analysis can consider, for example, many separate components using the same techniques. The author has done such an analysis [1] considering one additional component, nitric oxide. The required extensions to the analysis follow the same basic conservation equation for mass species.

2.3.4 General Governing Equation

Each of the governing conservation equations listed in Table IV, with the exception of the continuity equation, can be put into one general form. The finite-difference equations that are derived for all of the conservation equations are essentially identical. As will be explained, this will result in a large advantage to utilizing a common grid system for all of the dependent variables. Each of the governing equations can

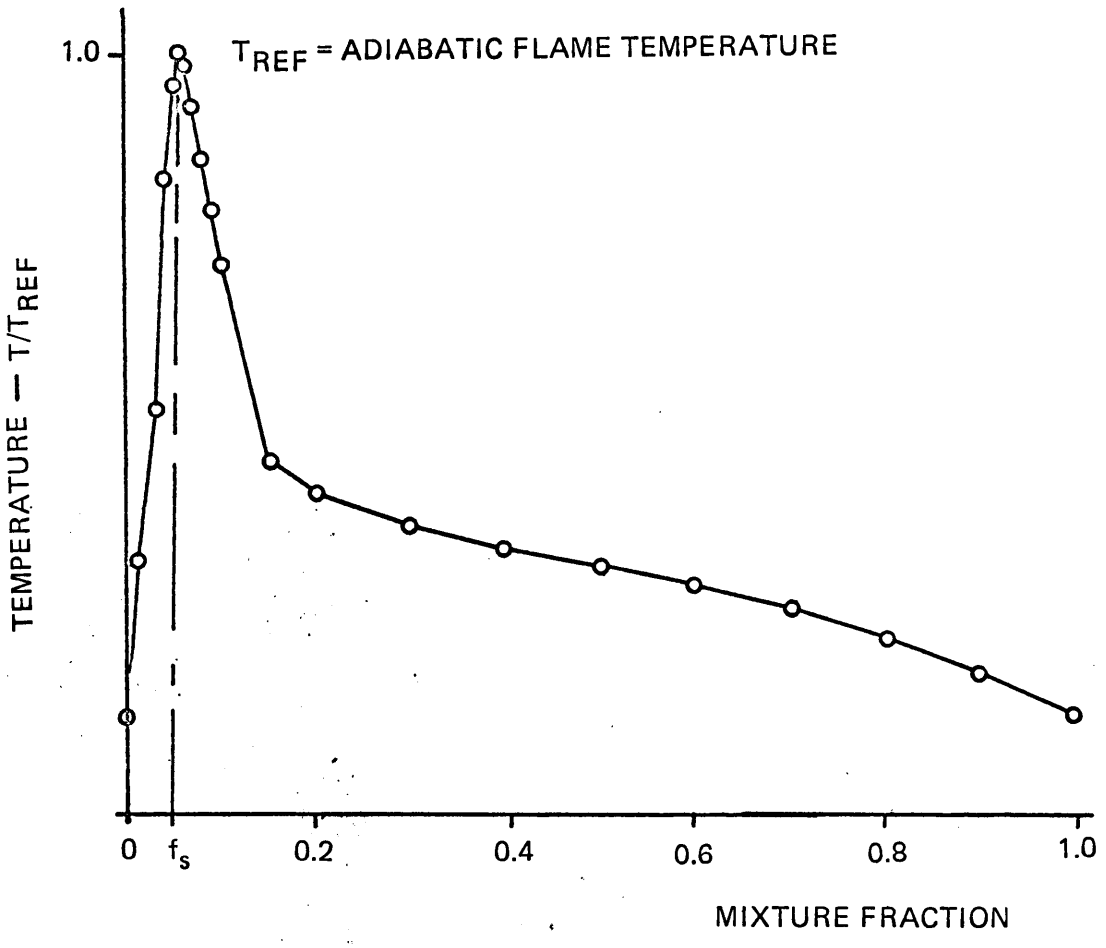

FIGURE 2.2 MIXTURE EQUILIBRIUM TEMPERATURE

be put into the general form

$$\text{div}[(\rho\bar{u}\phi) - \Gamma_\phi \text{grad}\,\phi] = S_\phi \tag{2.22}$$

which becomes for the axisymmetrical cylindrical coordinate system

$$\frac{\partial}{\partial x}\left\{\rho u\phi\right\} + \frac{1}{r}\frac{\partial}{\partial r}\left\{r\rho v\phi\right\} = \frac{\partial}{\partial x}\left\{\Gamma_\phi \frac{\partial \phi}{\partial x}\right\} + \frac{1}{r}\frac{\partial}{\partial r}\left\{r\Gamma_\phi \frac{\partial \phi}{\partial r}\right\} + S_\phi \tag{2.23}$$

where ϕ is the dependent variable under consideration and Γ_ϕ is the turbulent exchange coefficient for the dependent variable being considered. For example, with ϕ being the axial velocity, u, the turbulent exchange coefficient, Γ_u, is the effective viscosity. As in the previous examples, the terms on the left side of equation (2.23) represent the convective transport of the ϕ quantity and the first two terms on the right side of equation (2.23) represent the transport of the ϕ quantity by turbulent diffusion. The remaining term on the right side of the equation, S_ϕ, represents "sources" for the ϕ quantity. Table V shows each of the dependent variables and the respective source terms for each variable. Any terms not falling under the convection or diffusion classification are included in the source term. In the case of the axial velocity, the source term includes pressure gradient, viscosity gradient and density gradient terms. The source term can also be used to account for radiation heat transfer, internal energy generation, viscous shear work, etc. The source term is, in general, strongly nonlinear.

As each of the field variables is handled in an identical manner, the algebraic finite difference equations that are derived in the following sections are derived for the general dependent variable ϕ.

2.4 Finite-Difference Equations

Table V Source Terms for the Dependent Variables

Variable ϕ	Source Term $S\phi$
u	$\frac{\partial}{\partial x}\{\mu_t \frac{\partial u}{\partial x}\} + \frac{1}{r}\frac{\partial}{\partial r}\{\mu_t r \frac{\partial v}{\partial x}\} - \frac{\partial P}{\partial x}$
v	$\frac{\partial}{\partial x}\{\mu_t \frac{\partial u}{\partial r}\} + \frac{1}{r}\frac{\partial}{\partial r}\{\mu_t r \frac{\partial v}{\partial r}\} - \frac{2\mu_t v}{r^2} + \frac{\rho w^2}{r} - \frac{\partial P}{\partial r}$
w	$-(\frac{\mu_t}{r^2} + \frac{\rho v}{r} + \frac{1}{r}\frac{\partial \mu_t}{\partial r})w$
f	0
k	$G_k - \rho\varepsilon$
ε	$\frac{\varepsilon}{K}\{C_1 G_k - C_2 \rho\varepsilon\}$

where

G_k is the mean strain rate

$$G_k = \mu_t[2\{(\frac{\partial u}{\partial x})^2 + (\frac{\partial v}{\partial r})^2 + (\frac{v}{r})^2 + (r\frac{\partial}{\partial r}(\frac{w}{r}))^2\} + (\frac{\partial v}{\partial r} + \frac{\partial v}{\partial x})^2]$$

2.4.1 Grid System

An essential feature of the current solution procedure is the grid system. The dominant solution algorithms currently found in the literature use a staggered grid system. The current algorithm uses one common grid system for all variables. A typical grid system is shown in Fig. 2.3. This unified grid system is convenient and results in a simpler solution algorithm. The solution requires roughly one-fourth the computations required in a staggered grid system.

The grid system is divided into a number of cells, as shown. The key feature of this mesh is that all variables are located at the center of the cells. It will be shown that as a result of this approach, a single set of finite difference coefficients will suffice. This single set of coefficients is valid for all of the dependent variables. In addition, the nodal system allows for an extremely easy specification of both Dirichlet and Newman type boundary conditions by the use of image boundary points (IBP).

2.4.2 Central Difference Coefficients

There are several approaches found in the literature to obtain an algebraic finite difference equation from the governing partial differential equation [4,5,6]. The techniques range from direct substitution of the finite-difference approximations to the partial derivatives into the governing equations to more physically oriented control volume integrals. The latter approach is used here for several reasons. First, this approach allows a more straightforward inclusion of variable properties such as effective viscosity and density. In addition, this approach

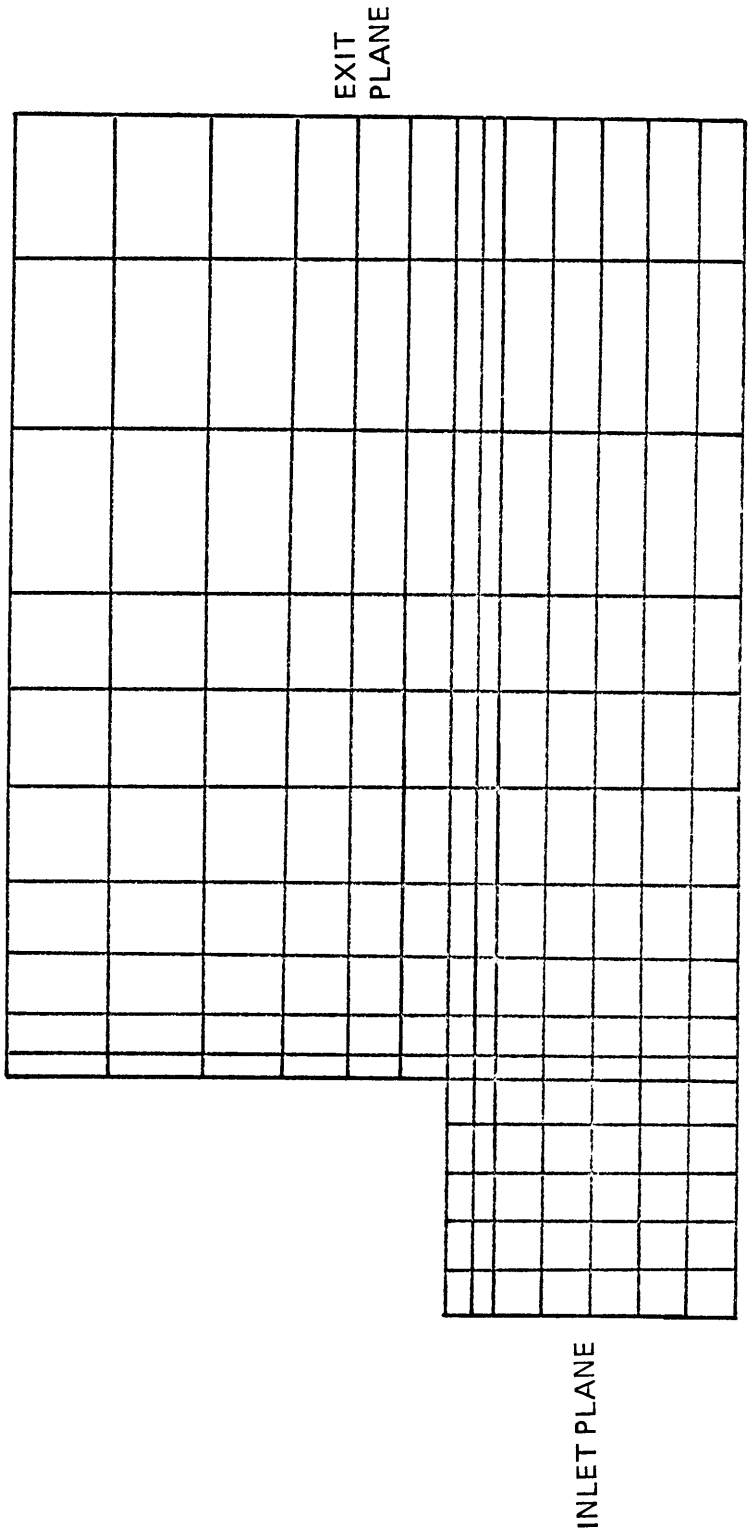

FIGURE 2.3 TYPICAL GRID SYSTEM

also allows an easier inclusion of specified flux boundary conditions. Finally, the control volume is well suited for deriving finite difference coefficients that will be valid for the general conservation equation rather than for a specific equation. A detailed description of the integration of the governing equation over the control volume is given in Appendix A. The results of this integration over the control volume, shown in Figure 2.4, are verbally

$$\text{Net Convection} + \text{Net Diffusion} = \text{Sources} \tag{2.24}$$

The convective and diffusion transport of ϕ across each face of the control volume is summed to equal the internal sources of ϕ within the volume. This practice is illustrated using the east face of the control volume as an example. The convection of ϕ across the east face of the control volume is given by

$$C_e = \rho_e A_e u_e \phi_e \tag{2.25}$$

The diffusion of ϕ across the east face of the control volume is given by

$$D_e = \Gamma_e A_e \frac{(\phi_E - \phi_p)}{\Delta x_e} \tag{2.26}$$

The generation, or source, of ϕ within the control volume is given by

$$\text{SOURCE} = S_\phi (\text{Vol}) \tag{2.27}$$

For the moment, a central difference will be employed to illustrate the calculation of the finite difference approximations, but as will be explained in the following sections, a special differencing procedure will be employed to ensure numerical stability of the solution procedure. Following the above procedure for the other three faces of the control volume, the following set of algebraic finite difference equations is produced [7]:

$$a_p \phi_p = \sum_i a_i \phi_i + S_{\phi_p}; \quad i = E, W, N, S \tag{2.28}$$

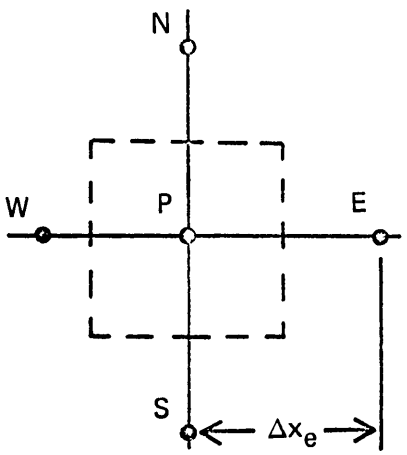

FIGURE 2.4 TYPICAL CONTROL VOLUME

where

$$a_p = \sum a_i \tag{2.29}$$

and

$$a_E = D_e - C_e/2 \tag{2.30}$$

$$a_W = D_w + C_w/2 \tag{2.31}$$

$$a_N = D_n - C_n/2 \tag{2.32}$$

$$a_S = D_s + C_s/2 \tag{2.33}$$

The preceding algebraic finite difference equation is strongly nonlinear. For example, if the field variable is the axial velocity, the east and west finite-difference coefficients depend strongly on the variable itself. There are a number of important stability criteria for a finite-difference equation such as equation (2.28). These criteria are discussed in the following section.

2.4.3 Upwind Differencing

In the previous section, the finite-difference coefficients were derived by using a central difference scheme. As shown most clearly by Spalding [37] and others [38, 4], the use of central differences can lead to difficulties with stability. Stability problems may be encountered when the convection terms are much larger than the diffusion terms across a particular control volume face. This stability problem is quite similar to that encountered in transient diffusion type problems such as heat conduction or neutron diffusion. The basic difficulty arises when the first derivatives, the convection terms, appearing in

the governing equation are large compared to the second derivatives, the diffusion terms.

In the following sections, the stability problem is discussed in terms more directly related to the physics of the problem in an attempt to show the basic cause and the cure for the stability problem. To begin, recall that the transport of the ϕ quantity across each face of the control volume face has two components, a convection component and a diffusion component. The relative magnitudes of these two terms is usually expressed in terms of a dimensionless parameter, the Peclet number. (The Peclet number is simply a cell Reynolds number if ϕ is velocity.) The Peclet number at the east face of the control volume is

$$Pe\Big|_e = \frac{\rho_e u_e \Delta x_\varepsilon}{\Gamma_e} \tag{2.34}$$

As shown by Spalding [36], if the Peclet number is greater than 2, the use of a central difference to represent the convection term results in an inherent instability. This approximation results in a violation of basic stability criteria for finite difference equations such as equation (2.28), i.e., a negative finite difference coefficient is produced. Physically, the large Peclet number signals the fact that the convection transport is much larger than the diffusion transport at this point in the flow field and it is thus impossible for the downstream value of the ϕ variable to have any influence at the upstream location. The cure for this stability problem, upwind (or donor cell) differencing, removes the influence of the downstream value by using a backwards or upwind difference to evaluate the term. It should be noted that upwind differencing is

not the only approach that can be used, but it is the most widely used. Other techniques, for example, utilize an artificial viscosity [4,38].

The differencing scheme that is employed is based on the usage of both central differences and upwind differences, depending on the local Peclet number at each face of the control volume. This may at first seem to be a cumbersome procedure, but as will be shown, it is a rather simple inclusion in the basic solution algorithm and, in fact, can significantly reduce the computation time since the use of the upwind difference will in effect make the problem locally a parabolic rather than an elliptic problem.

To illustrate the process, consider the transport coefficient across the east (e) face of the control volume shown in Fig. 2.4. As derived, the a_E finite difference coefficient is given by

$$a_E = D_e - C_e/2 \tag{2.35}$$

The above relation is based on the assumption that the value of the variable, ϕ, at the east boundary of the control volume is that obtained by the linear approximation

$$\phi_e = \frac{\phi_P + \phi_E}{2} \tag{2.36}$$

This also implies that a central difference is used to approximate the first derivative, convection term, in the governing equation. If the Peclet number is large, the convection transport is dominant and the value of the variable at the east face will be closer to either the east value or the value at the point itself, but it will not be the average value given by equation (2.36). Thus, if the velocity across the east

face is large and positive, the value of the variable at the face will be close to the value at the point itself, and, if the velocity is large and negative, the value of the variable at the east face will be close to the value at the east node. Thus for convection dominated flow, the upwind value is dominant. The criteria that is used to determine if the velocity value is large is the Peclet number. In addition, if the convection is dominant, the diffusion component is neglected. Thus, the transport across the face is calculated in three different cases using the "hybrid" differencing scheme of Spalding [36].

$$(1)\quad P_e < 2: \quad a_E = D_e - C_e/2 \tag{2.37}$$

$$(2)\quad P_e > -2: \quad a_E = -C \tag{2.38}$$

$$(3)\quad P_e > 2: \quad a_E = 0 \tag{2.39}$$

Case 1 is a central difference and cases 2 and 3 are upwind differences. Note that in case three the west coefficient for the adjacent node (E) will be given by

$$a_W = C \tag{2.40}$$

To put this procedure in perspective with, for example, boundary layer solutions, a brief explanation is necessary. If the east-west direction corresponds to the principle flow direction for the two-dimensional boundary layer equations, the boundary layer assumptions are that the diffusion term in that direction is neglected. This assumption corresponds to an infinite Peclet number and the following coefficients will always apply:

$$a_E = 0 \quad . \tag{2.41}$$

$$a_W = C_w \tag{2.42}$$

Note that the solution has in effect been upwind differenced and that the parabolic character of the problem has been retained, illustrated by the fact that the east coefficient is zero. Thus, in this case it is not possible for the downstream value of the variable, at the east point, to influence the upstream value. Note that the solution procedure that is used automatically checks the significance of the diffusion term. If it is not significant, it is not included. The result is that if the flow field is not elliptic, i.e., the diffusion terms are everywhere negligible, the problem is reduced to essentially a parabolic problem. It should be noted, however, that the pressure solution technique that is used does include the downstream value of pressure. The inclusion of this downstream pressure value prevents the current solution procedure from becoming a simple marching solution. The pressure term can be expressed in terms of a backwards difference, however, and then a marching or parabolic solution technique will result.

2.4.4 Stability Considerations

There are several general criteria for the stable solution of finite difference equations such as equation (2.28) that involve significant first and second derivatives. These criteria are for linear equations but are applied here to the iterative solution of a non-linear problem. Referring to equation (2.28), the conditions can be summarized as

$$\text{(1) all } a_i \geq 0 \tag{2.43}$$

$$(2) \quad a_p > 0 \tag{2.44}$$

$$(3) \quad a_p \geq \sum_i a_i \tag{2.45}$$

The presence of the source term also presents some difficulties, and these will be discussed separately. Note that by the upwind differencing scheme discussed previously, it has been insured that the first condition is satisfied at all times. To insure that the second condition is always satisfied, a slight modification to the ϕ value is used. For each control volume, if ϕ is a solution to the governing differential equation, then ϕ plus an arbitrary constant is also a solution to the governing equation. This approach is commonly encountered in conduction heat transfer, for example. Thus, let the dependent variable be defined by

$$\bar{\phi} = \phi + C \tag{2.46}$$

If the above relation is substituted into the governing equation and integrated over the control volume, the expression for a_p becomes

$$a_p = \sum a_i \tag{2.47}$$

Since it has already been insured that the a_i values are always positive, it has also been insured that both conditions 2 and 3 are satisfied. In this manner, all three of the stability criteria have been satisfied.

In addition to the previously mentioned stability problems, some difficulty may be encountered with the source term, S_ϕ. For some of the governing equations, the source term may be a negative function, and this may lead to difficulty, as reported by Gosman, et al [7] and Launder, et al [40]. To illustrate, consider the coriolis term in the tan-

tential momentum equation; i.e.,

$$\frac{\rho v w}{r} \tag{2.48}$$

This term is a function of the tangential velocity value and may be either positive or negative, depending on the sign of the radial velocity. An additional example is the dissipation of turbulence kinetic energy which will always be negative. The stability problems occur when the source term is negative. To illustrate the cure to the problem, the source term is split into a positive and negative component. The FDE becomes

$$a_p \phi_p = \sum a_i \phi_i + S_\phi + S_\phi^- \phi_p \tag{2.49}$$

The cure is to evaluate implicitly the negative source term. Noting that S_ϕ^- is a negative quantity, the equation is rearranged to yield

$$a_p' \phi_p = \{a_p - S_\phi^-\} \phi_p = \sum a_i \phi_i + S_\phi \tag{2.50}$$

where

$$a_p' = a_p - S_\phi' \tag{2.51}$$

Note that a_p' is a positive quantity and the algebraic finite difference equation still satisfies the previous stability criteria. This technique is very effective in stabilizing problems with large nonlinear source terms.

2.4.5 Boundary Conditions

Prior to discussing the technique that is used in the current analysis in applying the boundary conditions, the importance of the boundary

conditions should first be discussed. The specification of the boundary conditions and the procedure used in deriving the finite difference equations at the boundary nodes is the most important single aspect of any solution procedure. To illustrate this statement, consider the following fact. All flow problems, from a vortex sheet behind a blunt body to the boundary layer over a flat plate to a fully elliptic recirculating flow, may be described using the identical set of partial differential equations. The only variation from one problem to another is the boundary conditions. Thus an accurate representation of the boundary conditions is essential and the boundary area must be the most accurately represented area within the whole flow field since, in effect, the boundary conditions determine the complete solution.

The procedure that is employed here is quite similar to that employed in the codes developed at Los Alamos [6,10]. It should be pointed out, however, that these codes are based on a staggered grid system and the current approach is based on a unified grid system. The unified grid system also simplifies the inclusion of the boundary conditions. In addition, the approach used here is quite different from that employed in the Patankar-Spalding approach. The three approaches are illustrated in Fig. 2.5. The three techniques have been named: (a) extended cell, (b) image node point and (c) the image cell approach. The approach utilized in the current algorithm is called the image node point method (INP). The INP technique is a natural approach to use in a unified grid system and has several distinct advantages in such a system.

First, the quantity which is actually specified is the value of the particular dependent variable at the boundary itself. In addition, this

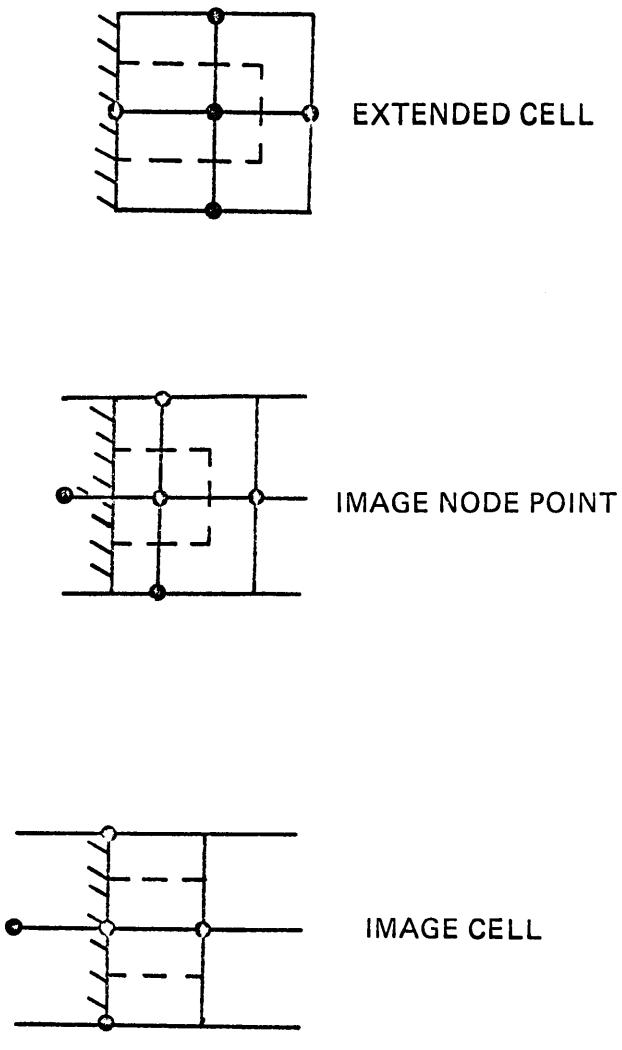

FIGURE 2.5 BOUNDARY CONTROL VOLUMES

required value is specified in a manner that does not require any special treatment of the governing finite difference equations at boundary nodes. This simplifies considerably the required computer code equations. The following examples will illustrate the process. Three basic types of boundary conditions are specified. They are:

(1) Dirichlet, ϕ_w = specified

(2) Newman, $\left.\frac{\partial \phi}{\partial n}\right|_w$ = specified

(3) Exit Plane - Continuative Boundary

All of the boundary conditions for any of the governing equations fall into one of these categories. For example, an adiabatic wall boundary condition is a boundary condition of the second type. The exit plane is in reality a form of the second boundary condition. The boundary conditions for each of the field variables is shown in Fig. 2.6 with the exception of the wall boundary conditions for k and ε which will be discussed separately. To illustrate the process, consider the axial momentum equations. There are four different possible boundary conditions that may occur for this equation. These four possibilities are illustrated in Fig. 2.7 as cells A, B, C and D. These are, respectively, an inlet boundary node, an exit boundary cell, a no-slip wall cell and a symmetry boundary cell. The basic procedure involves the use of the previously-mentioned image node point (INP). The boundary conditions are imposed by specifying a value for the INP variable which in effect specifies the boundary value for the variable at the boundary of the cell. For example, the no-slip wall condition is handled by setting

$$u_{C-1} = -u_C \tag{2.52}$$

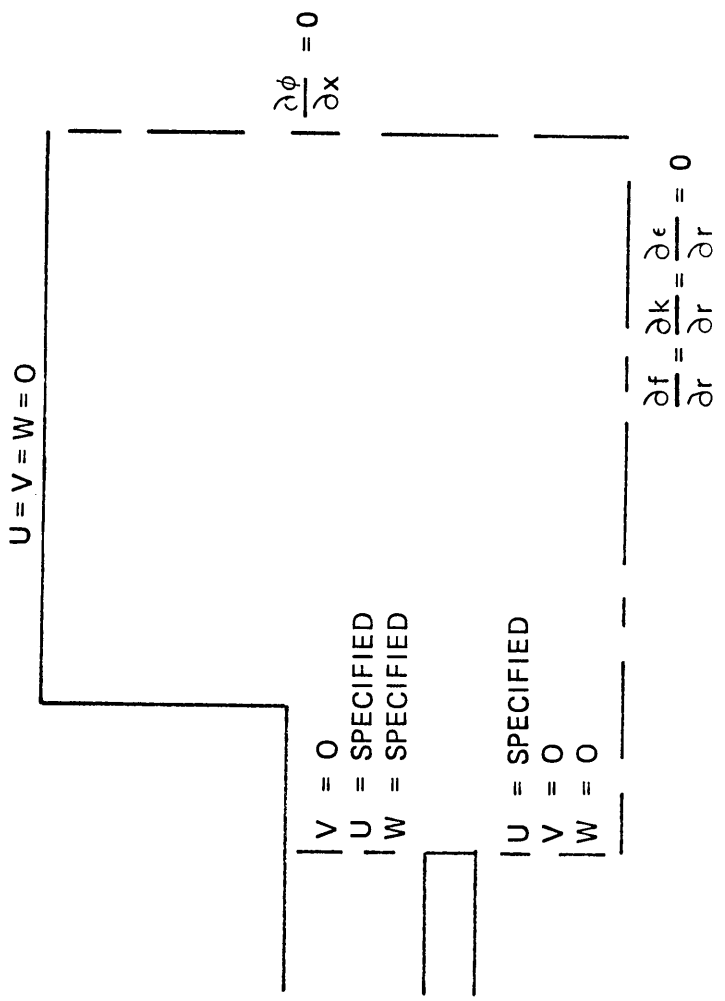

FIGURE 2.6 BOUNDARY CONDITIONS

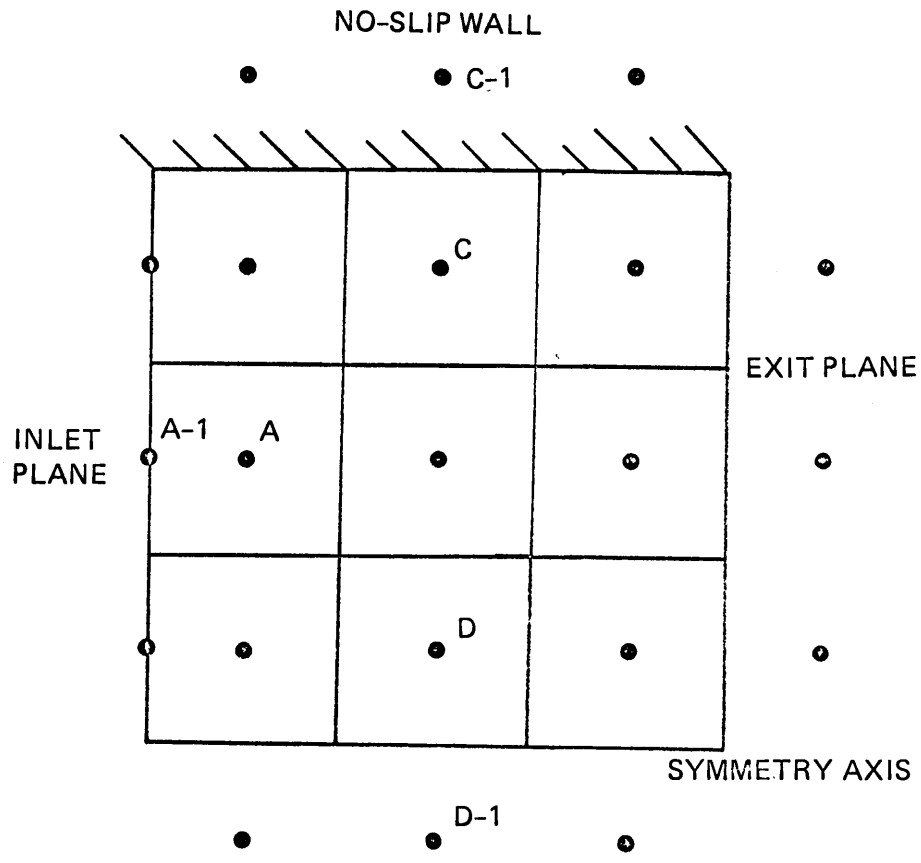

FIGURE 2.7 IMAGE NODE POINTS

Thus the velocity at the wall in the finite difference equations is

$$u_w = \frac{u_{C-1} + u_C}{2} = 0 \tag{2.53}$$

Note that the value of the velocity at the wall has been specified and, in addition, the normal gradient of the velocity at the wall is also calculated correctly without any special treatment. At the axis of symmetry, for example, the zero normal direction gradient condition is imposed by setting

$$u_{D-1} = u_D \tag{2.54}$$

Thus the procedure will easily handle any other basic types of boundary conditions that were previously outlined. The one exception is that on the inlet plane, the value at the actual inlet plane must be specified as illustrated by the u_{A-1} value shown in Fig. 2.7.

A particularly important boundary condition is the continuative boundary condition imposed on the exit plane. In general, two conditions are applied at the exit plane:

$$\left.\frac{\partial \phi}{\partial x}\right|_{exit} = 0 \tag{2.55}$$

$$\dot{m}_{exit} = \dot{m}_{inlet} \tag{2.56}$$

The first constraint is that the gradients of all variables are zero in the flow direction, and the second condition implies that the continuity equation is satisfied globally. The second condition is the one of particular interest. Because of the relatively weak nature of the first constraint, it is desirable to reduce as much as possible the

influence of the exit plant variables on the upstream values [40]. Because the flow will be positive and in general have a large Peclet number, in the majority of cases the finite difference coefficient that relates the influence of the downstream value is zero because of upwind differencing. Therefore, the only way the downstream value of axial velocity can influence the upstream value is via the continuity equation. This influence is reduced by the manner in which the continuative boundary condition is applied. The procedure is as follows. First the iterative solution of the governing equations at all interior points is carried out. The main point is that the continuative boundary condition is not applied until after the interior solution has been done. Second, the exit plane axial velocity is prescribed, based on the calculated interior values. At each exit plane image node point, then,

$$u_e^* = u_p \tag{2.57}$$

From these values, then, the total exit mass flow is calculated from

$$\dot{m}_{ex}^* = \sum_j u_e^* \rho_e A_e \tag{2.58}$$

To satisfy the continuity equation, this flow rate should equal the given inlet flow rate. If the flow rate does not meet this requirement, the exit velocity distribution is adjusted so that it does, i.e.,

$$F_m = \dot{m}_{in} / \dot{m}_{ex}^* \tag{2.59}$$

$$u_e = u_e^* F_m \tag{2.60}$$

The key point is that these adjustments are applied last in the calcula-

tion scheme, after all other calculations.

2.4.6 Turbulent Wall Functions

Special boundary conditions are employed for the calculation of turbulent flow near the walls. Following the procedure outlined by Spalding and Launder [36], the velocity profile adjacent to a wall is assumed to follow a universal law of the wall. The implications of the law of the wall are then included in the boundary conditions and the finite difference equations in the near-wall region. In particular, the law of the wall is used to calculate the shear stress at the wall. In addition, the special formulation is used to specify the dissipation rate, ε, in the near-wall region. Although the use of this assumed velocity profile in these calculations carries some significant assumptions [12, 36], this is the only practical approach that is currently available for the calculation of turbulent flows. The calculations in the near-wall region could be accomplished by employing a much finer grid system in this region. The grid system could be fine enough to carry the calculations to the extent of including the laminar sublayer. This approach is questionable however, since it would require considerable computation time and storage.

The assumed velocity profile in the near-wall region results in several implications in the solution algorithm. In the following sections, the additions to the algorithm are discussed.

The assumed velocity profile is given by

$$u^+ = \frac{1}{\kappa} \ln[Ey^+] \tag{2.61}$$

where

$$u^+ \equiv u/u_\tau \tag{2.62}$$

$$u_\tau \equiv \tau_w / [\rho c_D^{1/4} k^{1/2}] \tag{2.63}$$

and

$$y^+ \equiv c_D^{1/4} \rho k^{1/2} y / \mu_{ref} \tag{2.64}$$

The universal law is applied for y^+ greater than 11.5. It is assumed that the flow is fully turbulent and that the log-law profile is valid in this range. For y^+ less than 11.5, laminar calculations are used.

The log-law is used to specify the wall shear stress. The wall shear stress is then used as a boundary condition for the momentum equation for the flow parallel to the wall. In addition, the wall shear stress appears as a source term in the turbulent kinetic energy equation. For y^+ greater than 11.5, the wall shear stress is calculated from

$$\tau_w = \kappa c_D^{1/4} \rho u k^{1/2} / \ln\left[E \rho \delta k^{1/2} c_D^{1/4} / \mu_{ref}\right] \tag{2.65}$$

For y^+ less than 11.5, the wall shear stress is calculated from

$$\tau_w = \mu_r \left.\frac{\partial u}{\partial x}\right|_{wall} \tag{2.66}$$

The current approach uses the image node point to specify the wall shear stress implied by either equation (2.65) or (2.66). Assuming that the wall lies at the north face of the control volume, in the formulation of the finite-difference equations for the wall node the north coefficient for the axial momentum equation is

$$c_n = \left.\frac{\mu A}{\Delta x}\right|_n \tag{2.67}$$

The north coefficient represents the shear stress at the wall or

$$\tau_w = \mu \frac{u_N - u_p}{\Delta x} = -\mu \left[\frac{\partial u_p}{\Delta x}\right] \tag{2.68}$$

In the laminar calculations, the u_N value was set to give a zero velocity at the wall, i.e.,

$$u_N = -u_p \tag{2.69}$$

For the turbulent calculations, a velocity is specified at the image node point to give the correct shear stress at the wall. The image node point velocity is then calculated from

$$u_N = u_p + \frac{\tau_w \Delta x}{\mu} \tag{2.70}$$

The wall shear stress in equation (2.70) is calculated from either equation (2.65) or equation (2.66).

The second place that the wall shear stress is employed is in the source term for the turbulent kinetic energy. The source term is

$$S_k = G_k - \rho\varepsilon \tag{2.71}$$

But for the near-wall nodes, following the suggestion of Spalding and Pun [42], the source term is calculated from

$$S_k = \tau_w \frac{\partial u}{\partial y} - \frac{c_D \rho^2 k^2}{\mu_t} \tag{2.72}$$

or

$$S_k = \tau_w \frac{\partial u}{\partial y} - \frac{c_D \rho^2 k^2}{\tau_w} \frac{\partial u}{\partial y} \tag{2.73}$$

The one remaining requirement is the boundary condition for the dissipation rate. In the near-wall region, the length scale for the turbulence is assumed to be proportional to the distance from the wall. This results in a direct relation for the dissipation rate at the node adjacent to the wall, P. The dissipation rate is specified from

$$\varepsilon_p = \frac{c_D^{3/4} k_p^{3/2}}{\kappa\delta} \tag{2.74}$$

Note that the boundary condition for the dissipation rate is not at the wall but at the node adjacent to the wall. The influence of the adjacent values on the ε_p values is eliminated by setting S_p and S_p' to very large positive and very large negative values, respectively.

2.4.7 Solution of the Finite Difference Equations

At this point, a set of algebraic finite difference equations has been obtained, one for each node and for each variable. Each of the equations is of the form

$$a_p\phi_p = a_N\phi_N + a_S\phi_P + a_E\phi_E + a_W\phi_W + S_\phi \tag{2.75}$$

Thus, a set of coupled algebraic equations must be solved simultaneously. This set of equations is strongly nonlinear. The set of equations cannot be solved directly but must be solved by an iterative scheme. Various methods may be used, such as Gauss-Seidel iteration or Gaussian elimination, for example. A direct matrix inversion technique could be used, but this is not practical. The techniques used here have been called by Patankar, et al [5] the line-by-line (LBL) method. One constant coordinate line of the field is solved simultaneously. This technique is very efficient and takes advantage of the predominant flow direction, but at the same time preserves the full elliptic character of the governing flow equations.

As shown in Fig. 2.8, a simultaneous solution of each variable along a constant I-line is considered. It is assumed that all other variables are known and that the values of the variable under consideration, ϕ, are known everywhere except along the I-line. Thus the algebraic finite-difference equation is written as

$$a_P\phi_P = a_N\phi_N + a_S\phi_S + S_\phi' \tag{2.76}$$

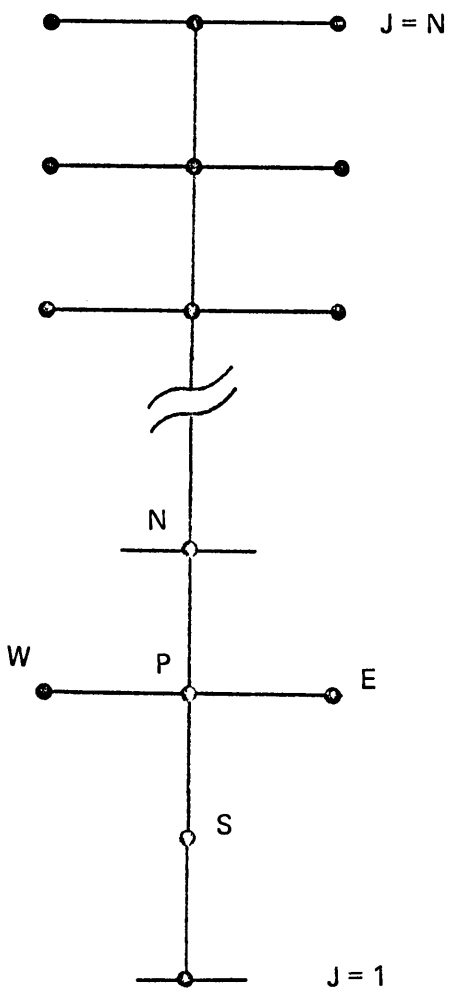

FIGURE 2.8 TRI-DIAGONAL SOLUTION ALGORITHM

where S'_ϕ is assumed to be a known constant for the current iteration. S'_ϕ is

$$S'_\phi = S_\phi + a_W\phi_W + a_E\phi_E \tag{2.77}$$

Note that this set of equations can be written in matrix form as

$$[A][\phi] = [S] \tag{2.78}$$

where the elements of the A matrix are the "a" coefficients appearing in equation (2.64). This is a tri-diagonal matrix and the set of equations can be solved simultaneously using the Thomas algorithm. With the boundary values of ϕ known at the (J=1) and (J=N) boundaries, the equations can be solved by the following scheme. The values of ϕ are computed from

$$\phi_j = G_j + H_j\phi_{j+1};\ j=N-1,\ N-2,\ \ldots,\ 1 \tag{2.79}$$

where for j=2, 3, 4, ..., N

$$G_j = \frac{S_{\phi_j} + a_S G_{j-1}}{a_p - a_S H_{J-1}} \tag{2.80}$$

$$H_j = \frac{a_N}{a_p - a_S H_{j-1}} \tag{2.81}$$

Thus the set of equations can be solved simultaneously by sweeping from 2 to N to calculate the G_j and H_j values and then sweeping from N to 2 to calculate the ϕ_j values. The boundary conditions at 1 and N are deduced from

$$\phi_1 = G_1 + H_1\phi_2 \tag{2.82}$$

Since ϕ_1 is known, the boundary condition is prescribed by setting

$$G_1 = \phi_1, \; H_1 = 0 \tag{2.83}$$

At the outer edge ϕ_N is known from a given boundary condition. This may be either a prescribed value or a prescribed gradient type of boundary condition.

2.5 Pressure Solution Procedure

As outlined earlier, the key feature of the pressure solution is the calculation of a pressure correction such that the continuity equation is satisfied. As shown earlier, it is not possible to express a strong relation between the velocity correction at the node itself and the pressure correction at the node itself if the same spacial location is shared. The required relation is of the form

$$u'_p = f(P'_p) \tag{2.84}$$

It will be shown, however, that this is not necessary. The approach that is utilized here is straightforward and does not depend on the use of a staggered grid system.

The continuity equation is applied to the same control volume as all other variables as illustrated in Fig. 2.9. Integrating this equation over the control volume results in the following relation which expresses the conservation of mass for the control volume.

$$\dot{m}_e - \dot{m}_w + \dot{m}_n - \dot{m}_s = 0 \tag{2.85}$$

This equation would be identically zero if the true solution that satis-

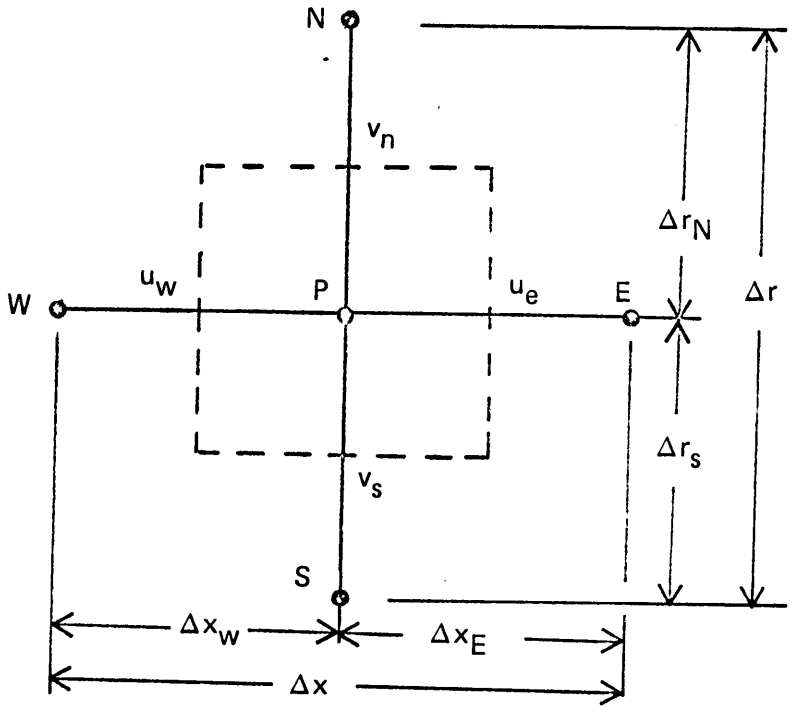

FIGURE 2.9 PRESSURE SOLUTION CONTROL VOLUME

fied both the momentum and continuity equations were available, but recall that in terms of the trial velocity field the continuity equation yields

$$\rho_e A_e u^*_e - \rho_w A_w u^*_w + \rho_n A_n v^*_n - \rho_s A_s v^*_s = D \qquad (2.86)$$

The trial velocity field does not satisfy continuity but has a non-zero residual, D. The key feature of the derivation of the pressure correction equation is that the velocity corrections at the control volume faces, not the node points, are expressed as functions of the pressure correction gradients.

In terms of the individual field variables, the continuity equation is, in terms of the true velocity,

$$\rho_e A_e u_e - \rho_w A_w u_w + \rho_n A_n v_n - \rho_s A_s v_n = 0 \qquad (2.87)$$

or in terms of the trial and correction velocities,

$$c_e(u^*_e+u'_e) - c_w(u^*_w+u'_w) + c_n(v^*_n+v'_n) - c_s(v^*_s+v'_s) = 0 \qquad (2.88)$$

where

$$c_e = \rho_e A_e \qquad (2.89)$$

$$c_n = \rho_n A_n \qquad (2.90)$$

$$c_s = \rho_s A_s \qquad (2.91)$$

$$c_w = \rho_w A_w \qquad (2.92)$$

Identical relations are used for the velocity corrections. Separating the trial and correction velocities gives

$$c_e u'_e - c_w u'_w + c_n v'_n - c_s v'_s = -D \tag{2.93}$$

where

$$D = c_e u^*_e - c_w u^*_w + c_n v^*_n - c_s v^*_s \tag{2.94}$$

Notice that if the trial velocity distribution satisfies continuity the source term or residual, D, will be zero. The key feature of this current approach is that it is assumed that the face or edge velocity and pressure corrections are related by

$$u'_e = D^e_u(P'_p - P'_E) \tag{2.95}$$

$$u'_w = D^w_u(P'_w - P'_p) \tag{2.96}$$

$$v'_n = D^n_v(P'_p - P'_N) \tag{2.97}$$

$$v'_s = D^s_v(P'_S - P'_p) \tag{2.98}$$

Substituting these relations into the continuity equation gives the required finite difference equation for the pressure corrections

$$c_e D^e_u(P'_p - P'_E) - c_w D^w_u(P'_w - P'_p) + c_n D^n_v(P'_p - P'_N) - c_s D^s_v(P'_S - P'_p) = -D \tag{2.99}$$

or

$$a_p P'_p = a_E P'_E + a_w P'_w + a_N P'_N + a_s P'_s - D \tag{2.100}$$

where

$$a_w = c_w D^w_u \tag{2.101}$$

$$a_E = c_E D^e_u \tag{2.102}$$

$$a_N = c_N D^n_v \tag{2.103}$$

$$a_S = c_S D_v^s \tag{2.104}$$

$$a_P = a_E + a_w + a_N + a_S \tag{2.105}$$

Notice that a finite difference equation has been derived which satisfies all the stability criteria also. The final requirement is the functions relating the pressure and velocity corrections, i.e.,

$$D_v^n,\ D_v^s,\ D_u^e,\ D_u^w \tag{2.106}$$

These relations may be easily derived by direct substitution into the axial and radial momentum equations. For example, consider the finite difference for the axial velocity

$$c_p u_p = \Sigma c_i u_i + S_u \tag{2.107}$$

Once the pressure field is corrected,

$$u_p' = u_p - u_p^* \tag{2.108}$$

Referring to Figure 2.9, assuming that the pressure correction varies linearly, a straightforward calculation gives

$$D_u^e = \tfrac{1}{4} \left.\frac{A_x}{c_p}\right|_E \frac{\Delta X_{EW}}{\Delta X_e} + \frac{A_x}{c_p}\bigg|_p \frac{\Delta X_{EW}}{\Delta X_p} \tag{2.109}$$

and similarly for the other faces of the control volume

$$D_u^w = \tfrac{1}{4} \left.\frac{A_x}{c_p}\right|_W \frac{\Delta X_{EW}}{\Delta X_w} + \left.\frac{A_x}{c_p}\right|_p \frac{\Delta X_{EW}}{\Delta X_p} \tag{2.110}$$

$$D_v^n = \tfrac{1}{4} \left.\frac{A_r}{c_p}\right|_N \frac{\Delta r_{NN}}{\Delta r_n} + \left.\frac{A_r}{c_p}\right|_p \frac{\Delta r_{NS}}{\Delta r_n} \tag{2.111}$$

$$D_v^s = \tfrac{1}{4}\left[\frac{Ar}{cp}_p \frac{r_{NS}}{r_s} + \frac{Ar}{cp}_S \frac{r_{SS}}{r_s}\right] \qquad (2.112)$$

2.5.1 Axial Pressure Correction

The preceding discussion centered on the local pressure correction at each control volume such that the continuity equation is satisfied over each control volume. In addition to this correction, a procedure is included to insure that at each axial location, the total axial flow rate is equal to the given inlet flow rate, $\dot{m}_{in}$.

At each axial location, the total axial flow rate is calculated from

$$\dot{m}_i^* = \sum_{\text{all } j} \rho_j A_j u_j \qquad (2.113)$$

The required flow rate correction is given by

$$\dot{m}_i' = \dot{m}_{in} - \dot{m}_i^* \qquad (2.114)$$

The axial mass flow rate is then corrected by applying a uniform velocity correction to all of the axial velocities at the axial location. The velocity correction is given by

$$\bar{u}' = \frac{\dot{m}_i'}{\sum_{\text{all } j} \rho_j A_j} \qquad (2.115)$$

To insure that the momentum equation remains satisfied, a simultaneous average axial pressure correction is also calculated. The pressure east of the axial velocity location is corrected to satisfy the momentum equation. Following the procedure outlined previously, the velocity and pressure corrections are related by

$$u'_j = D^u_j P'_E \tag{2.116}$$

Then, for all of the nodes at the axial location, define

$$D_T = \sum_{\text{all } j} \rho_j A_j D^u_j \tag{2.117}$$

The average pressure correction is given by

$$\overline{P}'_E = \frac{\dot{m}'_i}{D_T} \tag{2.118}$$

2.6 Sample Program

To illustrate the basic aspects of the solution process, a very simple problem for which an analytic solution is available was chosen. The problem is simply the developing laminar flow in a planar duct as shown in Fig. 2.10. The problem has a number of simplifying assumptions which are not required in the general solution procedure but have been made to illustrate the solution algorithm with as much of the complexity removed as possible. The following assumptions are made in this case:

- laminar flow
- isothermal
- incompressible
- uniform grid
- steady state
- two-dimensional

It should be emphasized that the current algorithm is not restricted to requiring these simplifications. In fact, the general algorithm can handle in the current form, or with some extensions:

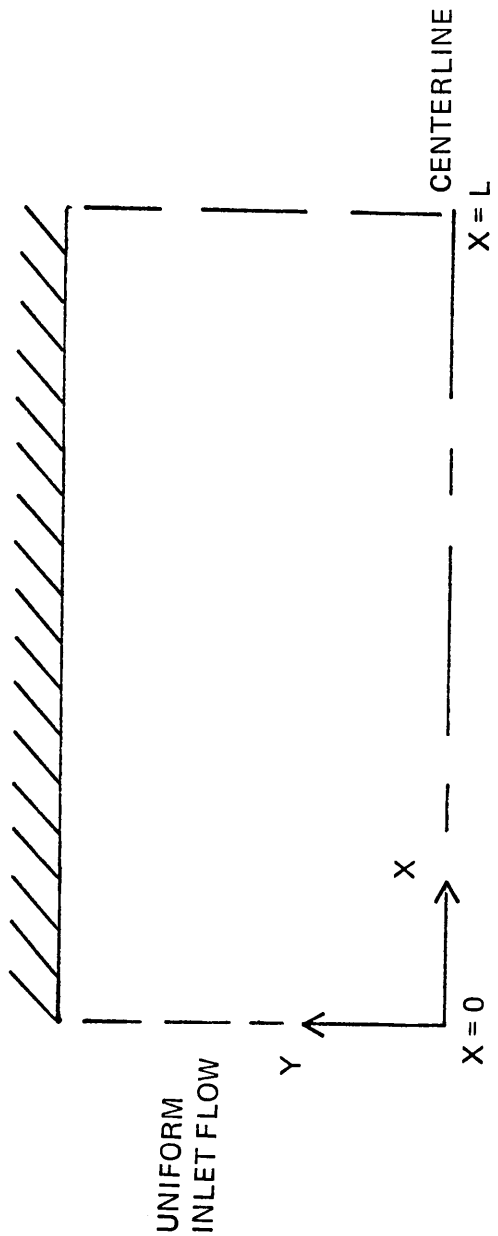

FIGURE 2.10 DUCT ENTRANCE PROBLEM

- turbulent flow
- reacting flow
- heat transfer
- arbitrary grid spacing
- compressible
- three-dimensional
- transient
- parabolic or elliptic

The basic program shown in Appendix A includes all of the essential features of the more general code. The sample program is set up for flow at a Reynolds number of 150 for comparison with known solutions.

3.0 EXPERIMENTAL APPARATUS

The experimental apparatus consisted essentially of a complete system for the combustion of a gaseous fuel under controlled input conditions using a laboratory scale swirl burner. In addition, instrumentation for the measurement of the detailed three-dimensional distributions of velocity was also provided. In the following sections, a brief description of this equipment is given. A more detailed description of the apparatus, along with a discussion of the actual design process for this equipment, may be found in reference 20. The following discussion is in three sections covering the swirl burner itself, the overall combustion system and, finally, the instrumentation system.

3.1 Swirl Burner

The burner that was used is illustrated in Fig. 3.1 along with the associated windbox assembly. The dimensions for the assembly are given in Table VI. The burner is a relatively small laboratory scale unit which features a very convenient means of varying the amount of swirl that is produced. As shown in Fig. 3.2, the variable swirl is achieved by using pairs of fixed and movable swirl generator blocks. This design was adapted from a design originally published by the International Flame Research Foundation [24]. This design allows for a very easy adjustment of the amount of swirl produced while at the same time producing a relatively small pressure drop through the burner. As shown in Fig. 3.2, the blocks are mounted on a backing plate in eight pairs. The inlet air can have either a radial or tangential direction depending on the position of the movable blocks. Rotation of the blocks by rotating the backing

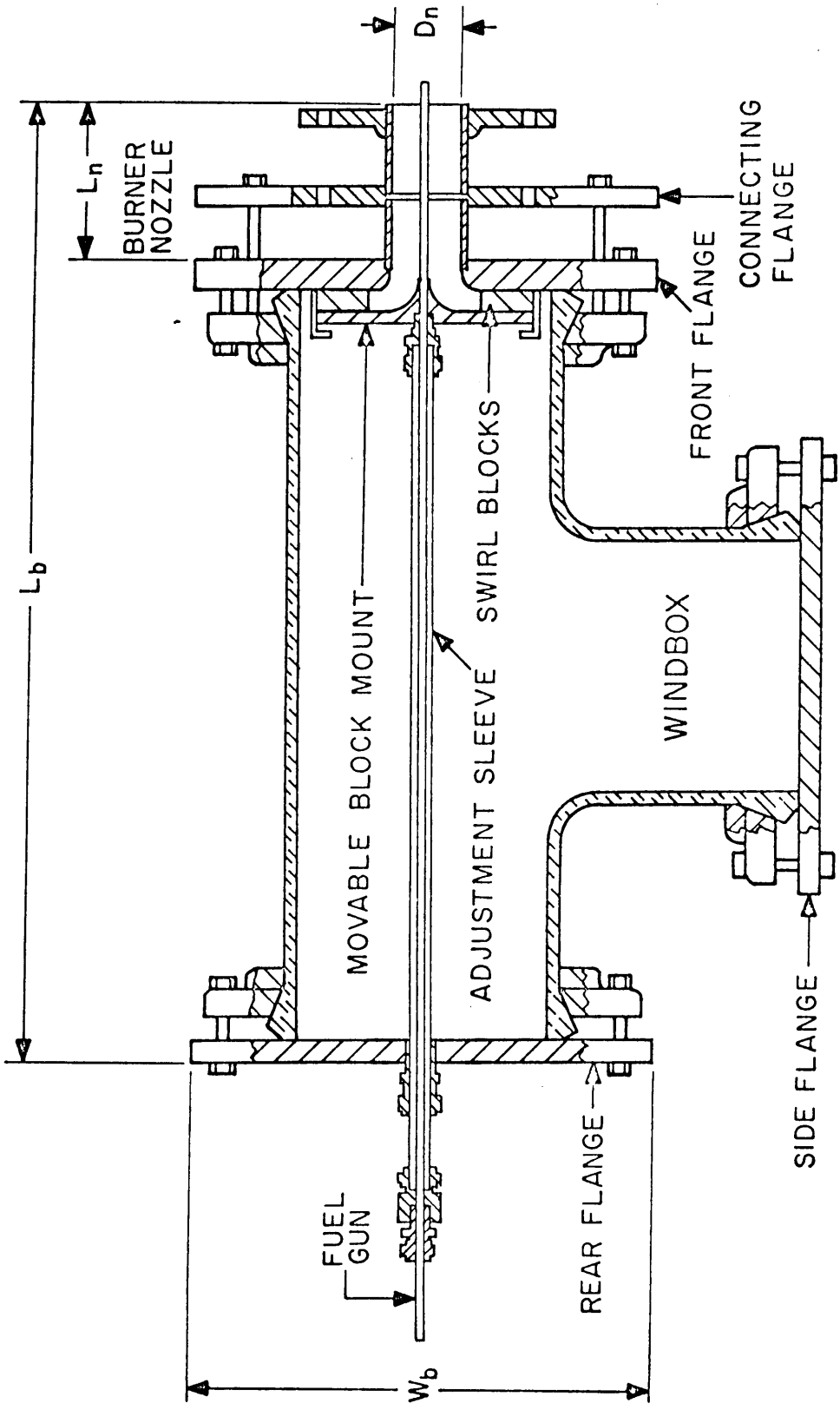

FIGURE 3.1 BURNER AND WINDBOX ASSEMBLY

Table VI

Dimensions of The Burner/Windbox Assembly

Description	Specification mm	(in.)
Overall		
Length, L_b	572	(22.5)
Width, W_b	279	(11.0)
Burner Nozzle		
Length, L_n	82.6	(3.25)
O.D.	48.3	(1.90)
I.D., D_n	45.0	(1.77)
Fuel Gun		
O.D., D_g	9.53	(0.375)
I.D.	7.75	(0.305)
Adjustment Sleeve		
O.D.	12.7	(0.500)
I.D.	10.6	(0.416)
Windbox (Tee)		
O.D.	169	(6.66)
I.D.	152	(6.00)

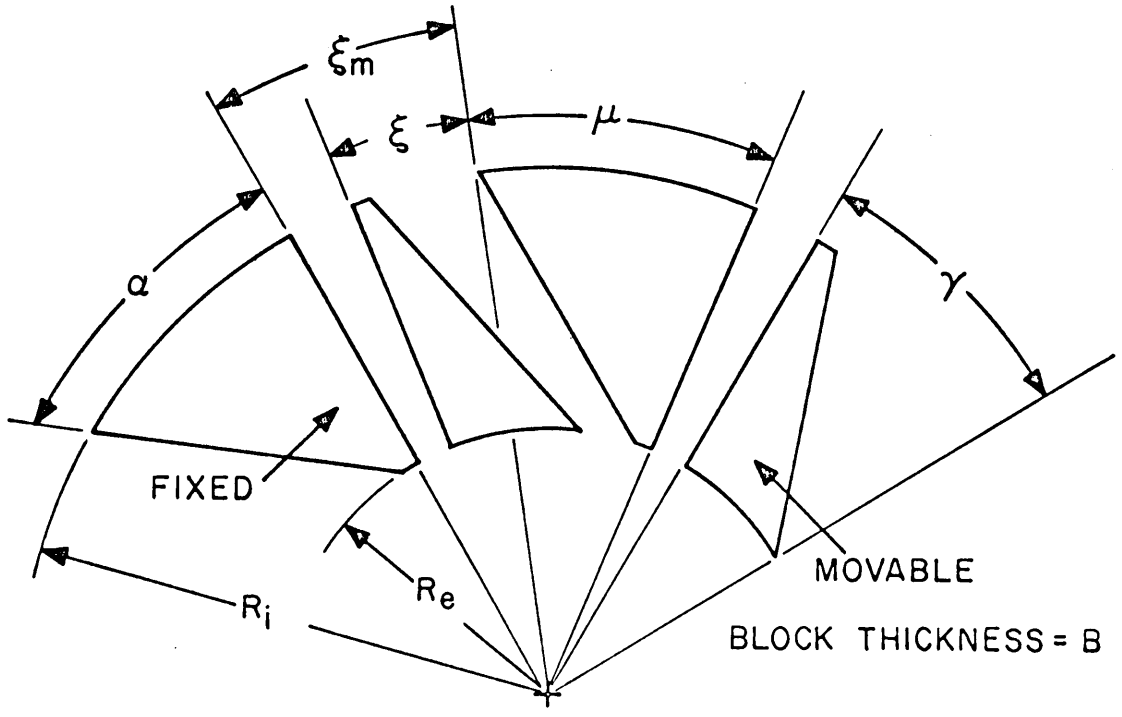

a. SWIRL BLOCK DIMENSIONS

b. AXIAL AIR ENTRY

c. TANGENTIAL AIR ENTRY

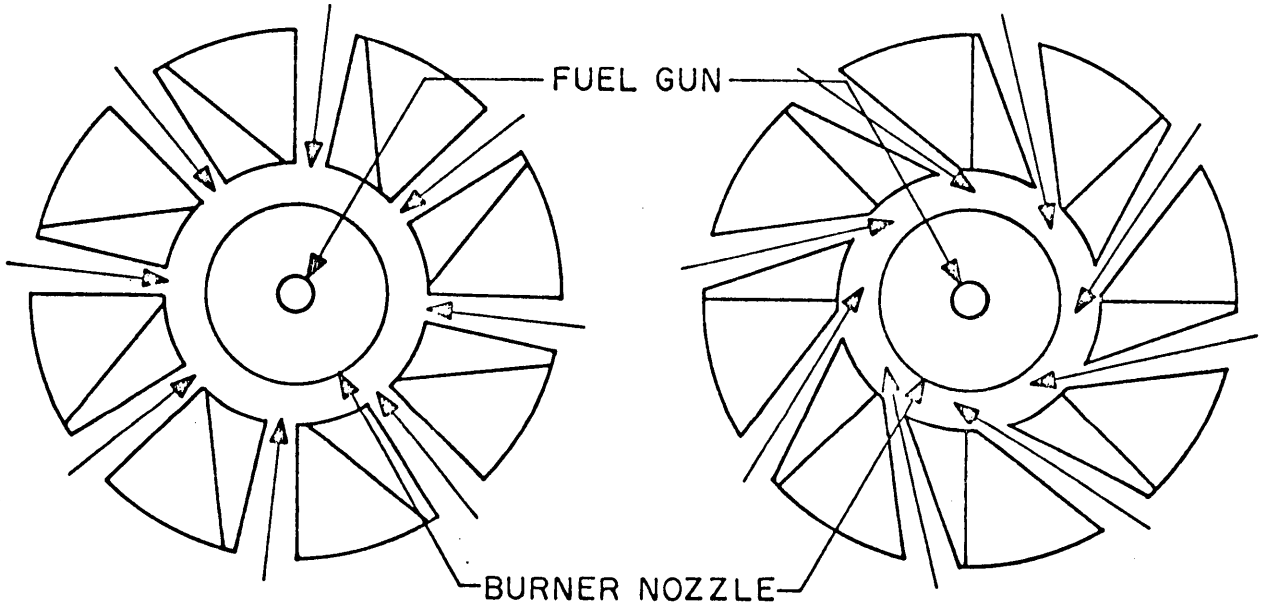

FIGURE 3.2 SWIRL BLOCKS

plate changes the angle, ξ, from zero to the maximum value shown in Fig. 3.2. In the actual design, the maximum angle is 12 degrees. A relationship for the theoretical swirl number that is produced by this arrangement was derived by Grant [20]. In the derivation, a very simple fluid flow model was assumed. The flow through the blocks was taken to be inviscid and one-dimensional. The resulting Swirl number that is produced is given by

$$S = 1.63 \left[1 - \frac{D_f^2}{D_n^2} \right] \frac{\xi/\xi_m}{(1-0.357\xi/\xi_m)^2} \beta \qquad (3.1)$$

where β, the fuel swirl factor, is defined as

$$\beta = \frac{1}{1 + \frac{1}{SG_{f\,m}^2} \left[\frac{D_n^2}{D_f^2} - 1 \right]} \qquad (3.2)$$

Utilizing this relation, the range of swirl numbers that may be produced with this burner is shown in Figures 3.3 and 3.4. The swirl number is a function of the fuel that is in use and the results shown are for the low HV fuel. As shown in Fig. 3.3, the diametral ratio also has a significant effect on the maximum swirl number that may be produced. In view of this fact, the burner design was modified to allow the diametral ratio to be changed easily as per the recommendation of Grant [20]. This design feature is illustrated in Fig. 3.5. For the results of the present investigation, the fuel used was the low HV gas and an optimum diametral ratio was found using a relation derived by Grant [20]. This optimum value is the diametral ratio producing the maximum swirl for a given

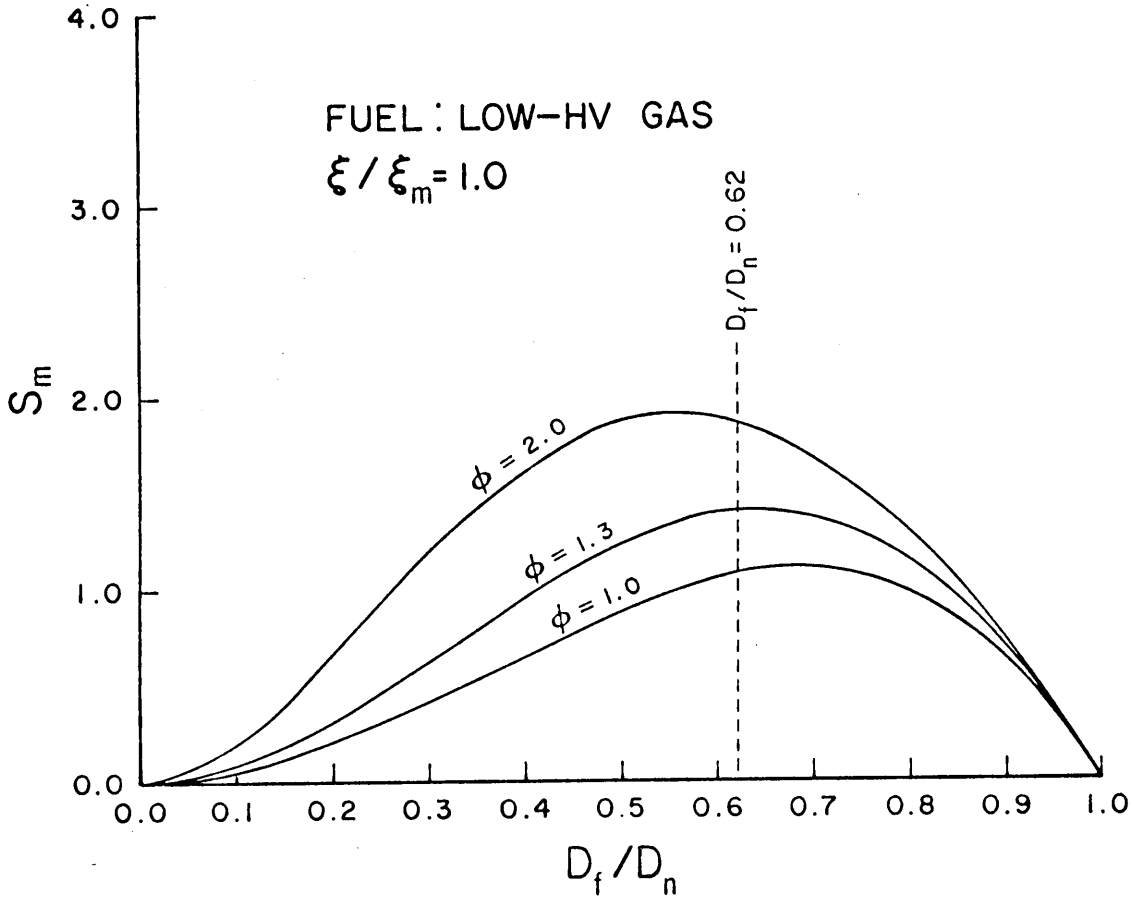

FIGURE 3.3 RANGE OF SWIRL NUMBER

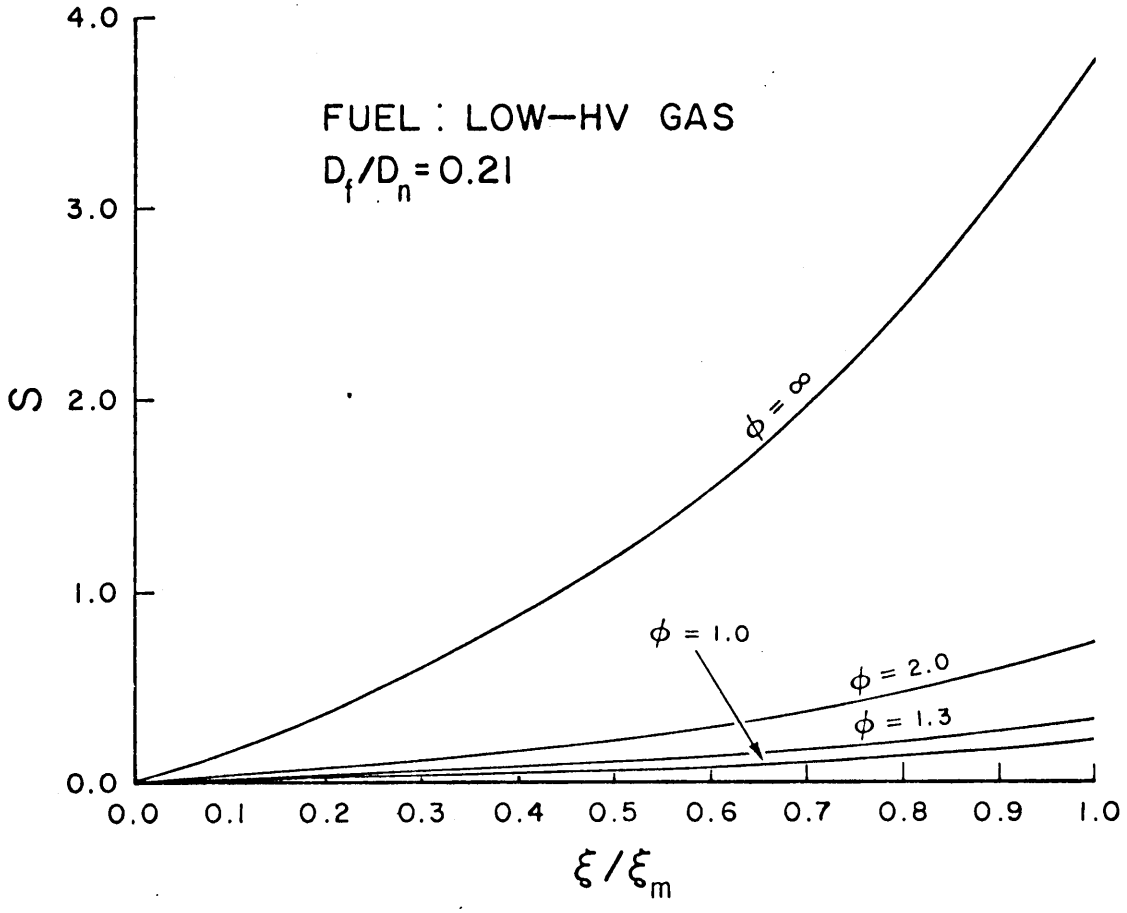

FIGURE 3.4 OPERATING SWIRL NUMBER RANGE

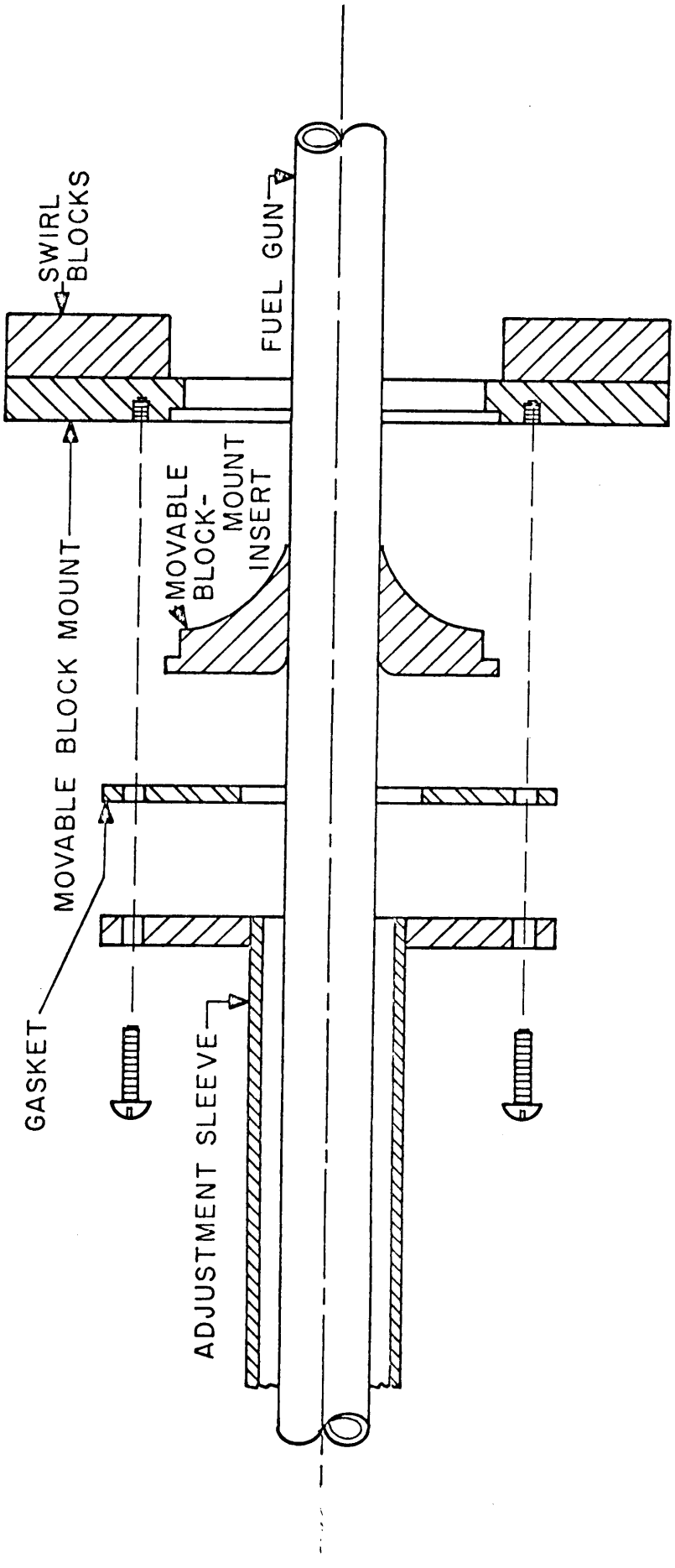

FIGURE 3.5 FUEL NOZZLE

block setting. Based on Grant's relation, a diametral ration of 0.62 was selected for the burner in the current work.

3.2 Combustion System

The combustion system consists of the swirl burner, the combustion chamber to which the swirl burner is mounted, and the associated piping and instrumentation for providing a measured flow of fuel and oxidant (air) to the system. The overall combustion system is illustrated pictorially in Fig. 3.6. A block diagram of the system showing the associated flow control and measurement system for the fuel and oxidant is shown in Fig. 3.7. The dimensions for the system are shown in Table VII.

As shown in Fig. 3.6, a traversing mechanism is mounted on top of the combustion chamber. This traversing system allows for the precise location of either a velocity or temperature probe within the combustion chamber. The top of the chamber has a section removed to facilitate the positioning of the velocity probe. This section is then covered by the moving plate shown in Fig. 3.6.

3.3 Instrumentation

The velocity profiles are measured using a five-hole pivot probe. The probe is a United Sensor type DC three-dimensional pressure probe. The measurement of the three velocity components and the local static pressure requires the determination of five pressure differences with the probe. The five pressure taps on the probe are connected to a Celesco variable-reluctance pressure transducer by a manifold arrangement. This arrangement allows the reading of the desired pressure by the single pressure transducer. The desired tap is selected by positioning a toggle

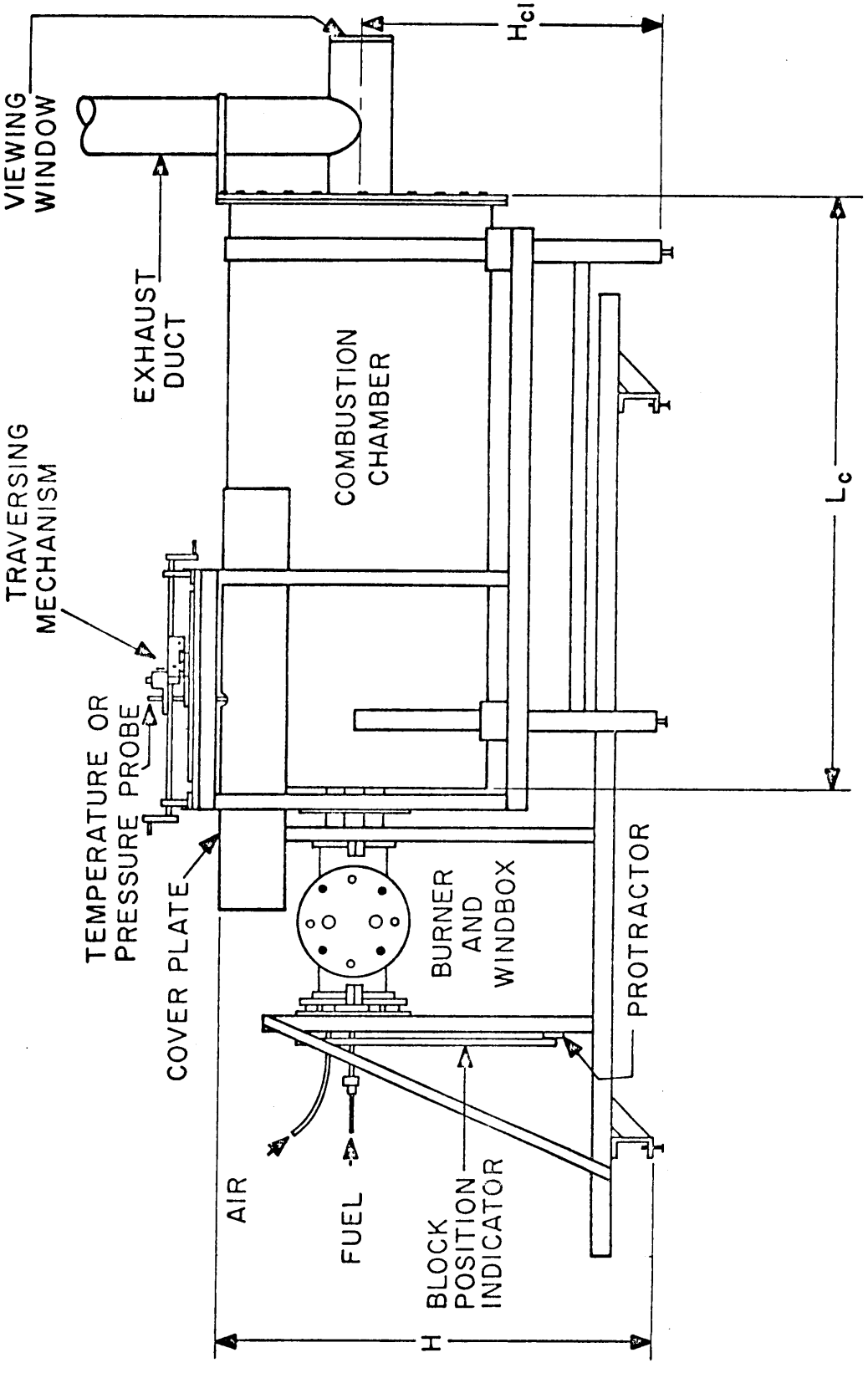

FIGURE 3.6 OVERALL COMBUSTION SYSTEM

Table VII

Dimensions of The Burner System

Description	Specification	
	m	(in.)
Overall		
Height, H	1.08	(46.5)
Length, L	2.87	(113)
Centerline Height, $H_{c\ell}$	0.84	(33)
Combustion Chamber		
Length, L_c	1.46	(57.5)
O.D.	0.67	(26.5)
I.D.	0.66	(26.0)

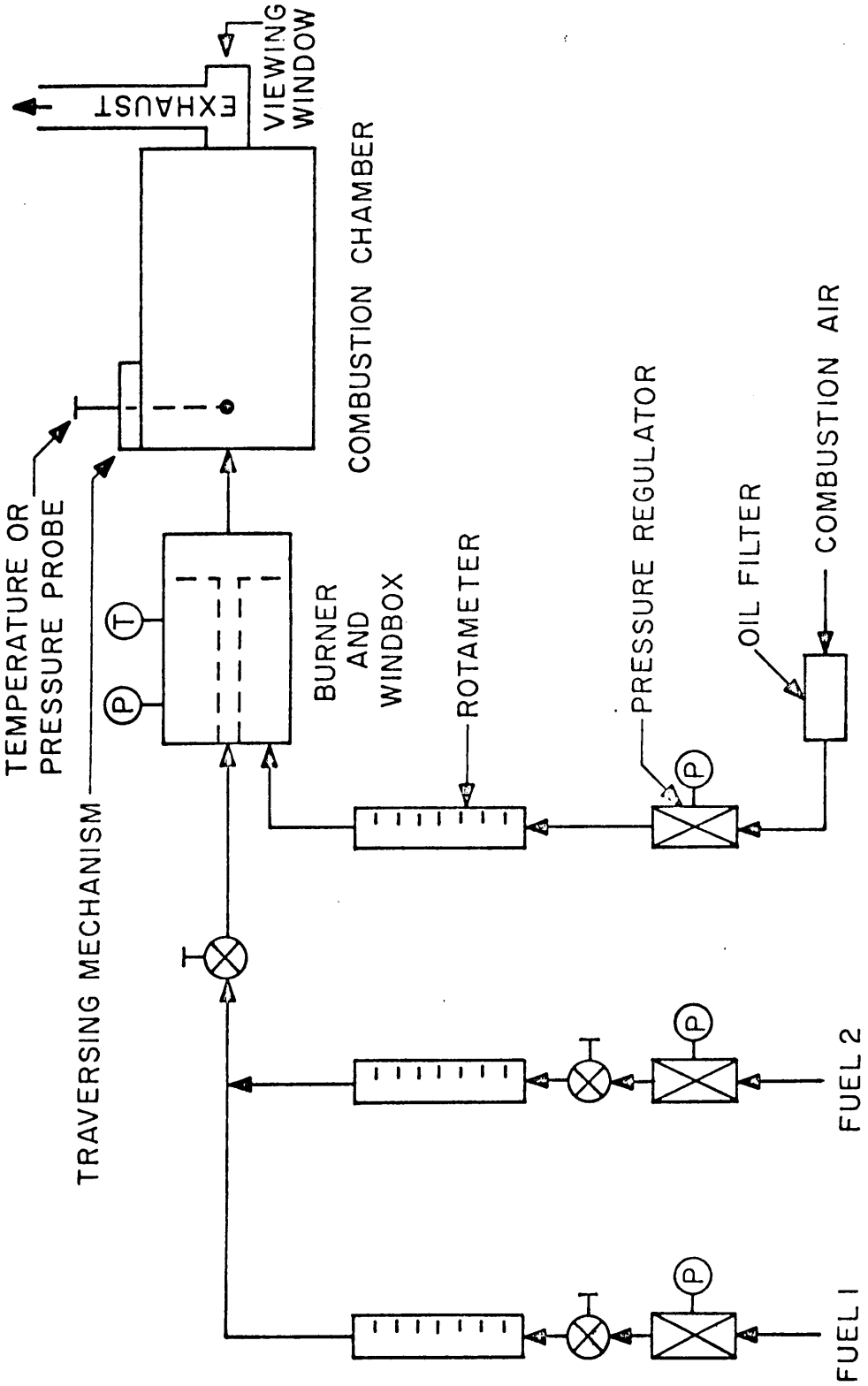

FIGURE 3.7 FLOW SYSTEM

valve. Calibration charts for the particular probe were supplied with the probe.

4. RESULTS

In this chapter, results are presented from calculations made using the sample program and the PRIMCO code. The results are separated into three general areas: one, the sample program results; two, test cases for PRIMCO; and three, comparisons of PRIMCO predictions and isothermal measurements from the experimental swirl burner.

4.1 Sample Program

The results from a typical run of the sample program for the calculation of the duct entrance problem are presented in Chapter 3 and are illustrated in Figure 4.1. This figure shows the centerline velocity in the duct as the flow develops. As shown in the figure, these calculations agree well with the analytic calculations of Schlichting [40] and the numerical predictions of Gosman, et al [5]. In addition, the fully developed velocity profile agrees with the known parabolic profile as shown in Fig. 4.2. This example problem requires approximately 50 iterations to obtain the accuracy shown in the figure. Note in particular that the form of the exit velocity profile is not assumed. The exit plane boundary conditions are simply the zero flow-direction gradients and the continuative outflow conditions as discussed in Chapter Two. A printout showing the predicted values is given in the appendix. Of particular interest in this printout is the static pressure distribution since, although the developing velocity profile is relatively familiar, more conventional calculation methods do not include the pressure as one of the dependent variables and its distribution is not usually presented. As shown, the pressure shows a significant axial gradient

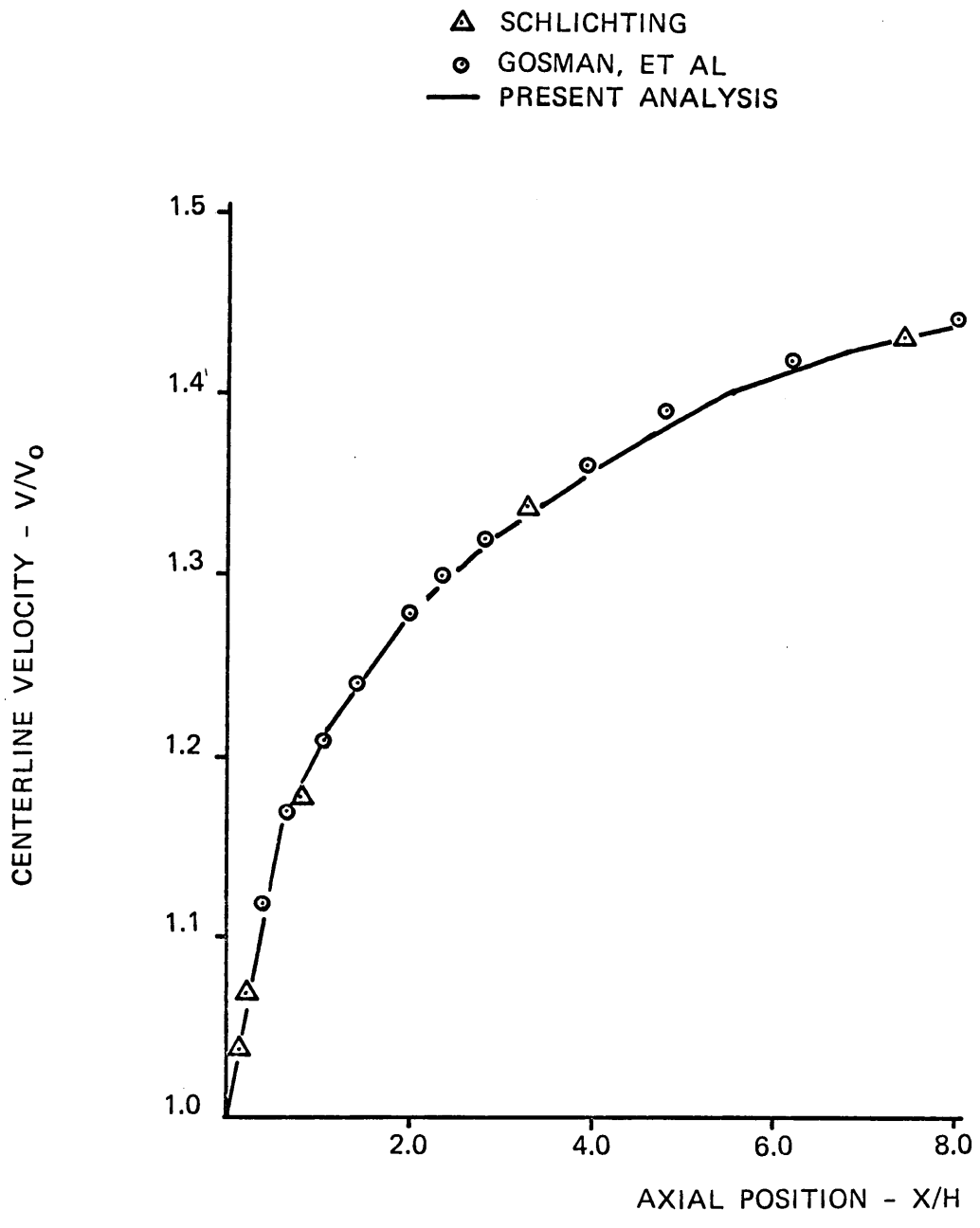

FIGURE 4.1 LAMINAR DUCT DEVELOPING VELOCITY

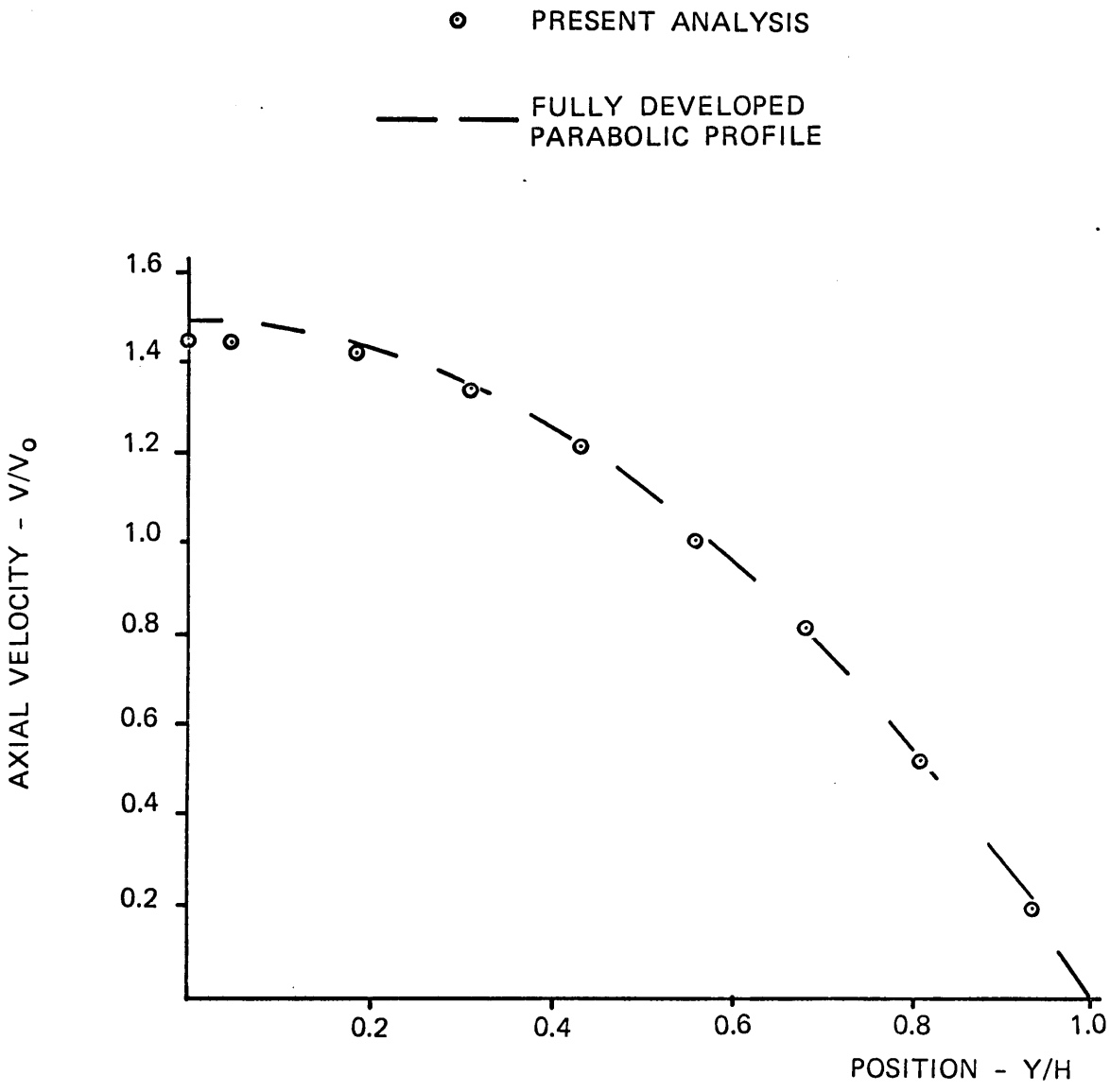

FIGURE 4.2 LAMINAR DUCT VELOCITY PROFILE

and a small radial gradient. The radial gradient also coincides with the small negative radial velocity distribution as the flow redistributes towards the centerline of the duct. These initial results illustrate clearly some of the relative merits of a primitive variables solution. The actual results of the calculations clearly exhibit the physical phenomenon that is familiar.

4.2 PRIMCO Test Cases

Several test cases were run for relatively simple problems to debug the PRIMCO code and to verify the results. The results for these test cases were then compared to results of computations published by Spalding and Pun [41] and to a known analytic solution in one case. The results published by Spalding and Pun were obtained from a code using a staggered grid and thus furnish some comparison of the staggered and non-staggered techniques. Two test cases were run for these comparisons.

4.2.1 Laminar Pipe Flow

The first test case is for the developing laminar flow in the entrance region of a pipe. This case provides two checks for the code. First, since the fully developed velocity profile is well established for the geometry, this provides a known solution to verify the code. The second check is to compare the detailed predictions for the distributions of the velocities and pressure in the developing region of the flow with the results of Spalding and Pun.

The laminar pipe flow test case was set up to duplicate the case presented by Spalding and Pun as closely as possible. The grid system

used in both cases had 10 axial and 10 radial nodes. The node points in the PRIMCO calculations coincided with the "main" node points in the staggered grid used by Spalding and Pun. An inlet Reynolds number based on the pipe radius of 100 was used in both cases.

The predicted axial velocity at the centerline of the pipe is shown in Fig. 4.3. As shown in the figure, the PRIMCO predictions agree well with those of Spalding and Pun. The predicted static pressure at the centerline is shown in Fig. 4.4. The predictions again agree well with those of Spalding and Pun. As noted, Fig. 4.4 shows only the centerline pressure; however, the radial pressure gradient predicted by both codes was extremely small. In addition, the radial velocities predicted by both codes was extremely small. The radial velocity at all points within the flow field was negative, as expected. The predicted axial velocity profile at a well-developed axial point is shown in Fig. 4.5. The PRIMCO results and those of Spalding and Pun showed no discernible difference in this case and only the PRIMCO results are shown on this plot.

Several features of these comparisons are a result of the difference between a staggered and a non-staggered grid system. As shown in Fig. 4.3, the axial velocity values from the PRIMCO results are at the main node points which coincide with the main node points in the Spalding and Pun analysis. Note, however, that the axial velocity values from the Spalding and Pun results are on the staggered locations between main node points. Also, as shown in Fig. 4.4, the static pressure values at the inlet area are somewhat different. The staggered approach implicitly assumes that the axial pressure gradient is zero at the inlet plane and

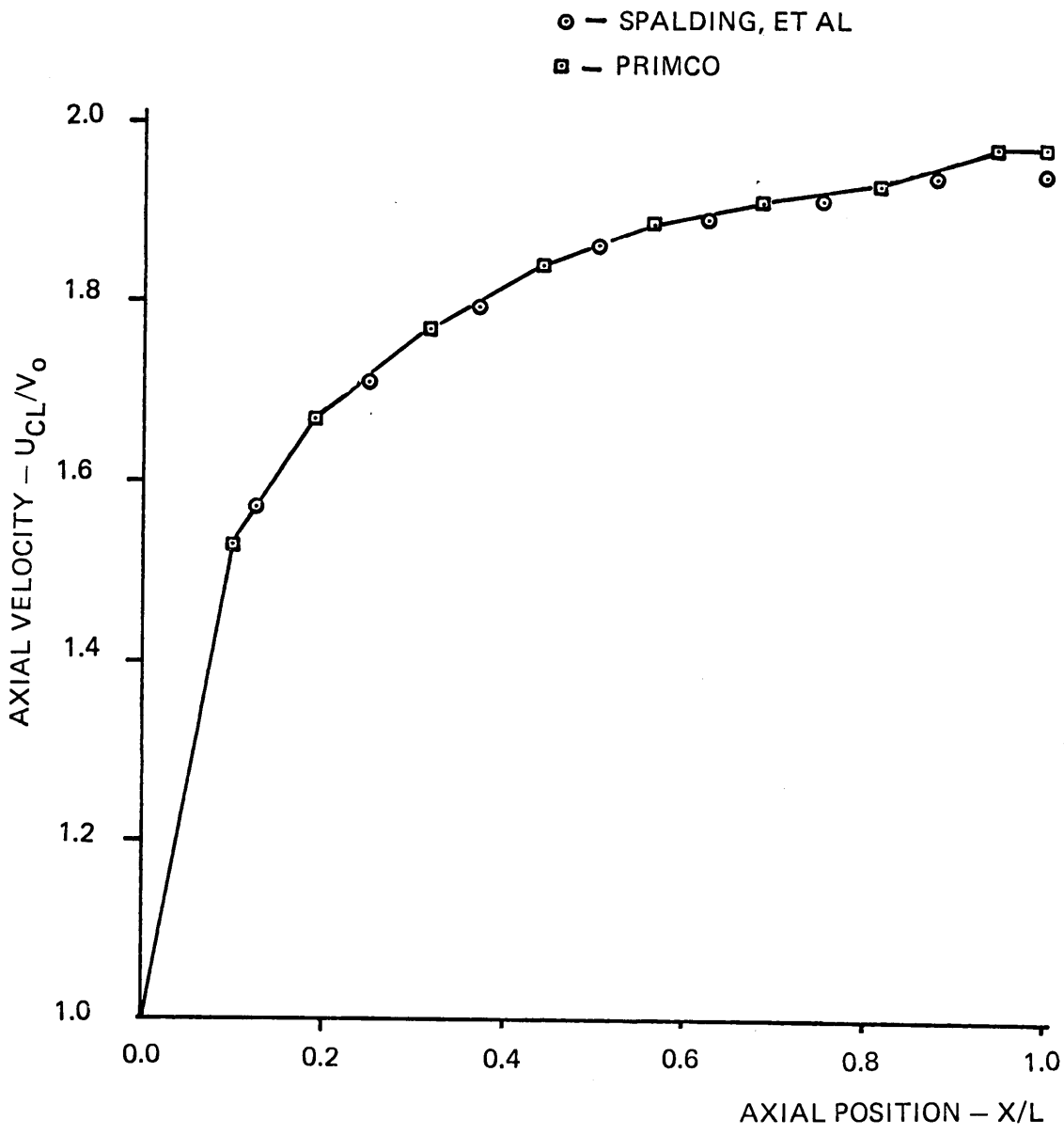

FIGURE 4.3 CENTERLINE AXIAL VELOCITY DISTRIBUTION

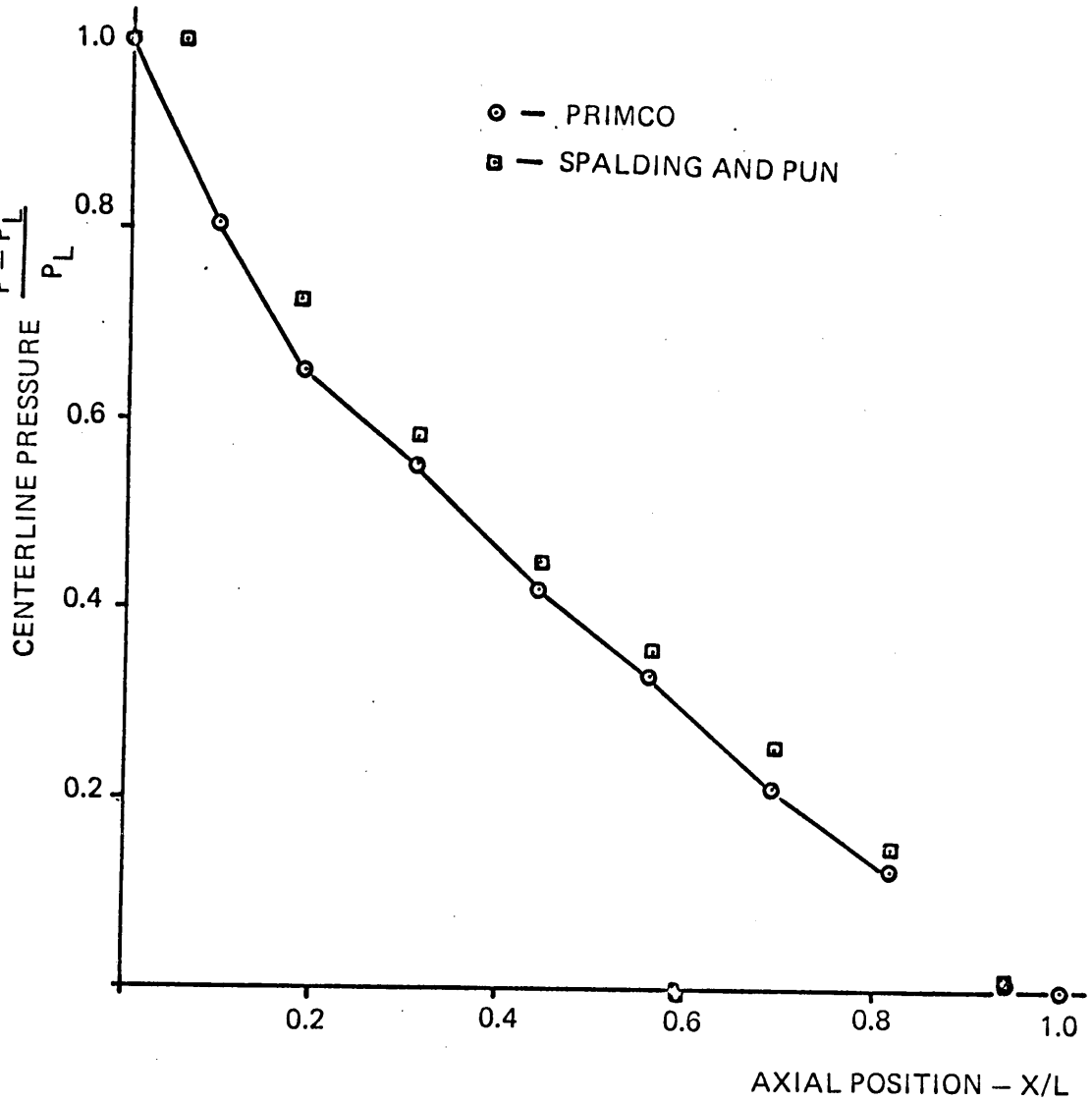

FIGURE 4.4 LAMINAR PIPE FLOW PRESSURE DISTRIBUTION

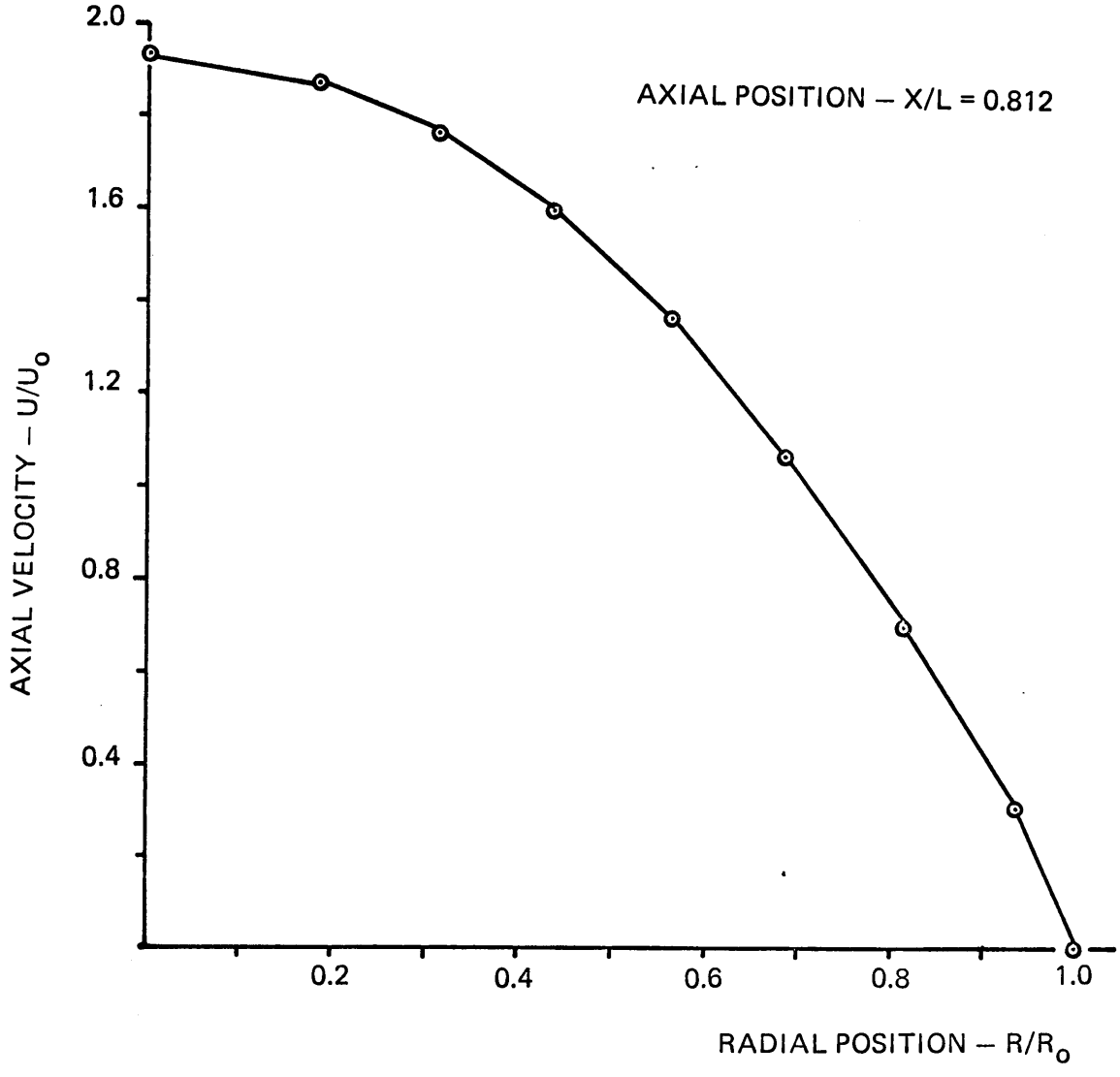

FIGURE 4.5 AXIAL VELOCITY PROFILE

the pressure at the inlet node is not presented. This is the reason for the difference in the results at the inlet plane area.

One interesting result is shown by both sets of predictions: There is a slight increase in the axial velocity at the exit plane. The effect is more significant in the PRIMCO results. This increase, as shown in Fig. 4.3, does not seem to follow the trend of the developing velocity profile. This departure from the developing flow pattern can be attributed to the application of the exit plane boundary condition. The influence of the exit plane boundary condition appears to be minimal at the upstream locations, however.

The computations shown for this case required approximately 40 iterations to provide adequate accuracy. The convergence rate is illustrated in Fig. 4.6. The parameter used to monitor the convergence is the sum of the absolute value of the continuity equation residual at all nodes. This quantity is normalized using the total mass flow rate. The normalized residual sum is calculated from the following relations.

$$R = \sum_{\text{all } i} \sum_{\text{all } j} \left| R_{ij} \right| \tag{4.1}$$

$$\tilde{R} = \frac{R}{\dot{m}_{in}} \tag{4.2}$$

Where R_{ij} is the continuity equation residual at the (i,j) cell.

4.2.2 Turbulent Pipe Flow

The second test case compared to results published by Spalding and Pun was for turbulent pipe flow. In this case the geometry is essentially

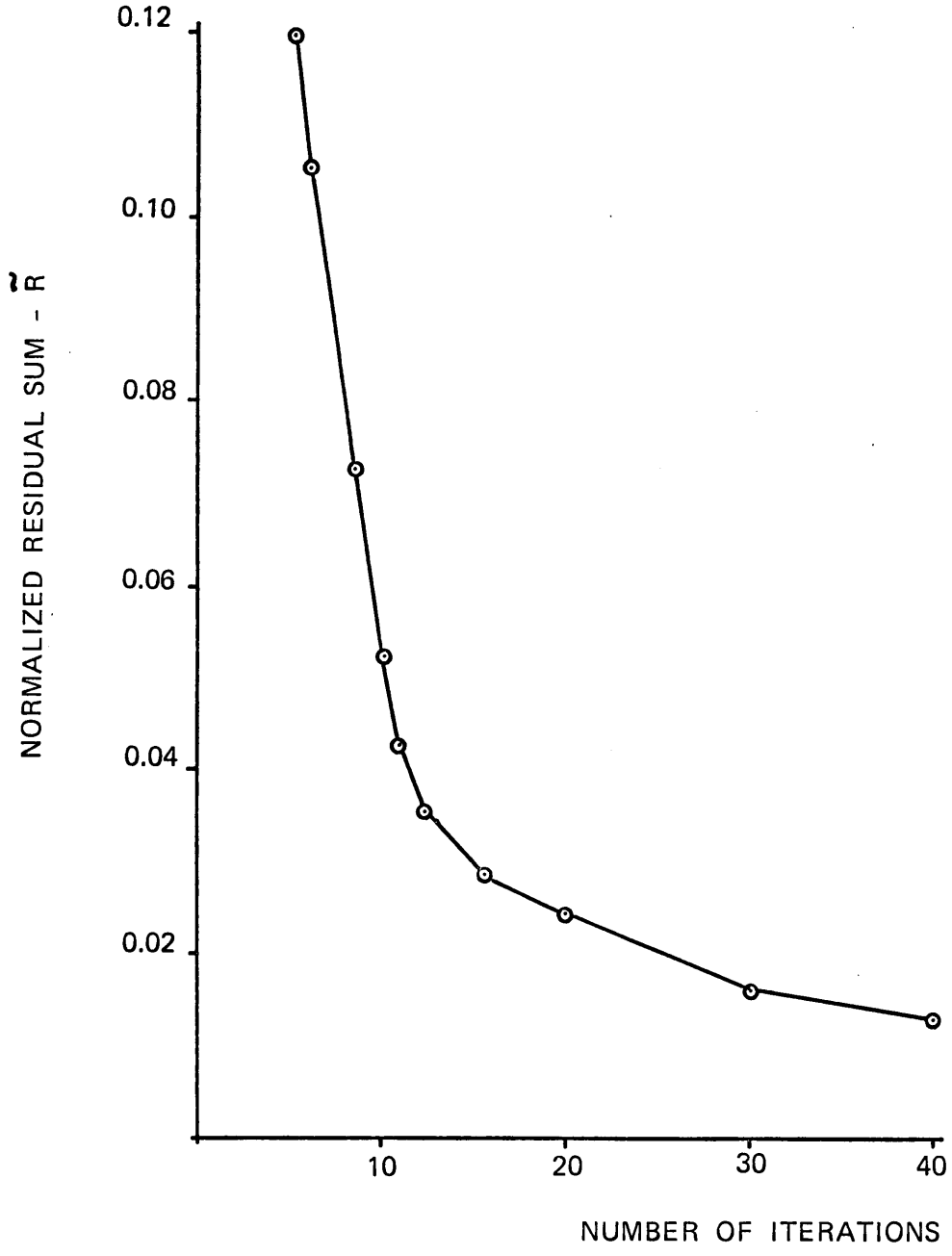

FIGURE 4.6 CONVERGENCE RATE

identical to the laminar pipe flow case. The pipe radius is the same and the radial grid spacing is the same. The only difference in the two grid systems is the axial spacing. A longer grid system was used for the turbulent case. As in the previous case, the main node points in the PRIMCO calculations coincide with the main node points in the Spalding-Pun analysis.

The two-equation turbulence model was employed in this case and wall-flux boundary conditions were also employed for this case. The inlet turbulence level is assumed to obey the following relation

$$k = 0.005\rho u_m^2 \tag{4.3}$$

The inlet dissipation rate was also assumed to be a constant value given by

$$\varepsilon = c_D k^{3/2}/(0.03R_o) \tag{4.4}$$

As in the laminar pipe flow case, the computed results were in close agreement with those published by Spalding and Pun. A comparison of the centerline axial velocity is shown in Fig. 4.7. In addition, a plot of the axial velocity distribution at a single axial station is shown in Fig. 4.8. In both cases, the results are in close agreement. Figure 4.9 shows the axial pressure distribution and as with the velocity predictions the two calculations agree.

Of particular interest in this case are the turbulence variables, the kinetic energy and the dissipation rate. A plot of the radial distribution of the turbulence kinetic energy at several axial stations is

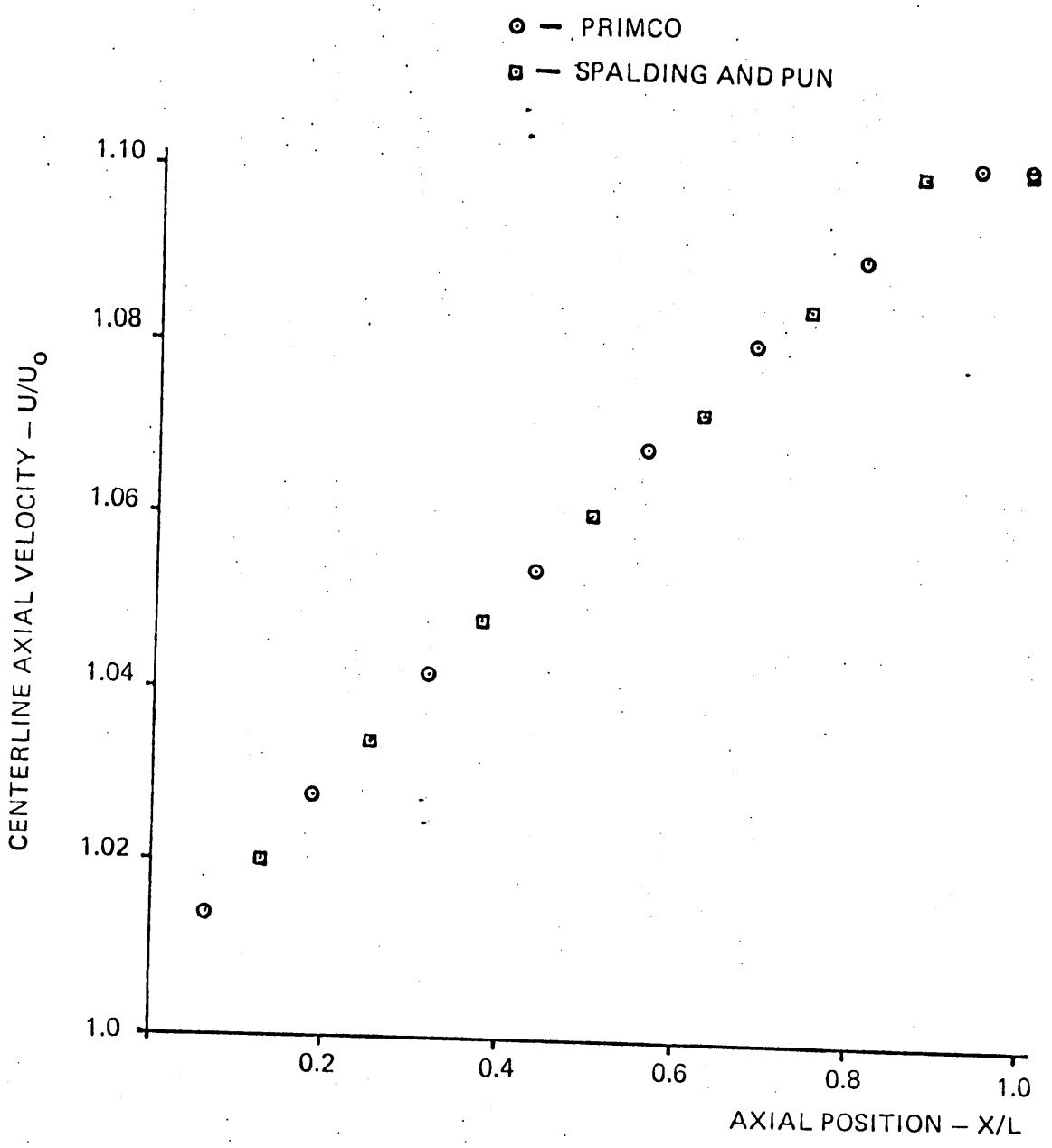

FIGURE 4.7 TURBULENT PIPE FLOW AXIAL VELOCITY

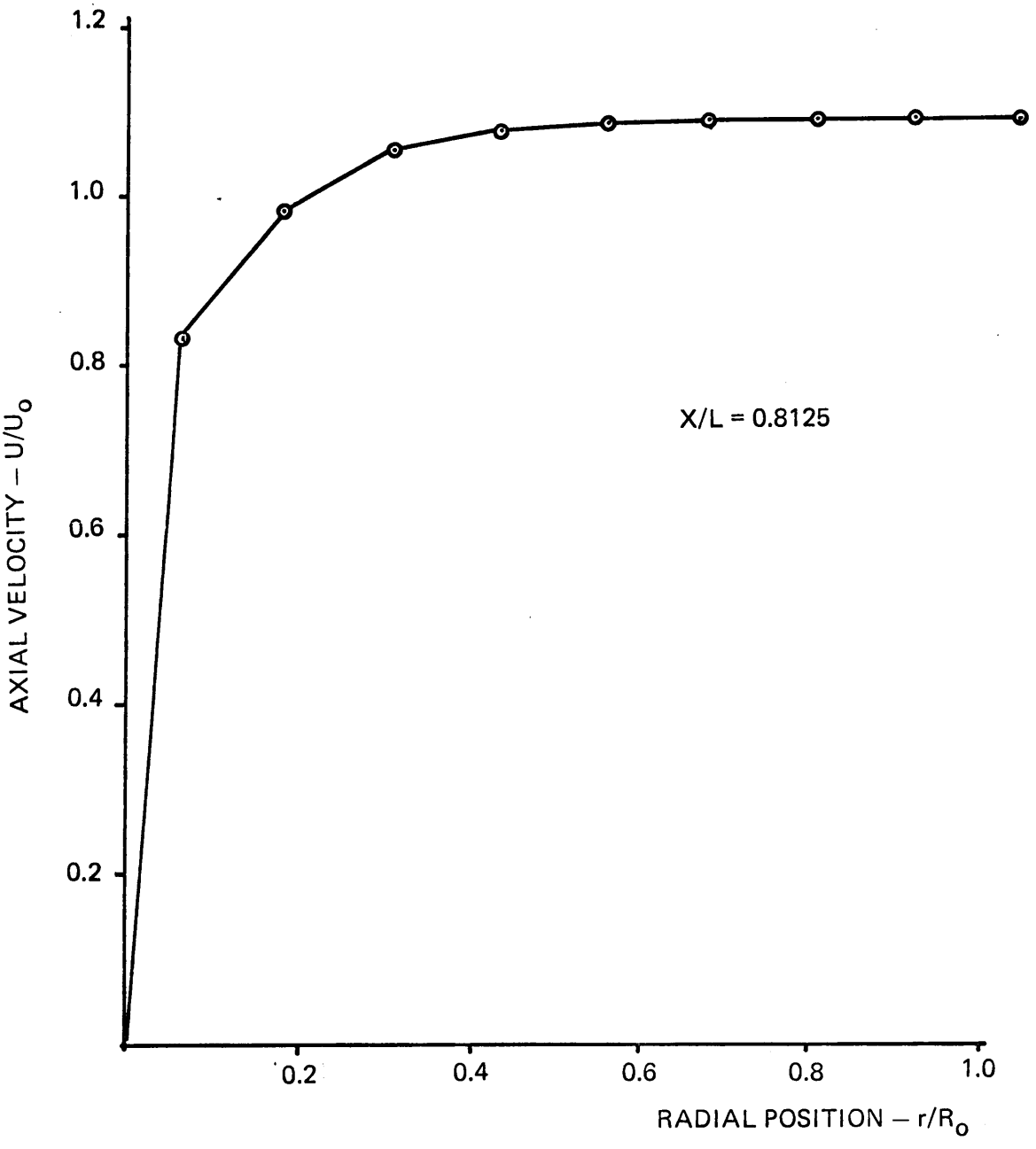

FIGURE 4.8 TURBULENT PIPE FLOW VELOCITY PROFILE

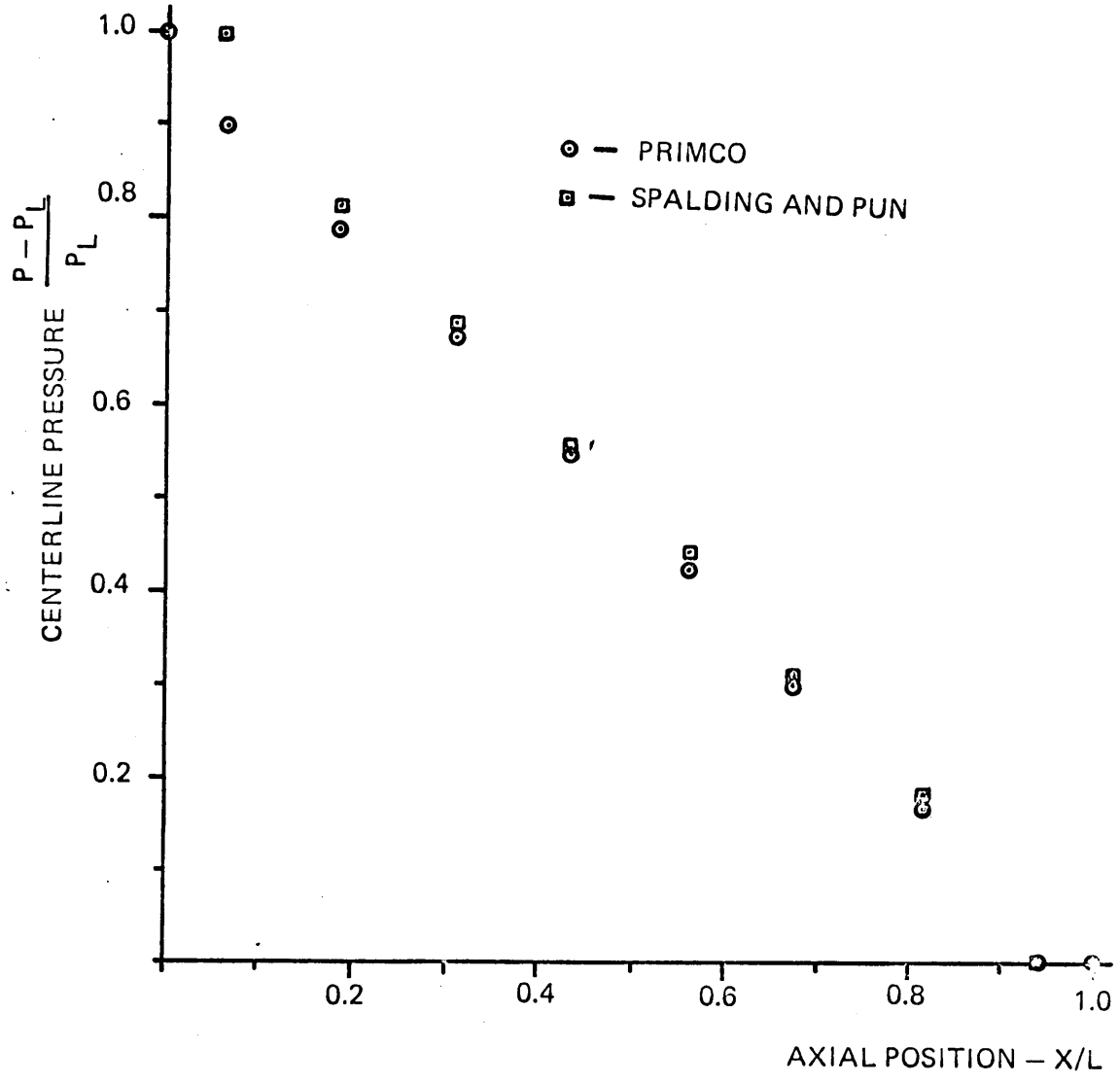

FIGURE 4.9 TURBULENT PIPE FLOW PRESSURE DISTRIBUTION

shown in Figure 4.10. Figure 4.11 shows a plot of the dissipation rate at the same axial stations. Note that the wall-flux boundary conditions are apparent as the source of turbulence energy at the near-wall region. Also note that the turbulence level decays to an almost uniform level at the center of the pipe. As the flow develops in the axial direction, the turbulence level is decaying although this is a relatively short length over which the flow is calculated.

Relaxation Factors

In general, the solution of such strongly nonlinear problems as those under consideration here requires special techniques to insure a stable and convergent solution. In the current analysis, a technique was used to under-relax the dependent variables during the solution process. The finite different equation for the variable ϕ at the node P may be solved directly for the new value of ϕ. The new estimate of ϕ is given by

$$\phi_P^* = \frac{\Sigma c_i \phi_i + S_\phi}{c_P}; \quad i = E, W, N, S \tag{4.5}$$

To reduce the rate of change in ϕ, the new value of ϕ is under-relaxed, i.e., the next estimate of ϕ in the solution process is calculated from

$$\phi_P = R\phi_P^* + (1-R)\phi_P^{Old} \tag{4.6}$$

The relaxation factor R varies in the range

$$0 < R \leq 1 \tag{4.7}$$

Using relaxation factors less than one slows down the solution process, but is necessary to insure stability. For the current problems,

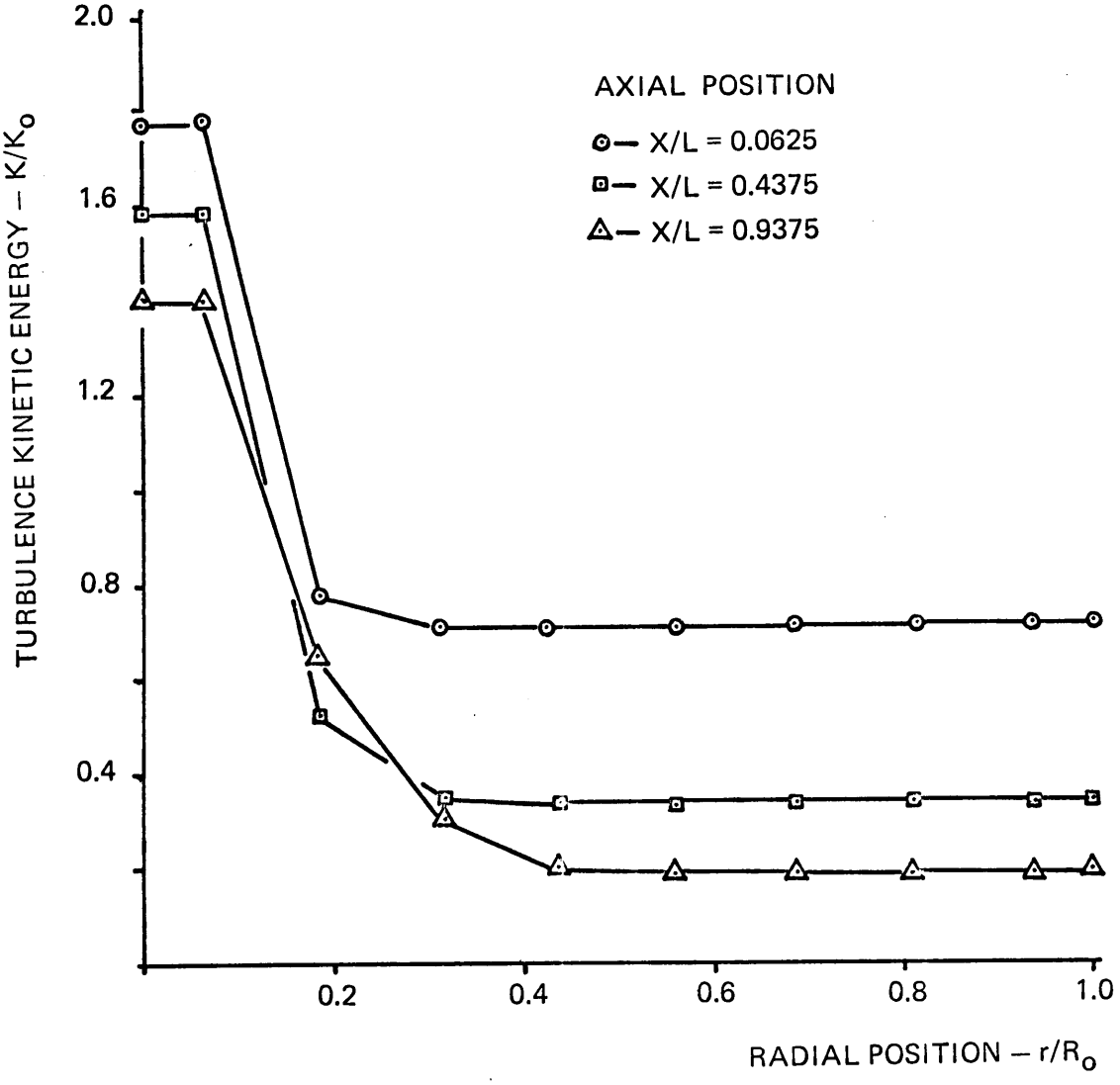

FIGURE 4.10 TURBULENCE KINETIC ENERGY

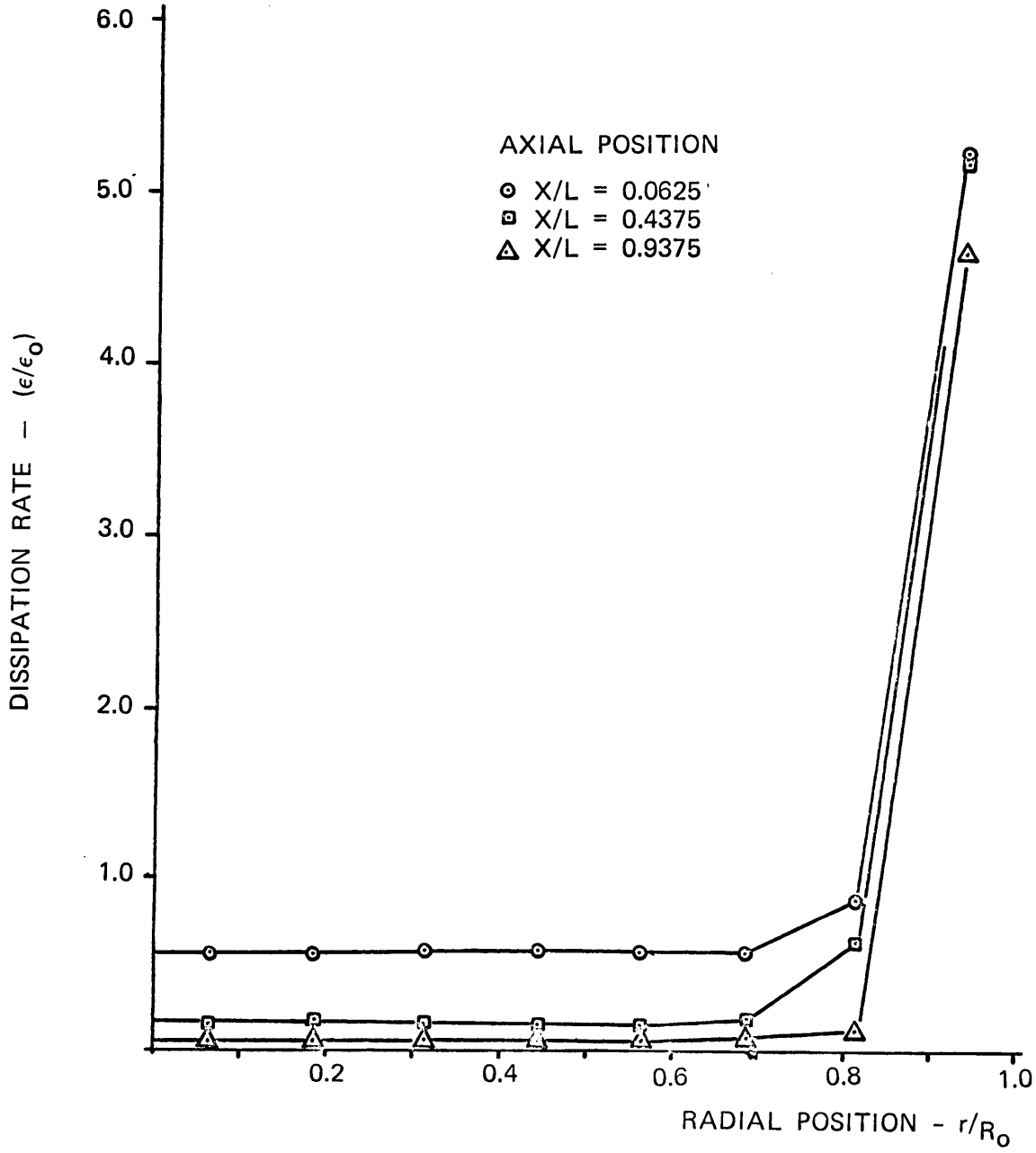

FIGURE 4.11 DISSIPATION RATE PROFILE

the relaxation factor for each dependent variable was not optimized. For the simpler problems, relaxation factors of one may be used without any stability problems. For the more complex swirling flows, including turbulence calculations, the relaxation factors shown in Table VIII were used.

4.3 Comparisons with Experimental Data

The final results to be presented are comparisons of predictions from PRIMCO with measured data from the experimental laboratory-scale burner. These comparisons are for isothermal flow in the lab-scale burner. The predicted velocity field from PRIMCO was compared to the experimentally measured velocity field for the isothermal air flow. The isothermal air flow case considered was chosen as representative of stable operating conditions with the low HV gas combustion. These calculations differ from those in the preceeding comparisons in three key areas; one, the presence of the swirl velocity, two, the complexity of the geometry involved, and three, the two inlet streams at different velocities.

The operating conditions for the isothermal example are shown in Table IX. As in the turbulent pipe flow example, the two equation turbulence model was employed in these calculations. All inlet velocities were assumed to be uniform and the inlet turbulence kinetic energy and dissipation rate were calculated as in the turbulent pipe flow example. A grid system of 481 nodes (24 x 21) was used.

Typically, the calculations involving swirl, the two-equation turbulence model, and more complex geometry converged much slower than

Table VIII Relaxation Factors

Variable	U	V	W	P	f	k	ε	μ_t
Factor	0.3	0.3	0.7	0.5	1.0	0.5	0.5	0.2

Table IX
Operating Conditions for Isothermal Measurements

Average Primary Inlet Velocity	61.5 m/sec.
Average Secondary Inlet Velocity	12.5 m/sec.
Average Tangential Inlet Velocity	9.0 m/sec.
Swirl Block Setting	0.40
Theoretical Inlet Swirl Number	0.62

the simpler examples already presented. Whereas the less complex examples, such as the turbulent pipe flow case, required 50 to 100 iterations to achieve an adequately converged solution, the swirling flow calculations require approximately 500 iterations to converge. For the more complex examples, the choice of initial estimates of the dependent variables and the optimization of relaxation factors is much more important.

The predicted and measured axial and swirl velocities are shown in Figures 4.12 through 4.19. In each of these figures, the velocity profile is shown as a function of the radial position. Each plot is at a fixed axial position. The axial position is measured from the inlet to the combustion chamber or the exit plane of the burner nozzle as shown in Fig. 3.1. All of the measurements were performed in the combustion chamber, as illustrated in Fig. 3.6. As shown in these figures, the measured and predicted results show excellent agreement. In particular, the swirl velocity predictions are quite interesting. The inlet swirl velocity prescribed as the inlet condition for the numerical computations was calculated from Grant's relationship, Eqn. 3.1. As shown in Figure 4.16, the peak swirl velocity at the inlet to the combustion chamber is slightly overpredicted. This is as expected since Grant's simplified analysis should overestimate the tangential velocity at the exit of the vanes. The swirl in this case is insufficient to produce a recirculating region similar to that shown in Figure 1.2. The swirl is sufficient to produce a significant deceleration of the high velocity primary fluid, as shown by the measured and predicted results.

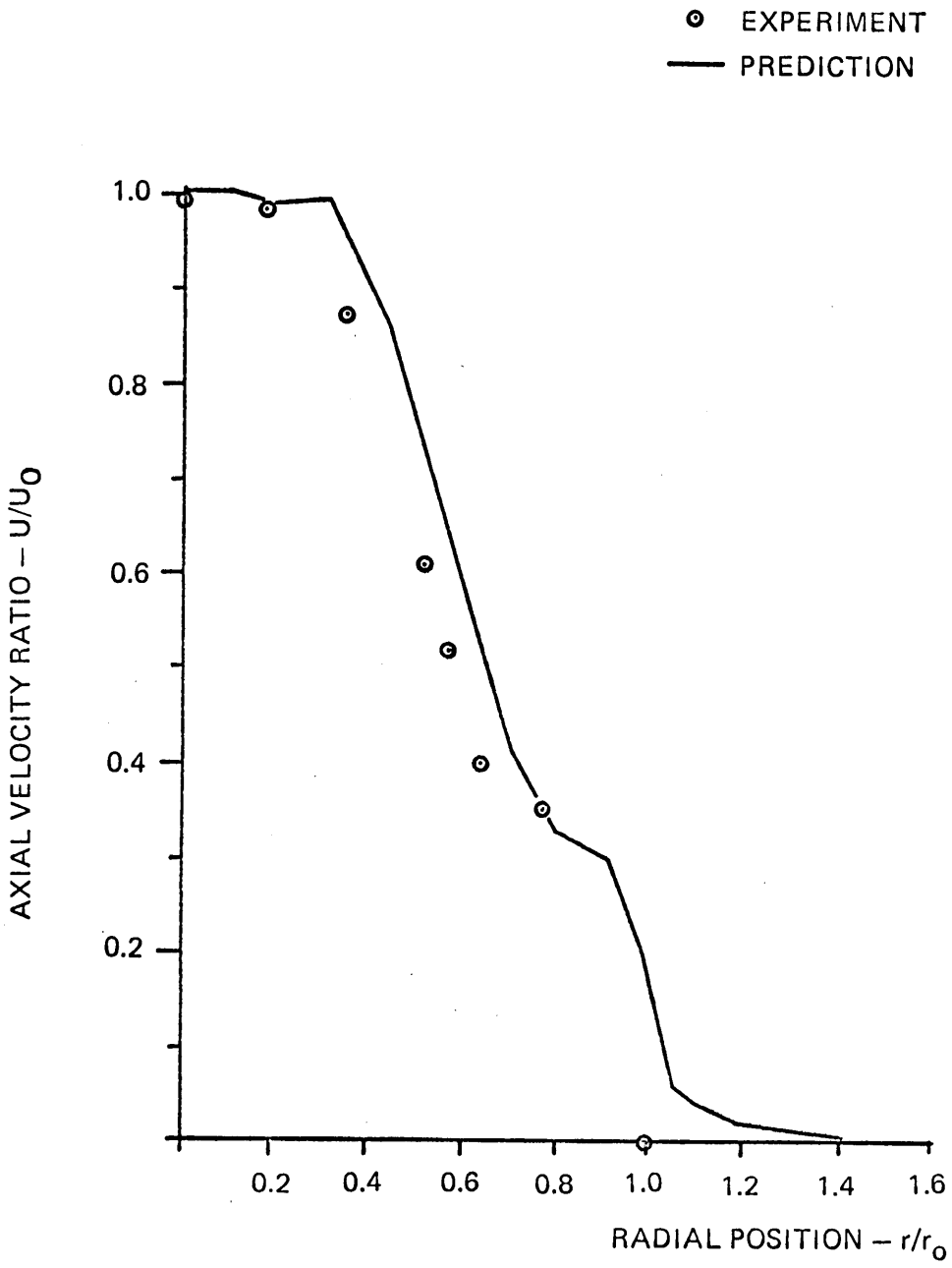

FIGURE 4.12 AXIAL VELOCITY DISTRIBUTION

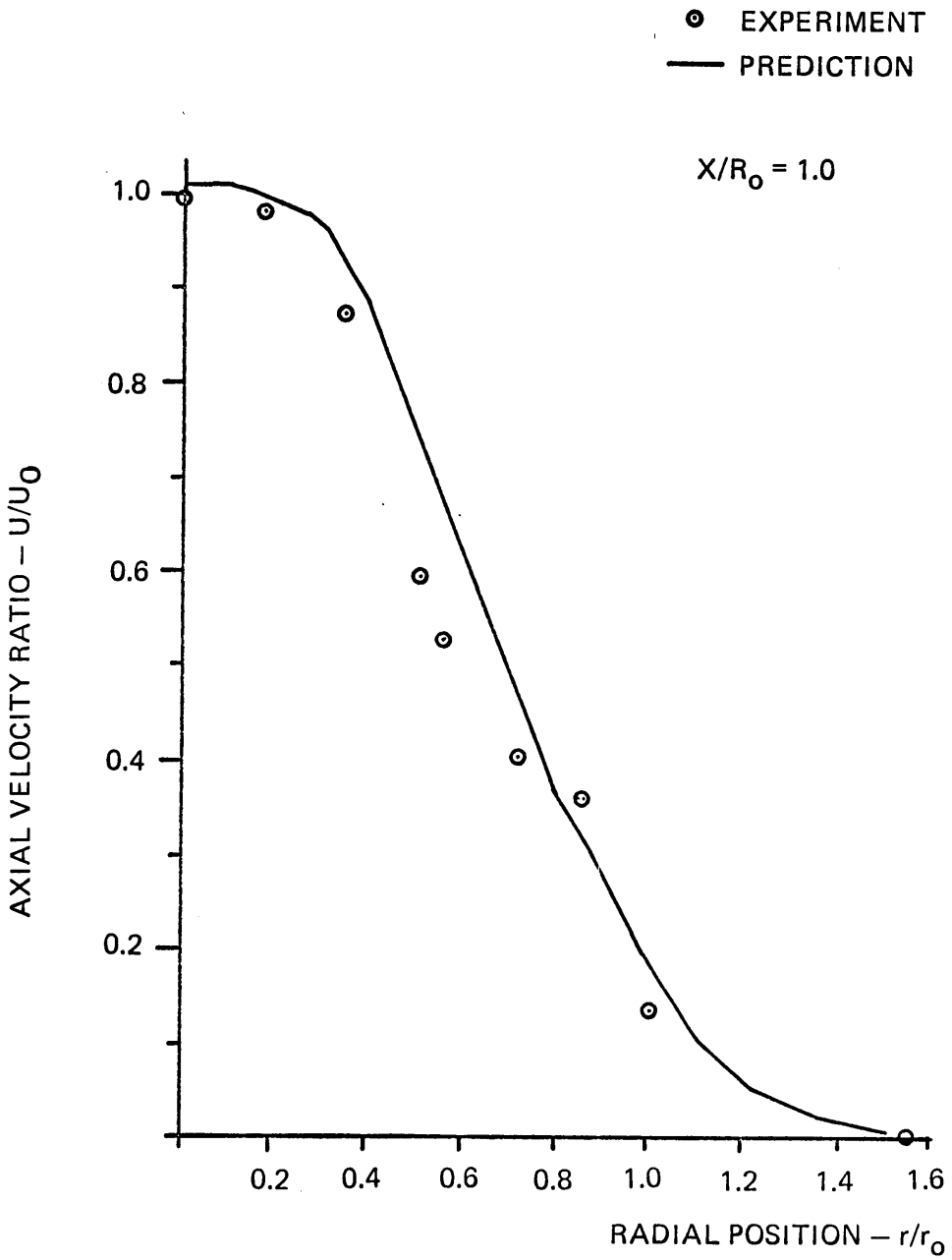

FIGURE 4.13 AXIAL VELOCITY DISTRIBUTION

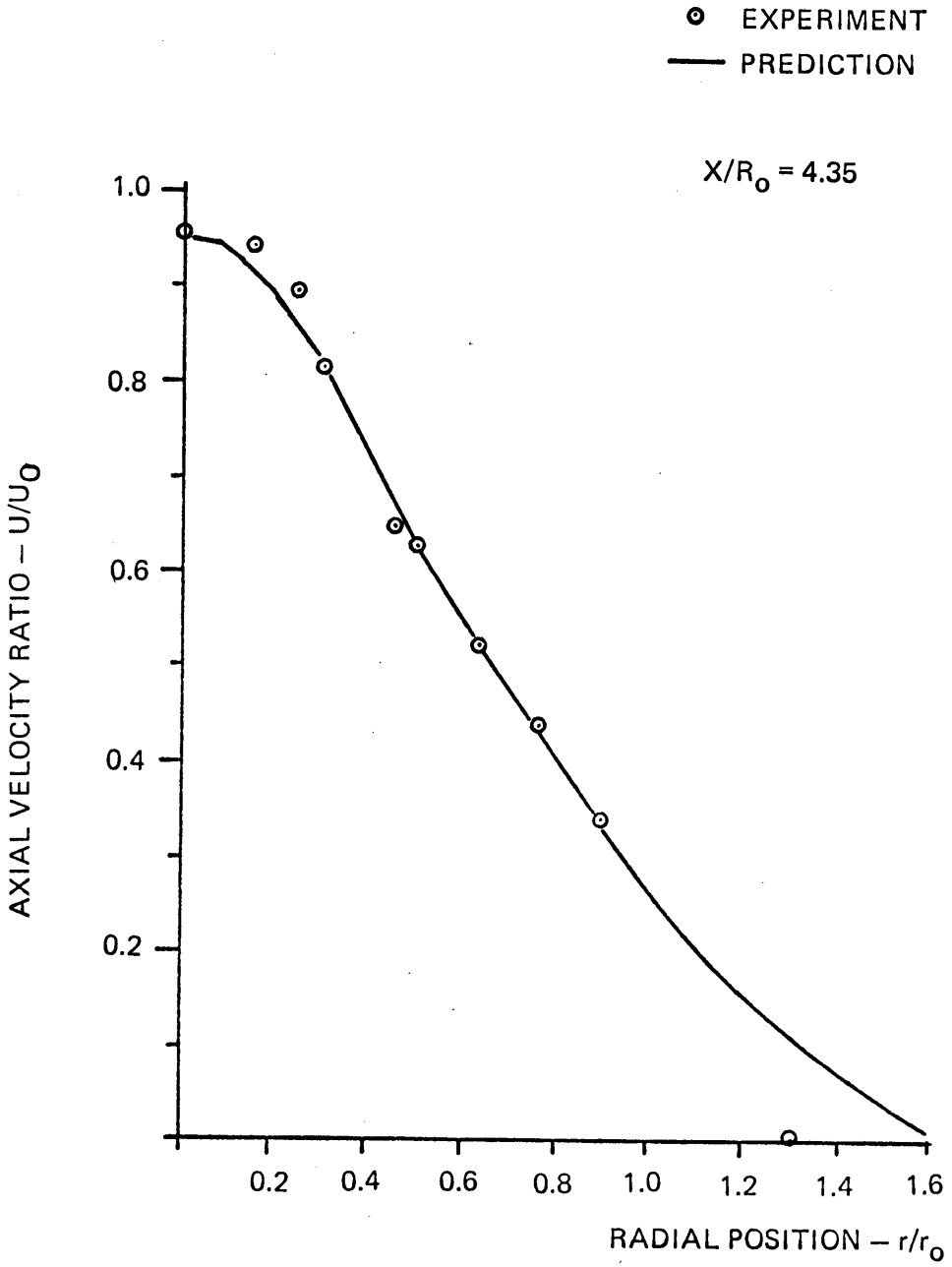

FIGURE 4.14 AXIAL VELOCITY DISTRIBUTION

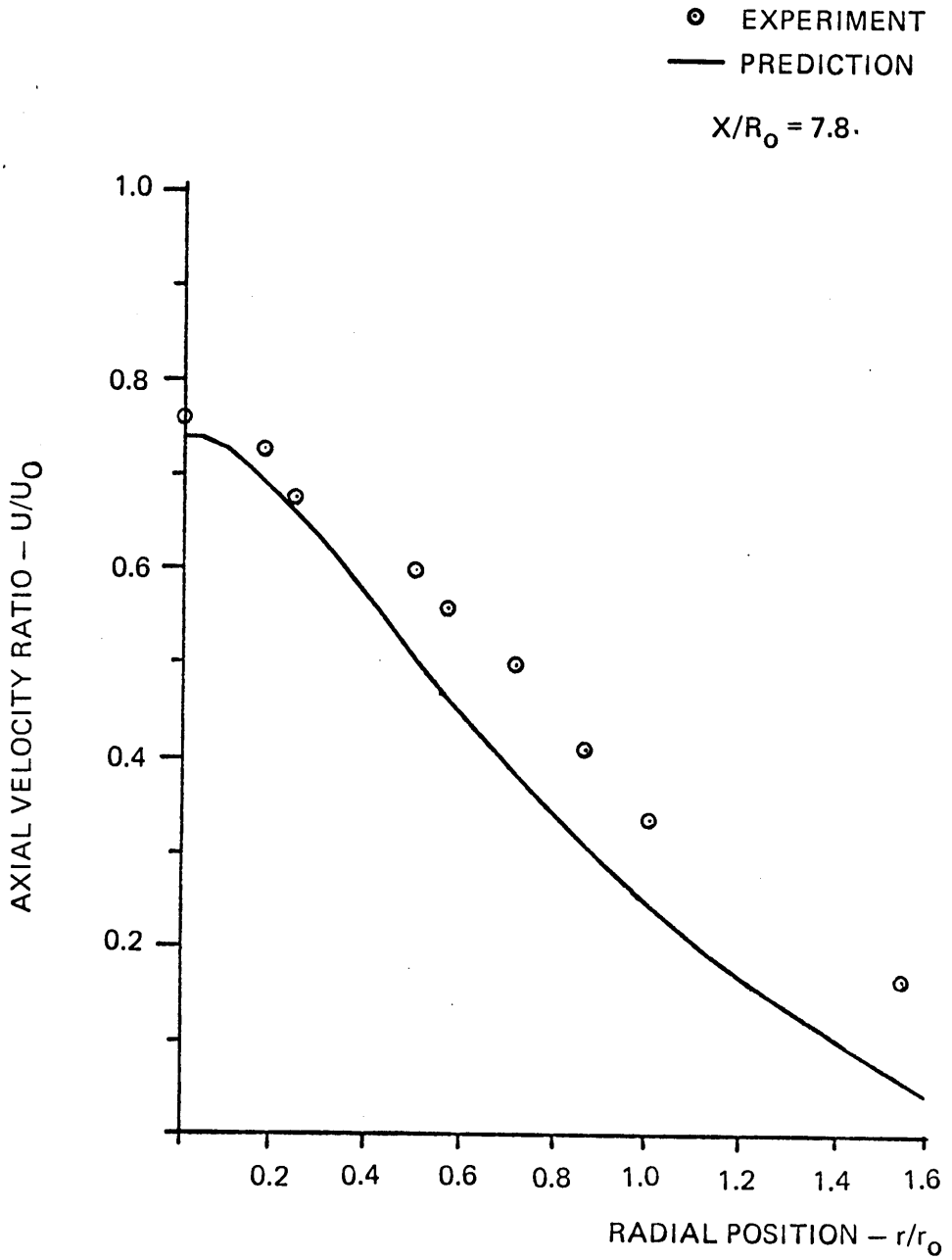

FIGURE 4.15 AXIAL VELOCITY DISTRIBUTION

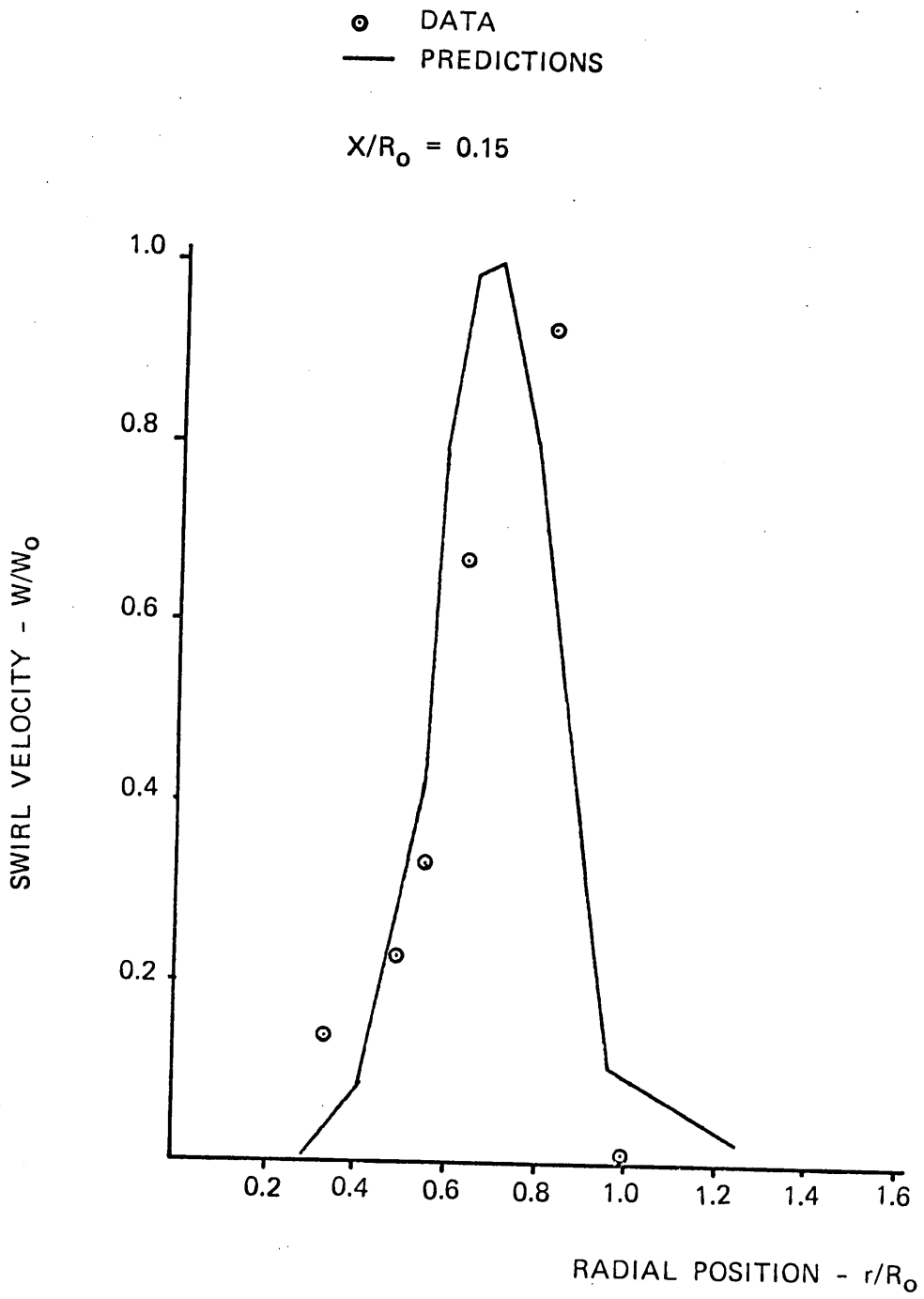

FIGURE 4.16 SWIRL VELOCITY DISTRIBUTION

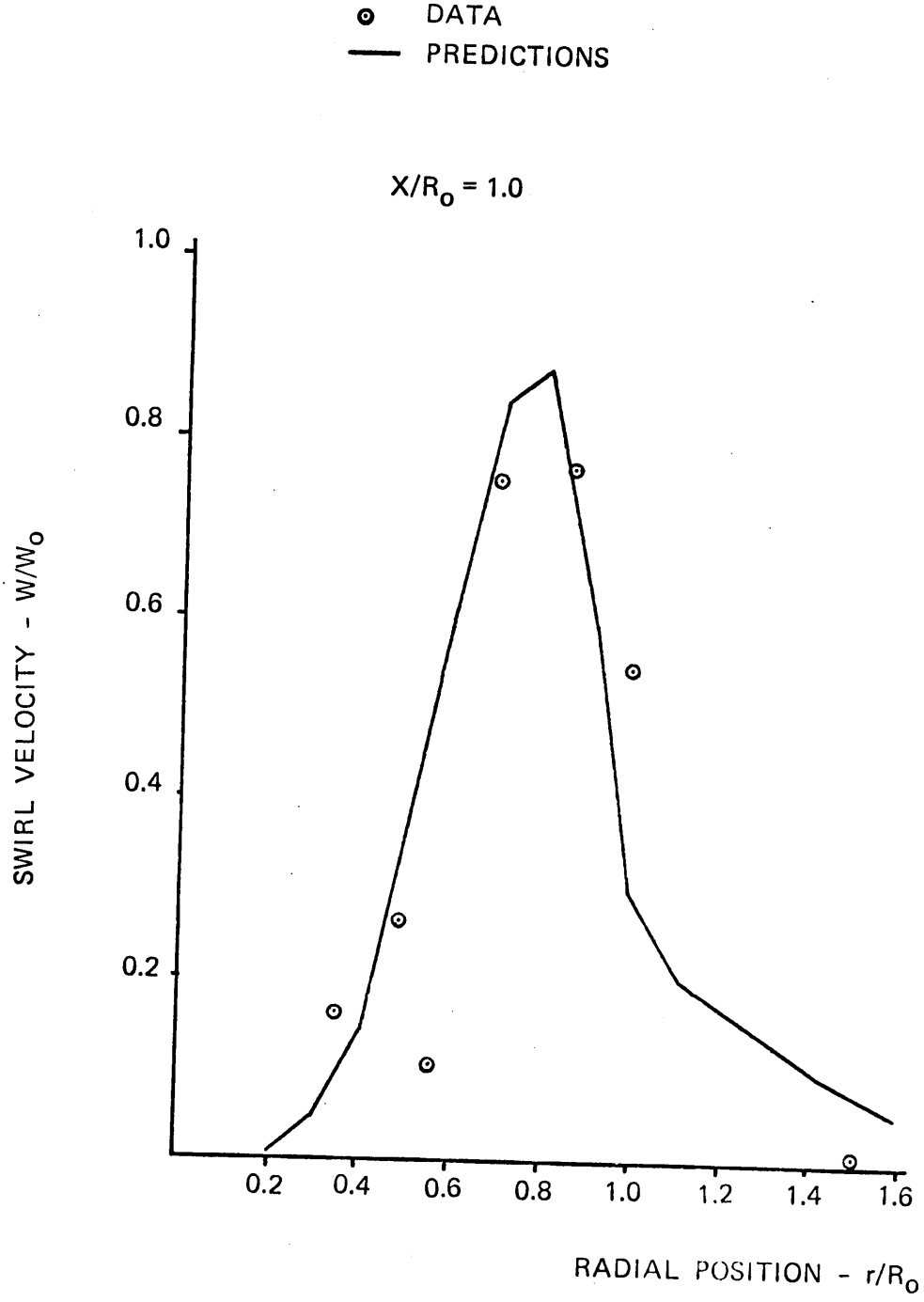

FIGURE 4.17 SWIRL VELOCITY DISTRIBUTION

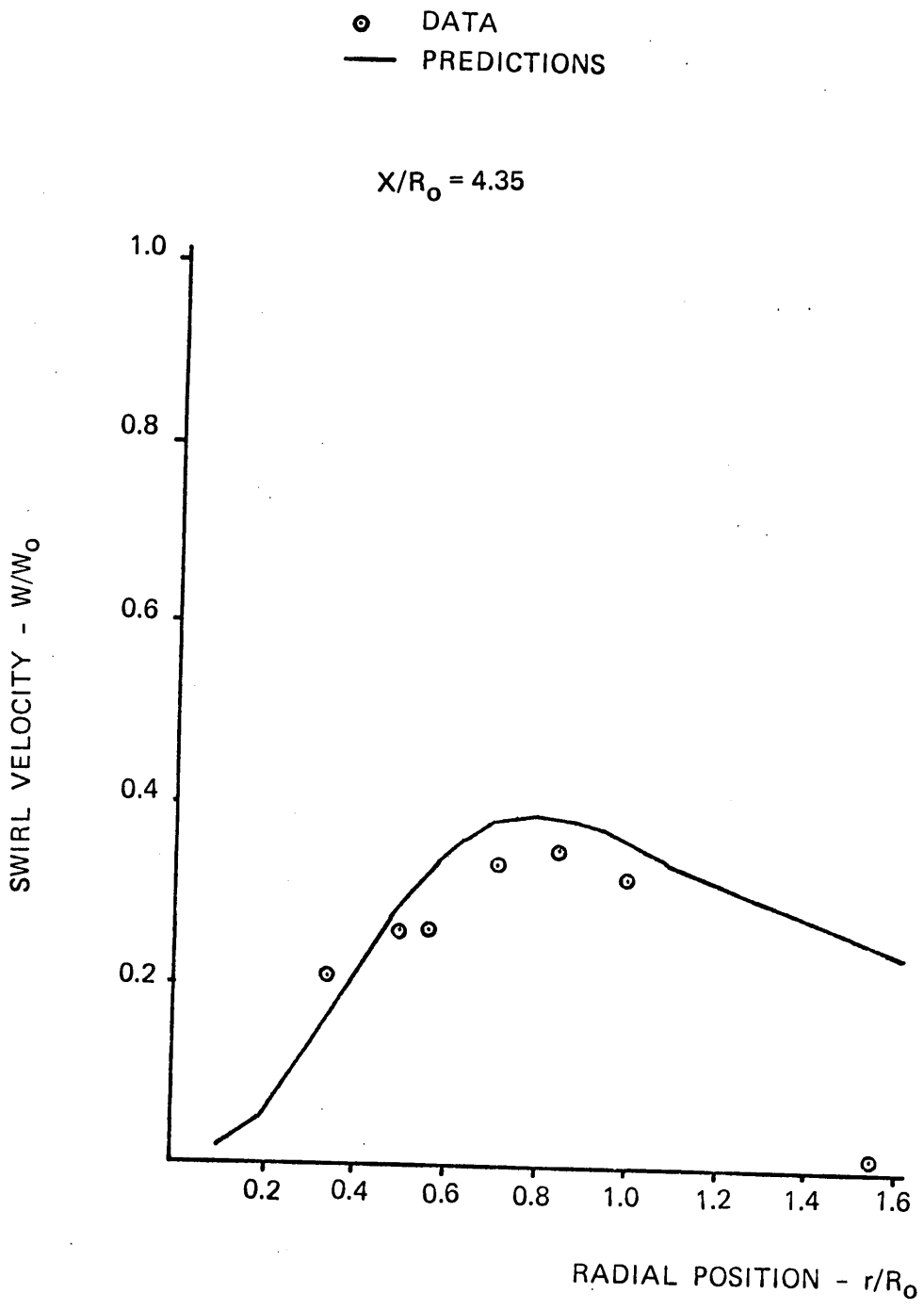

FIGURE 4.18 SWIRL VELOCITY DISTRIBUTION

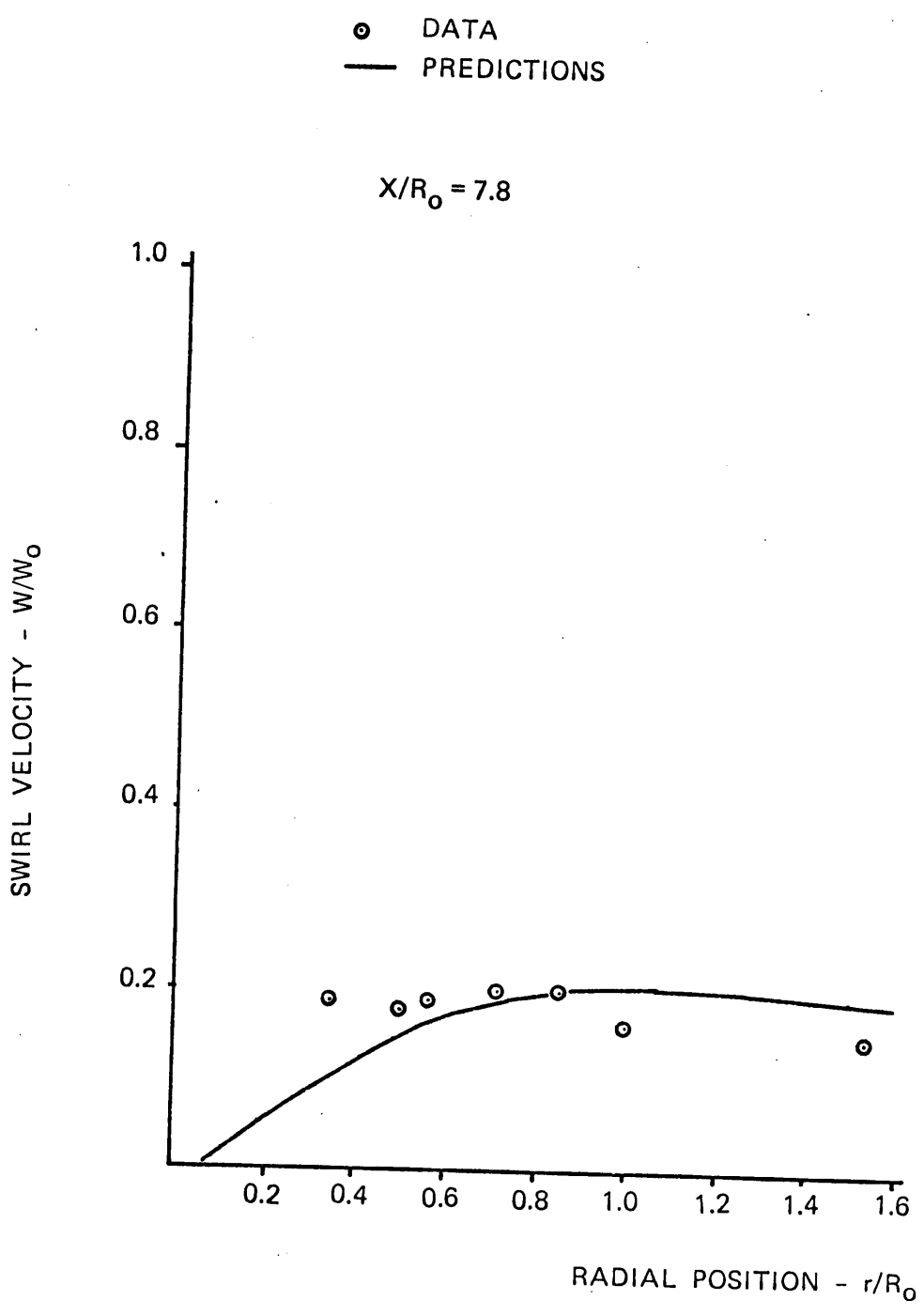

FIGURE 4.19 SWIRL VELOCITY DISTRIBUTION

Althouth there is no experimental data for comparison, it is interesting to note the predicted distribution of the turbulence kinetic energy. A plot of the radial distribution of the turbulence kinetic energy at three axial stations is shown in Figure 4.20. The first axial position is upstream of the combustion chamber. At this axial location, a single peak in the turbulence level is observed at the high shear boundary between the inlet primary and secondary flows. The second axial station is downstream of the combustion chamber inlet. At this axial station, there are two relative peaks in the turbulence energy. The first peak corresponds to the same peak shown at the first axial position. The second peak corresponds to the high-shear edge of the swirling jet. The profile at the last axial position shows the decay of the turbulence level towards a uniform level at the downstream station.

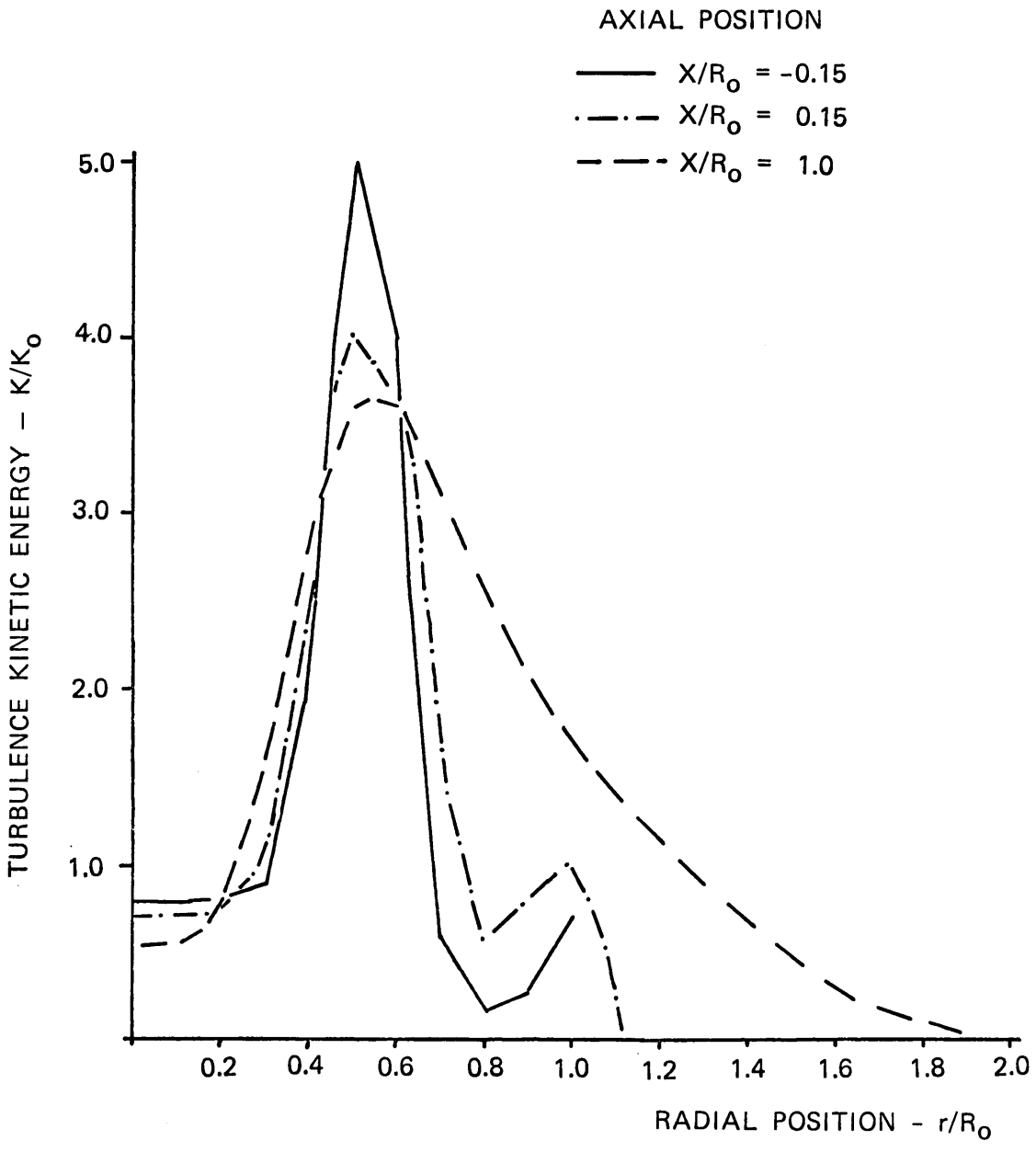

FIGURE 4.20 TURBULENCE KINETIC ENERGY PROFILE

5.0 SUMMARY AND CONCLUSIONS

This dissertation represents one phase of a larger overall project in combustion research. The overall project is aimed at developing complementary experimental and analytical techniques for the investigation of basic combustion processes involving swirl burners. The principle application in mind is the combustion of synthetic low HV gases. The objective of the current dissertation was to develop the required analytical techniques to model such a system and to demonstrate the validity of these techniques by comparison of predicted results and measured results for a laboratory scale swirl burner.

After a thorough review of the literature on numerical modeling techniques that could be applied to the analysis of a swirl burner for low HV gas combustion, the development of a numerical algorithm was initiated. The resulting computer code, PRIMCO, incorporates several features found in other such analyses appearing in the literature. The solution algorithm embodied in PRIMCO was given the acronum CENCIS (for CEntered-Cell-Implicitly-Staggered). The basic algorithm follows the work of Patankar and Spalding [7] and the work of Harlow and Welch [8] in a primitive variables (velocity and pressure) formulation of the Navier-Stokes equations. The algorithm also features an implicit pressure solution procedure which follows the previous work in this area. The main departure from the previous work in this area involves the use of a non-staggered grid system. The previous algorithms used staggered spacial locations for the velocity and pressure values.

The PRIMCO code is a two-dimensional axis symmetric analysis that includes variable density and viscosity effects. The code models

turbulent flow using a two-equation turbulence model to provide an effective viscosity. The current form of the code features a simplified infinite reaction rate combustion model. Radiation and conduction heat transfer are not accounted for.

The use of the non-staggered grid system in the current work has proved satisfactory for the class of problems that has been considered thus far. It should be noted, however, that a very limited class of problems has been considered here and that the staggered grid approach has been successfully applied to a very wide range of problems. In particular, the problems considered in the current work have been limited to flows where the flow is predominantly in one direction. The major portion of the pressure gradient has been in the principle flow direction. The CENCIS algorithm has not been used in a case where the principle flow direction may change in various regions of the geometry.

As part of the verification of the basic solution algorithms, a simplified code was developed to solve a basic test case. This sample code, CENCIS-T, was applied to calculate the developing laminar flow in a planar duct. The results of this analysis were compared to results of an analytical solution for this problem from Schlichting [43]. The results were also compared to numerical predictions for the problem obtained with a stream-function-vorticity formulation. The results were in agreement in all comparisons.

The PRIMCO computer code was verified by comparisons with results obtained from several sources including a known analytical solution, other numerical calculations, and experimental data. The PRIMCO predictions

for developing laminar pipe flow were compared to results obtained from numerical computations published by Spalding and Pun [41]. The PRIMCO results were also compared to the known fully developed velocity profile for laminar flow in a pipe. In both of these comparisons, the PRIMCO predictions were satisfactory and in close agreement.

The final step in the development process for the PRIMCO analysis was the comparison of PRIMCO predictions for the experimental swirl burner with the measured isothermal velocity distribution. The comparisons showed that the code could predict the performance in all areas of the flow field where measured data was available.

6. RECOMMENDATIONS

In the following section, recommendations for further areas of work are presented. The recommendations that are presented are limited to areas concerned with the current combustion project. There are numerous other possible applications of the numerical techniques presented here. The recommendations presented are separated into two general categories considering extensions to the existing analysis and additional experimental work.

6.1 Extensions to the Existing Analysis

There are several areas of improvement to the basic analysis that can readily be incorporated into the existing computer code. First, of prime importance to a combustion analysis in particular is the inclusion of heat transfer effects, particularly radiation heat transfer. Since this is a departure from the previous assumption of a physically controlled equilibrium combustion process, an additional partial differential equation will have to be added, i.e., the energy equation. The energy equation can readily be incorporated into the existing computer code since it can easily be put into the same form as the general conservation equation outlined in Chapter Two. The source term for the energy equation would include the radiation heat transfer, for example. Energy release terms for the combustion reactions can also be included in the source terms.

6.1.1 Radiation Heat Transfer

The radiation heat transfer can be handled in a manner that can be

conveniently included in the current solution algorithm. Such an approach is the finite-flux method outlined in reference [44]. This approach, combined with a specified surface temperature boundary condition, could be used to model combustion within a furnace, for example. The calculations can be used to predict the wall heat flux and other parameters of particular interest to furnace designers.

6.1.2 Reaction Kinetics

A second area of possible extension of the existing analysis would be to include a more complex combustion model in the analysis. Instead of the infinite rate reaction model employed in the current analysis, any number of finite-rate reactions may be considered. The number of reactions considered will be limited by computational limits of computer time and storage. Again, because of the structure of the CENCIS algorithm, this feature could be easily incorporated into the existing computer code. The governing equation for each reaction to be considered is the conservation of mass species for each species to be considered. For example, the formation of nitric oxide can be calculated from the conservation equation for the mass fraction of the NO. The source term in the governing equation in this case becomes, for example, an Arrhenius type rate equation. Note that this conservation equation also fits the form of the generalized conservation equation. The solution of this and other such similar equations will require little additional computation since the required finite difference coefficients are the same as for all of the previous equations.

6.1.3 Particle or Droplet Combustion

An additional area in which the analysis may be extended would be the extension of the analysis to model particulate or droplet combustion. This extension is more difficult than the two examples already discussed. This area is of particular practical importance, however, since this would allow the modeling of pulverized coal combustion and fuel oil combustion. Such particle-fluid models have been developed [35]. These models would be coupled with the momentum and mass conservation equations. These techniques consider the interaction of the fluid and particle components in the flow field.

6.2 Additional Experimental Studies

Further experimental work is required to use fully the potential of the existing experimental apparatus. The current work did not report temperature measurements and the current apparatus is capable of providing temperature measurements. The current work also only examined flow fields with relatively low swirl numbers. The flows did not include recirculation zones because of the relatively low swirl numbers. To achieve higher swirl numbers, however, the fuel would have to be introduced with a swirl component of velocity similar to that of the air. The idea of swirling the fuel, discussed by Grant also [19], seems to offer considerable benefit for the low HV gas combustion.

There are other areas of experimental investigation which are of considerable interest but would require considerably more experimental equipment than is currently available. These measurements would include local turbulence levels within the flow field, species concentration

profiles, and heat transfer rates. The current mathematical model with the two-equation turbulence model requires much additional experimental verification. One particular area of importance is the inlet turbulence level. That initial turbulence energy distribution must be specified as input to the numerical model. Experimental measurements are needed to provide guidelines for specifying these initial values of turbulence energy for various inlet geometries and flow conditions.

The state-of-the-art in the numerical computation of turbulent transport processes such as those under consideration here has reached the point that much more experimental work is needed to further develop and verify these techniques. These numerical techniques require more basic experimental measurements on very localized levels. The level of complexity and detail of numerical techniques and the level of complexity and detail in usable experimental data is directly related. The rate of progress in the development of numerical computations such as those presented here is strongly dependent on the availability of such data.

7.0 REFERENCES

[1] Rice, J. G., "The Modeling of Nitric Oxide Formation in a Swirl Burner with Flue Gas Recirculation", Master of Science Thesis, Virginia Polytechnic Institute and State University, September 1973.

[2] Gordon, S. and B. J. McBride, "Computer Program for Calculation of Complex Chemical Equilibrium Compositions, Rocket Performance, Incident and Reflected Shocks, and Chapman-Jonquet Detonations," NASA SP-273, Lewis Research Center, Cleveland, Ohio, 1971.

[3] Chigier, N. A. and J. M. Beér, "Velocity and Static Pressure Distributions in Swirling Air Jets Issuing from Annular and Divergent Nozzles," Transactions of the ASME, 86D, Journal of Basic Engineering, Vol 4, December 1964, pp. 788-796.

[4] Roache, P. J., Computational Fluid Dynamics, Hermosa, Albuquerque, New Mexico, 1972.

[5] Patankar, S. V. and D. B. Spalding, "Numerical Predictions of Three Dimensional Flows," Imperial College, Mechanical Engineering Dept., Report EF/TN/A/46, June 1976.

[6] Amsden, A. A. and F. H. Harlow, "The SMAC Method: A Numerical Technique for Calculating Incompressible Fluid Flows," Los Alamos Scientific Laboratory, Report LA-4370, Los Alamos, New Mexico, 1970.

[7] Gosman, A. D., W. M. Pun, A. K. Runchal, D. B. Spalding and M. Wolfshtein, Heat and Mass Transfer in Recirculating Flows, Academic Press, New York, 1969.

[8] Patankar, S. V., "Numerical Prediction of Three Dimensional Flows," Studies in Convection, edited by B. E. Launder, Vol 1, Academic Press, London, 1975, pp. 1-78.

[9] Caretto, L. S., A. D. Gosman, S. V. Pantankar and D. B. Spalding, "Two Calculation Procedures for Steady, Three Dimensional Flows with Recirculation," Proceedings of the Third International Conference on Numerical Methods in Fluid Dynamics, Paris, July 1972.

[10] Welch, J. E., F. H. Harlow, J. P. Shannon and B. J. Daly, "The MAC Method," Los Alamos Scientific Laboratory, Report LA-3425, Revised 1965.

[11] Hood, P. and C. Taylor, "Navier-Stokes Equations Using Mixed Interpolation," Finite Element Methods in Fluid Flow, UAH Press, Huntsville, Alabama, 1974.

[12] Launder, B. E. and D. B. Spalding, Mathematical Models of Turbulence, Academic Press, London, 1972.

[13] Buleev, N. I., "Theoretical Model of the Mechanism of Turbulent Exchange in Fluid Flows," Teploperedacha, USSR Academy of Sciences, p. 64, 1962.

[14] Chambers, T. L. and D. C. Wilcox, "Critical Examination of Two Equation Turbulence Closure Models for Boundary Layers," AIAA Journal, Vol 15, No 6, June 1977.

[15] Mellor, G. L. and H. J. Herring, "A Survey of Mean Turbulent Field Closure Models," AIAA Journal, Vol 11, May 1973.

[16] Kolmogorov, A. N., "Equations of Turbulent Motion of an Incompressible Turbulent Fluid," Izv. Akad. Navk. SSSR Ser Phys. VI, No. 1-2, p. 56, 1942.

[17] Jones, W. R. and Launder, B. E., "The Prediction of Laminarization with a 2-Equation Model of Turbulence," Int. J. of Heat and Mass Transfer 15, 301, 1972.

[18] Spalding, D. B., "The Calculation of the Length Scale of Turbulence in Some Turbulent Boundary Layers Remote from Walls," Imperial College, Heat Transfer Section Rep TWF/TN/31.

[19] Spalding, D. B., "The Prediction of Two Dimensional Steady Turbulent Flows," Imperial College, Heat Transfer Section Rep EF/TN/A/16.

[20] Grant, J. R., "Design and Operation of a Variable-Swirl Burner for Coal Gas Combustion Research," Master of Science Thesis, Virginia Polytechnic Institute and State University, November 1976.

[21] Lilly, D. G., "Swirl Flows in Combustion: A Review," AIAA Journal, Vol 15, No 8, August 1977.

[22] Chigier, N. A. and A. Chervinsky, "Experimental Investigation of Swirling Vortex Motion in Jets," Journal of Applied Mechanics, June 1967, pp. 443-451.

[23] Mathur, M. L. and N. R. L. Maccallum, "Swirling Air Jets Issuing from Vane Swirlers, Part I: Free Jets," Journal of the Institute of Fuel, May 1967, pp. 214-225.

[24] Leuckel, W., N. Fricker and K. Hein, "The Effect of Swirl on the Ignition Characteristics and Combustion Intensity of Pulverized-Coal and Natural Gas Flames," International Flame Research Foundation, Doc. No. TGK 20/a/45, 1970.

[25] Bafurwa, G. C. and N. R. L. Maccallum, "Turbulent Swirling Flames Issuing from Vane Swirlers," Doc. G02/CA/5, Eighteenth Meeting of the Aerodynamics Panel, Intl. Flame Research Foundation, Paris, July 1970.

[26] Syred, N., N. A. Chigier and J. M. Beér, "Flame Stabilization in Recirculation Zones of Jets with Swirl," Thirteenth Symposium (International) on Combustion, The Combustion Institute, Pittsburgh, 1972, pp. 617-624.

[27] Beltagui, S. A. and N. R. L. Maccallum, "Aerodynamics of Swirling Flames--Vane Generated Types," Combustion Institute, European Symposium, Academic Press, New York, 1973, pp. 559-564.

[28] Manheimer-Timant, Y., A. Segal and M. Wolfshtein, "Swirling Natural Gas Flames in Cylindrical Chambers," Combustion Institute, European Symposium, Academic Press, New York, 1973, pp. 571-576.

[29] Baker, R. J., P. Hutchinson, E. E. Rhalil and J. H. Whitelaw, "Measurements of Three Velocity Components in a Model Furnace With and Without Combustion," Fifteenth Symposium (International) on Combustion, Pittsburgh, 1974, pp. 553-571.

[30] Chigier, N. A. and K. Dvorak, "Laser Anemometer Measurements in Flames with Swirl," Fifteenth Symposium on Combustion (International), The Combustion Institute, Pittsburgh, 1974, pp. 573-585.

[31] Syred, N. and J. M. Beér, "Combustion in Swirling Flows: A Review," Combustion and Flame, Vol 23, 1974, pp. 143-201.

[32] Pillsburg, P. W., E. N. G. Cleary, P. P. Singh and R. M. Chamberlin, "Emission Results from Coal Gas Burning in Gas Turbine Combustors," January 1976, pp. 88-96.

[33] Klapatch, R. D. and G. E. Vitti, "Gas Turbine Combustor Test Results and Combined Cycle System," Combustion, Vol 45, No. 10, April 1974, pp. 35-38.

[34] Grant, J. R., J. G. Rice and W. C. Thomas, "The Combustion of a Low Heating Value Gas in a Swirl Burner," Presented at the Spring Meeting of the Combustion Institute, Cleveland, Ohio, March 1977.

[35] Hutchinson, P., E. E. Khalil, J. H. Whitelaw and G. Wigley, "The Calculation of Furnace-Flow Properties and Their Experimental Verification," ASME Paper No. 75HT-8, ASME, New York, April 1975.

[36] Launder, B. E. and D. B. Spalding, "The Numerical Computation of Turbulent Flows," Computer Methods in Applied Mechanics and Engineering, Vol 3, 1974, pp. 269-289.

[37] Spalding, D. B., "A Novel Finite Difference Formulation for Differential Expressions Involving Both First and Second Derivatives," International Journal of Numerical Methods in Engineering, No 4, 1972, pp. 551-559.

[38] Raithby, G. D., "A Critical Examination of Upstream Differenting Applied to Problems Involving Fluid Flow," Computer Methods in Applied Mechanics and Engineering, No 9, 1976, pp. 75-103.

[39] Roache, P. J., "On Artificial Viscosity," Journal of Computational Physics, Academic Press, Vol. 10, No. 2, October 1972.

[40] Launder, B. E. and U. Sha, "A Model for Turbulent Momentum and Heat Transfer in Large Rod Bundles," ANL-77-73, September 1977.

[41] Rivard, W. C., O. A. Farmer and T. D. Butler, "A Computer Program for Multicomponent Chemically Reactive Flows at All Speeds," Los Alamos Scientific Laboratory Report LA-5812, 1974.

[42] Pun, W. M. and D. B. Spalding, "A General Computer Program for Two Dimentionsal Elliptic Flows," Imperial College, London University, Report HTS/76/2, 1976.

[43] Schlichting, H., Boundary Layer Theory, McGraw-Hill, New York, 1968.

[44] Varma, S. A. and D. T. Pratt, "Anisotropic and Multiple Scattering of Thermal Radiation in Pulverized Coal Combustion," Seventeenth Symposium (International) on Combustion, The Combustion Institute, The University of Leeds, Leeds, England, 1978.

APPENDICES

Appendix A. Finite Difference Equations

The general governing equation in cylindrical coordinates is equation 2.2.3, which is repeated here as

$$\frac{\partial}{\partial x}\{\rho u\phi\} + \frac{1}{r}\frac{\partial}{\partial r}\{r\rho v\phi\} = \frac{\partial}{\partial x}\left\{\Gamma_\phi \frac{\partial \phi}{\partial x}\right\} + \frac{1}{r}\frac{\partial}{\partial r}\left\{r\Gamma_\phi \frac{\partial \phi}{\partial r}\right\} + S_\phi \qquad (A.1)$$

This equation is to be integrated over the control volume illustrated in Fig. A.1. The resulting integral is

$$\int_{x-}^{x+}\int_{r-}^{r+}\left[\frac{\partial}{\partial x}\{\rho u\phi\} + \frac{1}{r}\frac{\partial}{\partial r}\{r\rho v\phi\}\right] dxdr =$$

$$\int_{x-}^{x+}\int_{r-}^{r+}\left[\frac{\partial}{\partial x}\left\{\Gamma_\phi \frac{\partial \phi}{\partial x}\right\} + \frac{1}{r}\frac{\partial}{\partial r}\left\{r\Gamma_\phi \frac{\partial \phi}{\partial r}\right\}\right] dxdr$$

$$+ \int_{x-}^{x+}\int_{r-}^{r+} S_\varphi \, dxdr \qquad (A.2)$$

Each of the above integrals in equation A.2 may be integrated once to yield

$$\int_{r-}^{r+}\left[\rho u\phi|_{x+} - \rho u\phi|_{x-}\right] dr + \int_{x-}^{x+}\frac{1}{r}\left[r\rho v\phi|_{r+} - r\rho v\phi|_{r-}\right] dx$$

$$= \int_{r-}^{r+}\left[\Gamma_\phi \frac{\partial \phi}{\partial x}|_{x+} - \Gamma_\phi \frac{\partial \phi}{\partial x}|_{x-}\right] dr$$

$$+ \int_{x-}^{x+}\frac{1}{r}\left[\Gamma_\phi \frac{\partial \phi}{\partial r}|_{r+} - \Gamma_\phi \frac{\partial \phi}{\partial r}|_{r-}\right] dx + \Delta r\int_{x-}^{x+} S_\phi dx \qquad (A.3)$$

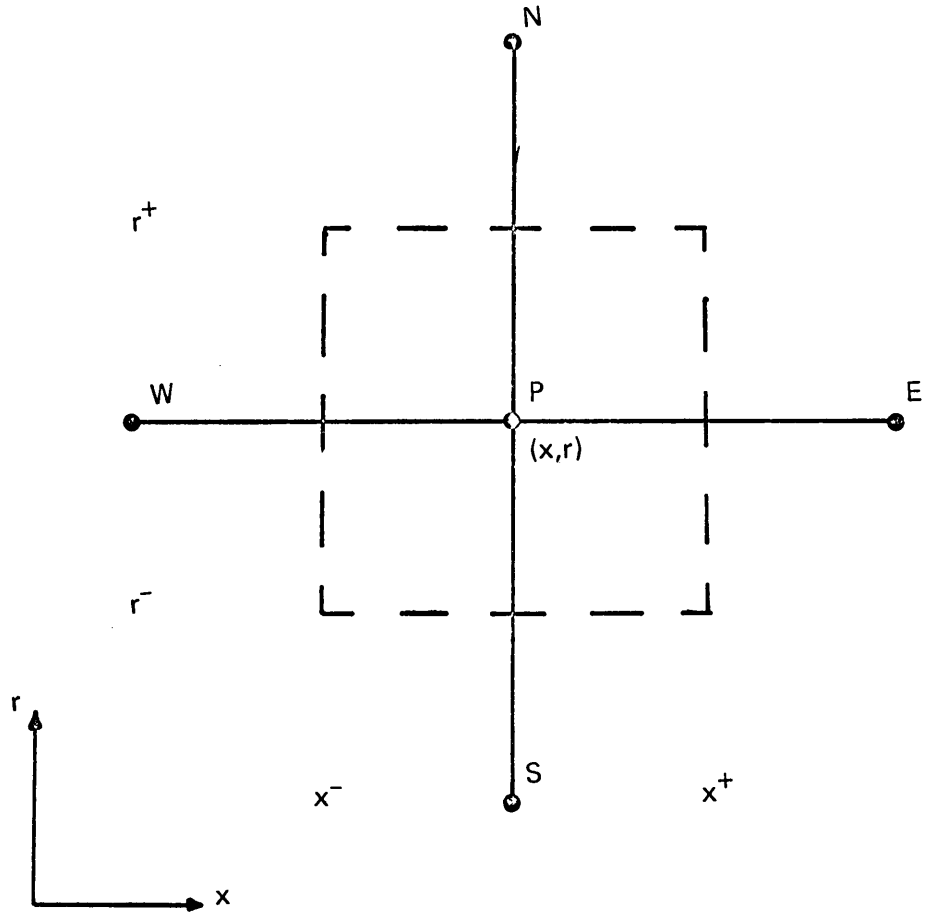

FIGURE A.1 CONTROL VOLUME

Notice that the mean value theorem was employed to evaluate integrals containing 1/r, i.e.,

$$\int_{r-}^{r+}\left[\frac{1}{r}\frac{\partial}{\partial r}\left\{r\rho v\phi\right\}\right]dr = \frac{1}{r_p}\int_{r-}^{r+}\frac{\partial}{\partial r}\left\{r\rho v\phi\right\}dr \tag{A.4}$$

Referring to Fig. A.1, the above expression is evaluated as

$$\int_{r-}^{r+}\frac{1}{r}\frac{\partial}{\partial r}\left\{r\rho v\phi\right\}dr = \frac{1}{r_p}\left[r\rho v\phi\Big|_{r+} - r\rho v\phi\Big|_{r-}\right] \tag{A.5}$$

Each of the integrals in equation A.3 is then integrated by assuming that each of the integrands is constant with respect to the dependent variable in that particular integral. The result of integrating equation (A.3) under this assumption is then

$$\left[\rho u\phi\Big|_{x+} - \rho u\phi\Big|_{x-}\right]\Delta r + \frac{1}{r_p}\left[r\rho v\phi\Big|_{r+} - r\rho v\phi_{r-}\right]\Delta x$$

$$= \left[\Gamma_\phi \frac{\partial\phi}{\partial x}\Big|_{x+} - \Gamma_\phi \frac{\partial\phi}{\partial x}\Big|_{x-}\right]\Delta r$$

$$+ \frac{1}{r_p}\left[r\Gamma_\phi \frac{\partial\phi}{\partial r}\Big|_{r+} - r\Gamma_\phi \frac{\partial\phi}{\partial r}\Big|_{r-}\right]\Delta x + S_\phi \Delta r\Delta x \tag{A.6}$$

Multiplying equation A.6 by r_p, yields

$$\rho u\phi\big|_{x+}A_x - \rho u\phi\big|_{x-}A_x + \rho v\phi\big|_{r+}A_{r+} - \rho v\phi\big|_{r-}A_{r-}$$

$$= \Gamma_\phi \frac{\partial\phi}{\partial x}_{x+}A_x - \Gamma_\phi \frac{\partial\phi}{\partial x}\Big|_{x-}A_{x-} + \Gamma_\phi \frac{\partial\phi}{\partial r}\Big|_{r+}A_{r+} - \Gamma_\phi \frac{\partial\phi}{\partial r}\Big|_{r-}A_{r-} \qquad (A.7)$$

Where the areas of each face of the control volume in Fig. A.1, per unit circumferential angle, are A_x, A_{r+}, and A_{r-}. These areas are given by

$$A_x = r_p\Delta r \qquad (A.8)$$

$$A_{r-} = r-\Delta x \qquad (A.9)$$

$$A_{r+} = r+\Delta x \qquad (A.10)$$

and the volume of the control volume per unit circumferential angle is

$$V = r_p\Delta r\Delta x \qquad (A.11)$$

Equation A.7 forms the basic finite difference equation. Note that the terms on the left side of equation A.7 comprise the net convective transport of ϕ for the control volume. The first four terms on the right side of equation A.7 form the net diffusive transport of ϕ for the control volume. The last term in equation A.7 represents the net source of ϕ within the control volume. Each of the terms appearing in equation A.7 must be evaluated in terms of the variables stored at the node locations. The node locations do not coincide with the control volume faces and therefore some scheme for interpolating the required values must be employed.

To illustrate the use of central differences, the convective and diffusive transport of ϕ across the east face of the control volume, with a uniform Δx and Δr, are given by

$$\rho u\phi\big|_{x+} A_x \simeq \left[\frac{P_e + P_p}{2}\right]\left[\frac{U_e + U_p}{2}\right]\left[\frac{\phi_e + \phi_p}{2}\right] r_p \Delta r \qquad (A.12)$$

$$\Gamma_\phi \frac{\partial \phi}{\partial x}\Big|_{x+} A_x \simeq \left[\frac{\Gamma_{\phi e} + \Gamma_{\phi p}}{2}\right]\left[\frac{\phi_e - \phi_p}{\Delta x}\right] r_p \Delta r \qquad (A.13)$$

Similar expressions are used for the remaining convective and diffusive terms at the other three faces. Finally, the source term, S_ϕ, is assumed constant over the control volume.

APPENDIX B.

Sample Program

```
      COMMON/FIELD/U(41,6),V(41,6),P(41,6),SU(41,6),SV(41,6)
      COMMON/GRID/X(11),Y(6),DX,DY,A,VOL
      COMMON/PROP/RHO,VISC,DIF
      COMMON/INDEX/IMAX,IM,JMAX,JM,KMAX,ITER,ITOTAL
      DX=0.025
      DY=DX
      A=DX
      VOL=A*DX
      RHO=0.075
      DATA U,V,P/246*20.,246*0.0,246*1.0/
      VISC=1.5E-4
      DIF=VISC*A/DX
      DATA IMAX,JMAX/21,6/
      JM=JMAX-1
      IM=IMAX-1
      DATA ITOTAL,IDBUG/50,0/
      KMAX=10
      IF(IDBUG.EQ.0) KMAX=3
      CALL CONTRL
      END
```

```
      SUBROUTINE CONTRL
      COMMON/CHECK/SCSUM,SMSUM
      COMMON/INDEX/IMAX,IM,JMAX,JM,KMAX,ITER,ITOTAL
C   FIRST ITERATION
      ITER=1
      ICOUNT=1
      IPRINT=10
      DO 10 I=2,IM
      CALL BOUND(I)
   10 CALL COEF(I)
      DO 1 I=2,IM
      CALL BOUND(I)
      CALL SOURCE(I)
      CALL COEF(I)
      CALL SOLVE(I,1)
      CALL COEF(I)
      CALL SOLVE(I,2)
      CALL COEF(I)
      CALL BOUND(I)
      CALL PRESS(I)
    1 CONTINUE
      CALL BOUND(IMAX)
      CALL PRINT
C   ITERATIVE LOOP
      DO 4 ITER=2,ITOTAL
      SCSUM=0.
      SMSUM=0.
      DO 3 I=2,IM
      CALL BOUND(I)
      CALL SOURCE(I)
      CALL SOLVE(I,1)
      CALL COEF(I)
```

```
      CALL SOLVE(I,2)
      CALL COEF(I)
      CALL BOUND(I)
      CALL PRESS(I)
    3 CONTINUE
      ICOUNT=ICOUNT+1
      CALL BOUND(IMAX)
      IF(ICOUNT.EQ.IPRINT) CALL PRINT
      IF(ICOUNT.EQ.IPRINT) ICOUNT=0
    4 CONTINUE
      RETURN
      END
```

```
      SUBROUTINE COEF(I)
      COMMON/FIELD/U(41,6),V(41,6),P(41,6),SU(41,6),SV(41,6)
      COMMON/COEFF/CE(41,6),CW(41,6),CN(41,6),CS(41,6),CP(41,6)
      COMMON/PROP/RHO,VISC,DIF
      COMMON/GRID/X(11),Y(6),DX,DY,A,VOL
      COMMON/INDEX/IMAX,IM,JMAX,JM,KMAX,ITER,ITOTAL
C
C
C     ENTRY XCOEF(I)
C
      DO 1 J=2,JM
      UE=(U(I+1,J)+U(I,J))/2.
      CONV=RHO*UE*A/2.
      CE(I,J)=AMAX1(DIF,ABS(CONV))-CONV
      UW=(U(I,J)+U(I-1,J))/2.
      CONV=RHO*UW*A/2.
      CW(I,J)=AMAX1(DIF,ABS(CONV))+CONV
    1 CONTINUE
C     RETURN
C
C
C     ENTRY YCOEF(I)
C
      CS(I,2)=DIF
      DO 2 J=2,JM
      VN=(V(I,J)+V(I,J+1))/2.
      CONV=RHO*VN*A/2.
      DIFU=AMAX1(DIF,ABS(CONV))
      CN(I,J)=DIFU-CONV
      CS(I,J+1)=DIFU+CONV
      CP(I,J)=CE(I,J)+CW(I,J)+CN(I,J)+CS(I,J)
    2 CONTINUE
```

```
RETURN
END
```

```
      SUBROUTINE SOLVE(I,K)
      COMMON/FIELD/U(41,6),V(41,6),P(41,6),SU(41,6),SV(41,6)
      COMMON/COEFF/CE(41,6),CW(41,6),CN(41,6),CS(41,6),CP(41,6)
      COMMON/INDEX/IMAX,IM,JMAX,JM,KMAX,ITER,ITOTAL
      COMMON/CHECK/SCSUM,SMSUM
      COMMON/SSOLV/ PHI(6),CON(6),G(6),H(6)
      DATA RECON,AIFAC,ILIM/0.5,1.0E-05,200/
      RELAX=RECON+(1.-RECON)*(FLOAT(ITER)/FLOAT(ILIM))
      RELAX=0.4
      AI=CP(2,2)*AIFAC
      IF((I.EQ.2).AND.(K.EQ.1)) SMSUM=0.0
      GO TO (1,3),K
    1 DO 2 J=2,JM
      CON(J)=SU(I,J)+CE(I,J)*U(I+1,J)+CW(I,J)*U(I-1,J)
    2 PHI(J)=U(I,J)
      PHI(1)=U(I,1)
      PHI(JMAX)=U(I,JMAX)
      GO TO 5
    3 DO 4 J=2,JM
      CON(J)=SV(I,J)+CW(I,J)*V(I-1,J)+CE(I,J)*V(I+1,J)
    4 PHI(J)=V(I,J)
      PHI(1)=V(I,1)
      PHI(JMAX)=V(I,JMAX)
    5 G(1)=PHI(1)
      H(1)=0.
      DO 6 J=2,JM
      CON(J)=CON(J)+AI*PHI(J)
      DENOM=(CP(I,J)+AI)-CS(I,J)*H(J-1)
      G(J)=(CON(J)+CS(I,J)*G(J-1))/DENOM
      H(J)=CN(I,J)/DENOM
    6 CONTINUE
      DO 7 JJ=2,JM
```

```
      J=JM+2-JJ
      PHI(J)=G(J)+H(J)*PHI(J+1)
    7 CONTINUE
      GO TO (8,10),K
    8 DO 9 J=1,JMAX
      UOLD=U(I,J)
      U(I,J)=UOLD*(1.-RELAX)+PHI(J)*RELAX
    9 SMSUM=SMSUM+ABS((UOLD-U(I,J))/U(I,J))
      GO TO 20
   10 DO 11 J=1,JMAX
      VOLD=V(I,J)
   11 V(I,J)=VOLD*(1.-RELAX)+PHI(J)*RELAX
   20 RETURN
      END
```

```
      SUBROUTINE SOURCE(I)
      COMMON/FIELD/U(41,6),V(41,6),P(41,6),SU(41,6),SV(41,6)
      COMMON/INDEX/IMAX,IM,JMAX,JM,KMAX,ITER,ITOTAL
      COMMON/GRID/X(11),Y(6),DX,DY,A,VOL
C SOURCE TERMS
C
      DO 11 J=2,JM
C  AXIAL VELOCITY
      PE=(P(I+1,J)+P(I,J))/2.
      PW=(P(I,J)+P(I-1,J))/2.
      DPDX=(PE-PW)/DX
      SU(I,J)=-DPDX*VOL
C  RADIAL VELOCITY
      PN=(P(I,J+1)+P(I,J))/2.
      PS=(P(I,J)+P(I,J-1))/2.
      DPDY=(PN-PS)/DY
      SV(I,J)=-DPDY*VOL
   11 CONTINUE
      RETURN
      END
```

```
      SUBROUTINE PRESS(I)
      DIMENSION PP(6),DVN(6),DVS(6),DUE(6),DUW(6),D(6),CPP(6)
      COMMON/CHECK/SCSUM,SMSUM
      COMMON/SSOLV/PHI(6),CON(6),G(6),H(6)
      COMMON/FIELD/U(41,6),V(41,6),P(41,6),SU(41,6),SV(41,6)
      COMMON/COEFF/CE(41,6),CW(41,6),CN(41,6),CS(41,6),CP(41,6)
      COMMON/INDEX/IMAX,IM,JMAX,JM,KMAX,ITER,ITOTAL
      COMMON/GRID/X(11),Y(6),DX,DY,A,VOL
      COMMON/PROP/RHO,VISC,DIF
      IF(I.EQ.2) SCSUM=0.
      DO 5 J=1,JMAX
    5 PP(J)=0.
      IF(I.EQ.2) PMIN=1.E 10
      DVN(JM)=0.0
      DVN(1)=0.0
      DO 1 J=2,JM
      DUW(J)=0.
      IF(I.NE.2) DUW(J)=VOL/(4.*CP(I-1,J)*DX)
      DUW(J)=0.
      DUE(J)=0.
      IF(I.NE.IM) DUE(J)=VOL/(4.*CP(I+1,J)*DX)
      DVS(J)=DVN(J-1)
      IF(J.EQ.JM) GO TO 2
      DVN(J)=VOL/((CP(I,J)+CP(I,J+1))*2.*DY)
    2 UE=(U(I,J)+U(I+1,J))/2.
      UW=(U(I,J)+U(I-1,J))/2.
      VN=(V(I,J)+V(I,J+1))/2.
      VS=(V(I,J)+V(I,J-1))/2.
      D(J)=RHO*A*(UE-UW+VN-VS)
      SCSUM=SCSUM+ABS(D(J))
      CPP(J)=RHO*A*(DUE(J)+DUW(J)+DVN(J)+DVS(J))
    1 CONTINUE
```

```
      DO 22 J=2,JM
   22 CON(J)=-D(J)
      G(1)=PP(1)
      H(1)=0.0
      DO 24 J=2,JM
      DENOM=CPP(J)-RHO*A*DVS(J)*H(J-1)
      G(J)=(CON(J)+RHO*A*DVS(J)*G(J-1))/DENOM
      H(J)=RHO*A*DVN(J)/DENOM
   24 CONTINUE
      DO 25 JJ=2,JM
      J=JM+2-JJ
      PP(J)=G(J)+H(J)*PP(J+1)
      P(I,J)=P(I,J)+PP(J)
      PMIN=AMIN1(P(I,J),PMIN)
   25 CONTINUE
      PP(JMAX)=PP(JM)
      PP(1)=PP(2)
C
      DO 3 J=2,JM
      PPN=(PP(J+1)+PP(J))/2.
      PPS=(PP(J-1)+PP(J))/2.
      IF(I.EQ.2) GO TO 4
C     U(I-1,J)=U(I-1,J)-VOL*PP(J)/(2.*CP(I-1,J)*DX)
    4 CONTINUE
      IF(I.EQ.IM) GO TO 6
      U(I+1,J)=U(I+1,J)+VOL*PP(J)/(2.*CP(I+1,J)*DX)
    6 CONTINUE
      V(I,J)=V(I,J)+VOL*(PPS-PPN)/(CP(I,J)*DY)
    3 CONTINUE
      IF(I.LT.IM) GO TO 11
      DO 12 I=1,IMAX
      DO 12 J=1,JMAX
```

```
      P(I,J)=P(I,J)-PMIN
   12 CONTINUE
   11 RETURN
      END
```

```
      SUBROUTINE BOUND(I)
      COMMON/GRID/X(11),Y(6),DX,DY,A,VOL
      COMMON/PROP/RHO,VISC,DIF
      COMMON/FIELD/U(41,6),V(41,6),P(41,6),SU(41,6),SV(41,6)
      COMMON/INDEX/IMAX,IM,JMAX,JM,KMAX,ITER,ITOTAL
      FLOWIN=RHO*U(1,1)*DX*FLOAT(JMAX-2)
C     AXIAL VELOCITY
      U(I,JMAX)=-U(I,JM)
      U(I,1)=U(I,2)
C     RADIAL VELOCITY
      V(I,JMAX)=-V(I,JM)
      V(I,1)=-V(I,2)
C     PRESSURE
      P(I,JMAX)=P(I,JM)
      P(I,1)=P(I,2)
C
C     EXIT PLANE BOUNDARY CONDITIONS
C
      IF(I.NE.IMAX) GO TO 4
      FLOW=0.
      DO 2 J=2,JM
      U(IMAX,J)=U(IM,J)
      FLOW=FLOW+RHO*A*U(IMAX,J)
    2 CONTINUE
      FACTOR=FLOWIN/FLOW
      DO 3 J=2,JM
      U(IMAX,J)=FACTOR*U(IM,J)
      V(IMAX,J)=V(IM,J)
      P(IMAX,J)=P(IM,J)
    3 CONTINUE
    4 CUNTINUE
      IF(I.NE.2) GO TO 6
```

```
      DO 5 J=2,JM
    5 P(1,J)=P(2,J)
    6 RETURN
      END
```

```
      SUBROUTINE PRINT
      COMMON/INDEX/IMAX,IM,JMAX,JM,KMAX,ITER,ITOTAL
      COMMON/CHECK/SCSUM,SMSUM
      COMMON/FIELD/U(41,6),V(41,6),P(41,6),SU(41,6),SV(41,6)
      DIMENSION TITLE(3)
      DATA TITLE/4HU-VE,4HV-VE,4HPRES/
C
C  PRINT OUT THE RESULTS
C
      WRITE(6,103) ITER,SMSUM,SCSUM
  103 FORMAT(//3X,5HAFTER,I3,11H ITERATIONS///
     2          3X,34HSUM OF MOMENTUM EQN RESIDUALS   = ,1PE10.3///
     3          3X,34HSUM OF CONTINUITY EQN RESIDUALS = ,1PE10.3//)
      DO 14 K=1,KMAX
      IPMAX=0
   10 WRITE(6,101) TITLE(K)
      IL=IPMAX+1
      IF(IMAX.LE.11) IPMAX=IMAX
      IF(IMAX.GT.11) IPMAX=IPMAX+11
      IF(IPMAX.GT.IMAX) IPMAX=IMAX
      DO 13 JJ=1,JMAX
      J=JMAX-JJ+1
      GO TO (7,8,9),K
    7 WRITE(6,100) (U(I,J),I=IL,IPMAX)
      GO TO 13
    8 WRITE(6,100) (V(I,J),I=IL,IPMAX)
      GO TO 13
    9 WRITE(6,100) (P(I,J),I=IL,IPMAX)
   13 CONTINUE
      IF(IPMAX.LT.IMAX) GO TO 10
   14 CONTINUE
  100 FORMAT(3X,11(1PE10.3))
```

```
101 FORMAT(//3X,1A4/)
    END
```

APPENDIX C.

Sample Program Results

AFTER 50 ITERATIONS

SUM OF MOMENTUM EQN RESIDUALS = 1.171E-01

SUM OF CONTINUITY EQN RESIDUALS = 4.347E-03

U-VE

1.000E+00	-4.598E-01	-2.906E-01	-2.375E-01	-2.193E-01
1.000E+00	4.598E-01	2.906E-01	2.375E-01	2.193E-01
1.000E+00	8.112E-01	7.010E-01	6.269E-01	5.887E-01
1.000E+00	9.858E-01	9.552E-01	9.100E-01	8.771E-01
1.000E+00	1.081E+00	1.104E+00	1.096E+00	1.083E+00
1.000E+00	1.135E+00	1.189E+00	1.211E+00	1.216E+00
1.000E+00	1.164E+00	1.235E+00	1.277E+00	1.301E+00
1.000E+00	1.179E+00	1.258E+00	1.313E+00	1.347E+00
1.000E+00	1.185E+00	1.268E+00	1.328E+00	1.367E+00
1.000E+00	1.185E+00	1.268E+00	1.328E+00	1.367E+00

-2.095E-01	-2.031E-01	-1.981E-01	-1.963E-01	-1.945E-01
2.095E-01	2.031E-01	1.981E-01	1.963E-01	1.963E-01
5.662E-01	5.515E-01	5.414E-01	5.335E-01	5.335E-01
8.540E-01	8.378E-01	8.263E-01	8.170E-01	8.170E-01
1.070E+00	1.059E+00	1.051E+00	1.044E+00	1.044E+00
1.219E+00	1.219E+00	1.217E+00	1.216E+00	1.216E+00
1.315E+00	1.325E+00	1.331E+00	1.336E+00	1.336E+00
1.371E+00	1.388E+00	1.401E+00	1.411E+00	1.411E+00
1.395E+00	1.417E+00	1.434E+00	1.446E+00	1.446E+00
1.395E+00	1.417E+00	1.434E+00	1.446E+00	1.445E+00

V-VE

0.000E-01 3.425E-02 5.578E-03 1.028E-03 3.726E-04
0.000E-01-4.254E-02-5.076E-03-6.672E-04-8.218E-05
0.000E-01-8.242E-02-1.716E-02-6.462E-03-2.714E-03
0.000E-01-9.132E-02-2.350E-02-1.189E-02-6.157E-03
0.000E-01-8.832E-02-2.473E-02-1.427E-02-8.314E-03
0.000E-01-7.277E-02-2.199E-02-1.404E-02-8.830E-03
0.000E-01-5.598E-02-1.710E-02-1.134E-02-7.485E-03
0.000E-01-3.292E-02-1.064E-02-7.438E-03-5.050E-03
0.000E-01-1.232E-02-3.687E-03-2.477E-03-1.709E-03
0.000E-01 1.232E-02 3.687E-03 2.477E-03 1.709E-03

2.294E-04 1.665E-04 1.030E-04 3.065E-04 0.000E-01
-6.646E-05-8.195E-05 4.549E-06-3.065E-04 0.000E-01
-1.560E-03-1.057E-03-6.836E-04-9.602E-04 0.000E-01
-3.792E-03-2.557E-03-1.790E-03-1.729E-03 0.000E-01
-5.488E-03-3.827E-03-2.767E-03-2.443E-03 0.000E-01
-6.138E-03-4.426E-03-3.291E-03-2.818E-03 0.000E-01
-5.416E-03-4.024E-03-3.055E-03-2.631E-03 0.000E-01
-3.730E-03-2.819E-03-2.175E-03-1.868E-03 0.000E-01
-1.288E-03-9.879E-04-7.667E-04-6.727E-04 0.000E-01
1.288E-03 9.879E-04 7.667E-04 6.727E-04 0.000E-01

PRES

0.000E-01-1.004E-01-2.804E-01-3.708E-01-4.467E-01
0.000E-01-1.004E-01-2.804E-01-3.708E-01-4.467E-01
0.000E-01-1.109E-01-2.782E-01-3.700E-01-4.464E-01
0.000E-01-1.217E-01-2.742E-01-3.691E-01-4.461E-01
0.000E-01-1.304E-01-2.693E-01-3.680E-01-4.458E-01
0.000E-01-1.369E-01-2.644E-01-3.668E-01-4.454E-01
0.000E-01-1.415E-01-2.604E-01-3.659E-01-4.450E-01
0.000E-01-1.444E-01-2.575E-01-3.652E-01-4.447E-01
0.000E-01-1.458E-01-2.561E-01-3.648E-01-4.446E-01
0.000E-01-1.460E-01-2.560E-01-3.648E-01-4.446E-01

-5.145E-01-5.778E-01-6.386E-01-7.048E-01-7.450E-01
-5.145E-01-5.778E-01-6.386E-01-7.048E-01-7.450E-01
-5.143E-01-5.777E-01-6.386E-01-7.048E-01-7.450E-01
-5.142E-01-5.776E-01-6.385E-01-7.048E-01-7.450E-01
-5.141E-01-5.775E-01-6.385E-01-7.048E-01-7.450E-01
-5.139E-01-5.774E-01-6.385E-01-7.048E-01-7.450E-01
-5.137E-01-5.773E-01-6.384E-01-7.048E-01-7.450E-01
-5.136E-01-5.772E-01-6.384E-01-7.048E-01-7.450E-01
-5.135E-01-5.772E-01-6.383E-01-7.048E-01-7.450E-01
-5.135E-01-5.772E-01-6.383E-01-7.048E-01-7.450E-01

The vita has been removed from the scanned document

EXPERIMENTAL AND PREDICTED PERFORMANCE FOR THE COMBUSTION OF A LOW HEATING VALUE GAS IN A SWIRL BURNER

by

James G. Rice

(ABSTRACT)

The combustion of a low heating value gas in a swirl burner is investigated. The investigation covers the development of a finite difference analysis of the flow and combustion processes in such a burner. In conjunction with the analytical work, an experimental program was conducted to provide detailed measurements of the three-dimensional velocity distributions within the flow field. The dissertation emphasizes the development and solution of the mathematical model.

The finite difference analysis uses the primitive variables of velocity and pressure to describe the flow field. Features of the solution algorithms of several previous authors are incorporated into the analysis. A unique feature of the current approach is the use of a non-staggered grid system. An additional feature is a very straightforward technique for handling boundary conditions which eliminates the need for special treatment of the finite difference equations at boundary points. The solution algorithm is given the acronym CENSIS, derived from CENtered-Cell-Implicitly-Staggered. To illustrate the incorporation of the algorithm into a computer code, a sample program is developed to solve a simplified problem which has a closed form solution. This program, CENCIS-T, is included. Calculations are presented for the swirl burner, and the predicted results are compared with experimental data. The pro-

gram used for the calculation of swirl burner performance is a more general code called PRIMCO. The PRIMCO code includes variable density and viscosity effects and incorporates a two-equation turbulence model for the Reynolds stress terms. The PRIMCO code also uses a simplified, infinite reaction-rate combustion model.

Because of the use of the non-staggered grid system, the CENCIS solution algorithm is less complicated than previous algorithms. As compared to a staggered grid system approach, the current algorithm requires approximately one-third the computations of the former approach. These advantages make this approach considerably easier to code and relatively easy to apply.